NEW COMPUTATIONAL METHODS AND ALGORITHMS FOR SEMICONDUCTOR SCIENCE AND NANOTECHNOLOGY

Benjamin C. Gamoke

Submitted to the faculty of the University Graduate School in

partial fulfillment of the requirements for the degree

Doctor of Philosophy

in the Department of Chemistry,

Indiana University

April 2015

Accepted by the Graduate Faculty, Indiana Universty, in partial fulfillment of the requirements for the degree of Doctor of Philosophy.

Doctoral Committee

_____
Krishnan Raghavachari, PhD

_____
Caroline Chick Jarrold, PhD

_____
Romualdo deSouza, PhD

_____
Randall Bramley, PhD

January 22nd, 2015

Acknowledgements

I would like to thank those who provided support and guidance during my studies at Indiana University. Most importantly, I have immense gratitude for Distinguished Professor Krishnan Raghavachari as my research advisor. He has provided indispensible guidance and patience, which has led to my development as a researcher and scientist. Professor Caroline Jarrold, Professor Srinivasan Iyengar, Professor Randall Bramley Provost Professor Romualdo deSouza, Herman T. Briscoe Professor Dennis Peters, Professor Harold Evans, Professor Paul Purdom, Jr., and Distinguished Professor Peter Orteleva, have also been vital to my development throughout the graduate program, by bringing new insights and ideas to the work presented in this document.

I am appreciative to have to opportunity to interact and learn from the previous and current members of the Raghavachari group. Previous group members, Dr. Ujjal Das, Dr. Hrant Hratchian, Dr. Nicholas Mayhall, Dr. Parathasarthi Ramakrishnan, and Dr. Aliaksandr Krukau, have all provided invaluable, ideas and support. In particular, I thank Dr. Raghunath Ramabhadran for his friendship and encouragement. I am also indebted to Dr. Jovan Jose, Dr. Debashis Adhikari, Arjun Saha, Manisha Ray, Victoria Erdely, Benjamin Noffke, Arkajyoti Sengupta, Daniel Beckett, Deyaa

AbuSalim, Edwin Becher, Arefin Chowdhury, and Corrine Kumar, for having the opportunity to learn and collaborate with an amazing group of talented coworkers.

I would also like to acknowledge my peers who joined Indiana University to study physical chemistry in 2009 for their encouragement throughout graduate school. We created a welcoming environment to take great leaps forward in chemistry together. The professional and personal connections I have made with Dr. Sarah Waller, Ryan Biczo, Mallory Mueller, Junjie Li, Amanda Leer, and Irma Hamilton will always be remembered and cherished.

Benjamin C. Gamoke

Bloomington, IN

22nd January 2015

Preface

Semiconductors are a very important class of materials. These systems have been influential in the development of modern electronics, as their electronic and structural properties are useful in integrated circuits,[1] lasers,[2] solar cells,[3] and other high performance technology. The definitive property of a semiconductor is the minimum energy required to induce an electronic excited state. Materials with very low or zero energies to undergo these transitions are classified as metallic, while other materials with very large transition energies are insulators.[4] Semiconductors have electronic transitions between those of metallic and insulating materials (e.g., 1.1 eV for silicon).[5]

The electronic properties that lead to this defined excitation energy come from the formation of extended systems from individual atoms. When two atoms are brought together, the atomic orbitals belonging to each atom interact, leading to linear combinations of these orbitals, subject to symmetry requirements. This results in bonding and anti-bonding molecular orbitals, formed by constructive and destructive combinations of the atomic orbitals. These orbitals are traditionally occupied by the “aufbau” principle, which states that the orbitals with the lowest energy are

occupied first. Many electronic configurations exist, with the most stable being referred to as the ground state.

As additional atoms are allowed to interact, more molecular orbitals are formed. The additional orbitals fall into specific energy regions, which converge to form bands as number of atoms approaches infinity. As these bands can classified by different types of bonding interactions of a molecular system's electronic structure, the band that contains the highest lying electrons is typically referred to as the valence band, while the lowest energy band that is unoccupied is known as the conduction band. These classifications hold true for insulators and semiconductors because of their associated *band gap*, or the energy required to undergo the lowest energy excitation from the valence band to the conduction band.

It is convenient to describe extended systems in terms of a unit cell, which is the smallest possible unit in either one-, two-, or three-dimensional space that can describe an infinite system. One-dimensional systems can effectively describe an infinitely long polymer or a nanoribbon. Two-dimensional units cells are typically used to describe surfaces of extended systems with an approximate thickness. As the thickness of the unit cell is several atomic layers

deep, it can approximately describe a bulk material's surface. However, as the number of atomic layers used to describe a unit cell decreases, it is best for describing "2D" molecules, like graphene or graphene sheets. Similarly, three-dimensional unit cells describe periodic bulk materials.

Each unit cell used for calculations in molecular systems contains a set of atoms and a corresponding set of translation vectors, described in terms of real space, whose linear combinations periodically translate the unit cell through n-dimensional space. A reciprocal space can be defined for this set of vectors by Fourier transform to momentum space.[6] This space can be used to define a set of molecular orbitals at point *k*, convenient for analysis of the electronic structure of a molecular system.

A band gap associated with any semiconductor is either classified as a *direct* or *indirect* band gap. If the highest energy point of the valence band and lowest energy point in the conduction band occur at the same *k* point in momentum space, then the band gap is known as a direct band gap (e.g., GaAs). For any other band gap, one where the relevant points in momentum

space that are involved in the electronic excitation are not equal, defines a semiconductor with an indirect band gap (e.g., silicon).

Along with electronic properties of a semiconductor, the structural features at the interface of the material are also important, as it is important for applications in microelectronics, sensing, and lubrication. The periodic surface facets can be described from Miller indices, which describes a plane from the perpendicular of a linear combination of the three spatial vectors of a 3-dimensional unit cell from the bulk material. By convention, Miller indices are a set of n indices, corresponding to the dimensional space of the unit cell, which designate an integer multiple of each translation vector, which are summed together. From this vector addition, the orthogonal plane is defined, which in turn defines the surface.

To illustrate this concept, Figure P.1 shows a primitive unit cell for bulk silicon. It contains two atoms, each of which are covalently bonded to four atoms, one of which is an intracell atom. From the set of translation vectors, two important planes of silicon are defined by their Miller indices, the Si(111) and Si(100) planes. Cleaving the (111) plane leads to breaking one covalent bond from each silicon atom, leading to a surface that has one unpaired

electron on each unsaturated atom, as shown in Figure P.2. When a surface from the (100) plane is formed, two covalent bonds are broken on each atom, creating an energetic instability. Geometric reconstruction occurs on this surface by creating surface dimers, which decrease the number of unpaired electrons to one per surface atom. There are two different bonding models that can describe the surface, causing symmetric and asymmetric surface dimers. Asymmetric dimers are caused by a dimer bond with ionic character, as the oxidized silicon atom has a larger preferred bonding angle than the reduced surface atom. Symmetric dimers are described by a covalent bonding between the two surface atoms. The reconstruction of the Si(100) surface to symmetric dimers is shown in Figure P.3.

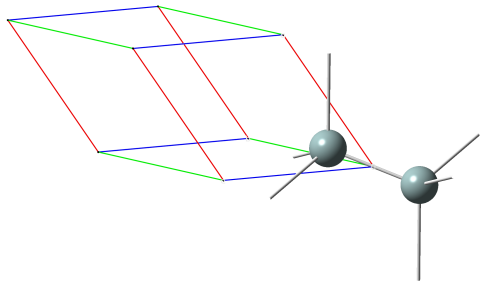

Figure P.1. A primitive unit cell for bulk silicon. The three translation vectors are represented by the blue, red, and green lines for their direction and magnitude.

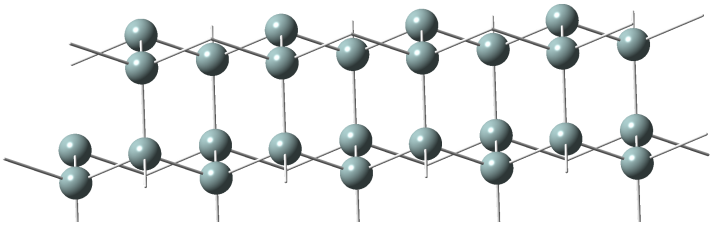

Figure P.2. A side view of the Si(111) surface. The surface is truncated for clarity, as lines that extend to other atoms refer to covalent to nearby atoms in the material.

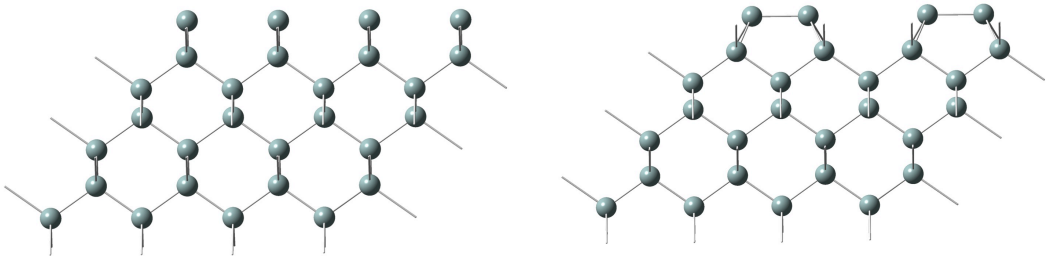

Figure P.3. A side view of the unreconstructed Si(100) surface (left) and reconstructed symmetric dimer surface (right).

Many challenges still exist in computational methods for calculating structural and electronic properties of materials systems. From the approximations that are imposed by standard models can lead to failures that lead to inaccurate or faulty results. We have identified several such deficiencies in this thesis and have

proposed new computational strategies to solve them in a satisfactory manner. Many of these new strategies involve composite hybrid techniques and are described below.

Computational chemistry is having a significant impact on the materials community. It uses computational techniques and algorithms to provide tools that yield insight into the behavior of complex systems. Not only does computational chemistry verify experimentally measured properties and behavior, but also provides a mechanism for predictions of new processes and chemical reactions not yet observed experimentally.

Developments in *ab initio* computational chemistry that emphasize high accuracy using quantum mechanics have traditionally focused on the study of small molecules. The steep scaling of accurate calculations does not permit such studies to be directly performed on large molecules. For example, 2nd Order Møller Plesset Perturbation Theory, (MP2), scales as O(N^5), and coupled cluster theory including single and double excitations and perturbative triple excitations, CCSD(T), scales as O(N^7), where N is the number of basis functions.[7] This high order scaling is prohibitively expensive for many large chemical systems. To remedy this problem, composite techniques are employed where

regions of a molecular system can be truncated to reduce computational cost and keep only the chemically relevant interactions to be described with a high level of accuracy.

The ONIOM methodology,[8] which is based on previous composite techniques, the Integrated Molecular Orbital Molecular Mechanics (IMOMM)[9] and Integrated Molecular Orbital Molecular Orbital (IMOMO) methods,[9] is an extrapolation-based technique that integrates several calculations using multiple levels of theory (Molecular Mechanics and Quantum Mechanics based methods) to approach relative energies and geometries that are in agreement with results from calculations that would otherwise be prohibitively expensive. ONIOM and similar hybrid methods require the atoms in the molecular system to be assigned to one or more regions. Each region has its own uniquely assigned computational method appropriate for its contribution to the overall molecular properties of interest.

In a 2-layer ONIOM calculation, the entire system is defined to be the "real" system. The region of the molecule that requires the most rigorous analysis and is therefore adequately described with a "high" level of theory is classified as the "model" system.

Using this nomenclature for a two-layer ONIOM calculation, the energy is defined as:

$$E_{ONIOM} = E_{low,real} - E_{low,model} + E_{high,model} \quad (3)$$

The total energies derived from this method contain little meaning. However, ONIOM excels at describing relative energies at a high level of accuracy, similar to that of performing the entire molecular system at the high level of theory chosen in the model system. This reason can be clearly identified when the absolute energy of the real system at a high level of theory is written as:

$$E_{high,real} = E_{low,real} - E_{low,model} + E_{high,model} + \Delta \quad (4)$$

Assuming the scalar Δ, which describes the difference between the total energy of the full system at the high level of theory and that obtained by ONIOM, is constant between any two structures, relative energies will be accurate due to error cancellation.[8a]

Gradients are obtained in a manner similar to the energies in the ONIOM formalism.

$$\frac{dE_{ONIOM}}{dq} = \frac{dE_{high,model}}{dq} \cdot J + \frac{dE_{low,real}}{dq} - \frac{dE_{low,model}}{dq} \cdot J \quad (5)$$

J is the Jacbobian required to describe how the separate regions couple and q is the geometrical coordinates.[10] The additive nature of the forces makes their computations simple and appropriate for molecular optimization.

Bonds are broken at the boundary between any two regions in order to create model systems that can be computationally achievable with higher levels of theory. If these broken bonds are left untreated, the newly defined but incomplete chemical structures will be in an electronic state and environment very different from the corresponding region in the full molecular system. In order to overcome this deficiency in hybrid methods, one often employs hydrogen link atoms to saturate the broken covalent bonds. The corresponding gradients associated with the presence of link atoms at regional boundaries are handled by the Jacobian, *J*, mentioned in the previous paragraph.

While ONIOM and other methods have been developed for the treatment of large systems, there are many instances where such standard models do not perform well. For example, truncation of a "model" system with hydrogen atoms will be poor when the atom being replaced from the "full" system has a substantially greater electronegativity, such as the truncation of a broken Si–O bond in silicon dioxide with a Si–H bond. Other truncation effects can lead to drastic deficiencies in a model system, particularly when describing materials systems.

In Chapter 1, a pseudoatom formulation for divalent silicon is presented which corrects a problem critical for describing Si(100) surface chemistry. The hydrogen link atom treatment, described above for creating truncated systems, leads to a drastic failure of the geometries for cluster and slab calculations. A pseudoatom can be used in place of hydrogen link atoms in order to describe truncated Si(100) systems to avoid this issue.[11] The effective potential parameters of our pseudoatom are obtained by fitting to information on both Si–Si and Si–O bonds, making our pseudoatom transferable for different bonding situations. We show the applications of the pseudoatom approach in small molecules and surface models, and also discuss its ability to describe heteroatomic bonds using multiple theoretical methods. Similar pseudoatom parameters are also derived and tested for monovalent silicon, divalent carbon, and monovalent carbon.

The accurate modeling of adsorbates on periodic surfaces at low coverages is computationally inefficient with current methodologies, typically requiring large unit cells to minimize unphysical intercell interactions. We propose a novel composite method in Chapter 2 that effectively cancels the adsorbate-adsorbate interactions that are otherwise present in such slab calculations. Our method provides a good description of the entire

potential energy surface, and yields geometrical relaxations at the low coverage limit on periodic surfaces requiring only small unit cells. Simple organic adsorbates have been studied on Si(111) and C(111) surfaces to illustrate the applicability of this new computational approach.

In Chapter 3, the ability to cancel spurious interactions has been further explored and generalized to overcome other challenges in modeling molecular systems. Other intercell interactions can occur when modeling materials or surface chemistry. Cluster models commonly use hydrogen atoms to saturate dangling bonds created due to truncation.[12] While this is adequate for many molecular systems, it is not adequate for many important problems involving surface chemistry where multiple covalent bonds to a single atom are severed between layers. We explore an alternative scheme to remedy the unphysical hydrogen-hydrogen link atom interactions that lead to catastrophic geometry distortions in Si(100) cluster models. Since these overall repulsive interactions are spurious and derived from truncation, we attempt to effectively remove them from the calculation in order to successfully model the Si(100) cluster using standard link atom treatments. A composite energy scheme is described by a set of well-defined fragments that can effectively cancel the unphysical

link atom interactions. This hybrid potential energy can then be minimized with respect to the geometrical parameters, yielding physically realistic structures that are not adversely impacted by the unphysical steric interactions.

Further, complex interactions between different portions of a large molecule can be difficult to analyze and understand through traditional electronic structure calculations. The physical consequences of each individual pairwise interaction that is contained inside a molecule cannot be quantified in a straightforward fashion with standard methods. By creating a set of molecular fragments, a novel composite energy method is proposed that can explore changes in a molecule caused by removing selected nonbonded interactions between different portions of a molecule. Energies and forces are easily obtained with this composite approach, allowing geometry optimizations that lead to chemically meaningful structures that describe how the omitted interactions contribute to the local geometrical minima. We illustrate the application of our new hybrid scheme by computing the influence of intramolecular hydrogen bonding interactions in two small molecules, 1,6-(g+G+TG+g+)-hexanediol and cis-1,4-cyclohexanediol. The resulting structural changes show some novel aspects that are interpreted to yield key physical insights. We

demonstrate that the composite method can be extended to larger molecular systems by showing its application on a Si(100) surface model containing interactions between dissociated ammonia on adjacent surface dimers. The method is robust and should be applicable for other large molecular studies, such as those in materials systems and biomolecules.

In Chapter 4, computational methods used to predict and identify x-ray photoelectron spectroscopy (XPS) are described. The spectra obtained are useful for the characterization of molecules and bulk material for chemical composition and bonding environments.[13] Because of the complex processes that occur during ionization of a system, calculation and assignment of peaks can be formidable. Therefore it is important to calculate spectroscopic features in an accurate but computationally tractable manner. Findings from these investigations are reported.

Further developments in each of these areas are reported in the prospectus, following the chapters of the main text. Current progress has been developed to solve further related problems in this field. Preliminary explorations and methods are reported to address future topics that are relevant to emerging techniques in modeling materials systems.

References

1. (a) Appelbaum, I.; Huang, B.; Monsma, D. J., Electronic measurement and control of spin transport in silicon. *Nature* **2007,** *447* (7142), 295-298; (b) del Alamo, J. A., Nanometre-scale electronics with III-V compound semiconductors. *Nature* **2011,** *479* (7373), 317-323; (c) Flatte, M. E., Solid-state physics: Silicon spintronics warms up. *Nature* **2009,** *462* (7272), 419-420.

2. (a) Ledentsov, N. N.; Ustinov, V. M.; Shchukin, V. A.; Kop'ev, P. S.; Alferov, Z. I.; Bimberg, D., Quantum dot heterostructures: Fabrication, properties, lasers (Review). *Semiconductors* **1998,** *32* (4), 343-365; (b) Pavesi, L., Will silicon be the photonic material of the third millenium? *Journal of Physics: Condensed Matter* **2003,** *15* (26), R1169; (c) Zavada, J. M.; Duhua, Z., Luminescence properties of erbium in III–V compound semiconductors. *Solid-State Electronics* **1995,** *38* (7), 1285-1293.

3. (a) Atwater, H. A.; Polman, A., Plasmonics for improved photovoltaic devices. *Nat Mater* **2010,** *9* (3), 205-213; (b) Grätzel, M., Dye-sensitized solar cells. *Journal of Photochemistry and Photobiology C: Photochemistry Reviews* **2003,** *4* (2), 145-153.

4. Madou, M. J., Solid-state physics, fluidics, and analytical techniques in micro- and nanotechnology, 3d ed. 2011.

5. Nelson, V., *Introduction to renewable energy*. CRC Press: 2011.

6. Ooi, L.-l., *Principles of x-ray crystallography*. Oxford ; New York : Oxford University Press, 2010.: 2010.

7. Jensen, F., *Introduction to Computational Chemistry*. 2 ed.; Wiley: 2006.

8. (a) Svensson, M.; Humbel, S.; Froese, R. D. J.; Matsubara, T.; Sieber, S.; Morokuma, K., ONIOM: A Multilayered Integrated MO + MM Method for Geometry Optimizations and Single Point Energy Predictions. A Test for Diels–Alder Reactions and Pt(P(t-Bu)3)2 + H2 Oxidative Addition. *The Journal of Physical Chemistry* **1996,** *100* (50), 19357-19363; (b) Vreven, T.; Byun, K. S.; Komáromi, I.; Dapprich, S.; Montgomery, J. A.; Morokuma, K.; Frisch, M. J., Combining Quantum Mechanics Methods with Molecular Mechanics Methods in ONIOM. *Journal of Chemical Theory and Computation* **2006,** *2* (3), 815-826.

9. Svensson, M.; Humbel, S.; Morokuma, K., Energetics using the single point IMOMO (integrated molecular orbital+molecular orbital) calculations: Choices of computational levels and model system. *Journal of Chemical Physics* **1996,** *105* (9), 3654-3661.

10. Vreven, T.; Morokuma, K.; Farkas, Ö.; Schlegel, H. B.; Frisch, M. J., Geometry optimization with QM/MM, ONIOM, and other combined methods. I. Microiterations and constraints. *Journal of Computational Chemistry* **2003,** *24* (6), 760-769.

11. Krüger, T.; Sax, A. F., Oligovalent link atoms in embedding calculations. *Journal of Computational Chemistry* **2002,** *23* (3), 371.

12. Yip, S., *Handbook of Materials Modeling. [electronic resource].* Dordrecht : Springer, 2005.: 2005.

13. Bureau, C.; Kranias, S., Accurate Density-Functional Calculation of Core XPS Spectra: Simulating Chemisorption and Intermolecular Effects on Real Systems? In *Quantum Systems in Chemistry and Physics Volume 2*, Hernández-Laguna, A.; Maruani, J.; McWeeny, R.; Wilson, S., Eds. Springer Netherlands: 2000; Vol. 2/3, pp 41-56.

Benjamin Gamoke

NEW COMPUTATIONAL METHODS AND ALGORITHMS FOR SEMICONDUCTOR SCIENCE AND NANOTECHNOLOGY

The design and implementation of sophisticated computational methods and algorithms are critical to solve problems in nanotechnology and semiconductor science. Two key methods will be described to overcome challenges in contemporary surface science. The first method will focus on accurately cancelling interactions in a molecular system, such as modeling adsorbates on periodic surfaces at low coverages, a problem for which current methodologies are computationally inefficient. The second method pertains to the accurate calculation of core-ionization energies through X-ray photoelectron spectroscopy. The development can provide assignment of peaks in X-ray photoelectron spectra, which can determine the chemical composition and bonding environment of surface species. Finally, illustrative surface-adsorbate and gas-phase studies using the developed methods will also be featured.

Krishnan Raghavachari, PhD

Caroline Chick Jarrold, PhD

Romualdo deSouza, PhD

Randall Bramley, PhD

Table of Contents

List of Tables

List of Figures

Chapter One

Divalent Pseudoatoms for Modeling Si(100) Surfaces

1.1. Introduction

Developments in computational chemistry that emphasize high accuracy using quantum mechanical methods have mostly focused on smaller molecular systems, where the number of atoms is constrained by current computational resources and technology. Molecular mechanics, using various force fields,[1] or semi-empirical methods such as AM1[2] or PM6,[3] have been methods of choice for large molecular systems because of their favorable scaling with the number of atoms in the molecule. However, recent developments have made it possible to apply *ab initio* methods for large systems while avoiding the scaling issues that occur even with relatively efficient DFT methods. These developments include hybrid methods such as QM/QM,[4] QM/MM,[5] and in general, ONIOM[6] hybrid methods. These procedures require the molecular system to be split into at least two different regions, each region having its own uniquely assigned computational method appropriate for its contribution to the overall molecular properties. Typically, regions where bonds are being created or broken are modeled with a more rigorous *ab initio* method, with the rest of the molecule being

treated with an approximate, but computationally efficient model. Essentially, such hybrid methods make use of the fact that interesting chemistry typically occurs locally.[6a, 7]

Bonds have to be frequently broken at the boundary between any two regions in order to create model systems that can be computationally achievable with higher levels of theory. If these broken bonds are left untreated, the newly defined, but valence-incomplete, chemical structures will be in an electronic state and environment very different from the corresponding region in the complete system. In order to overcome this deficiency in hybrid methods, one often employs hydrogen link atoms to saturate the broken covalent bonds. In some cases, replacement of an atom with a hydrogen link atom may be an appropriate approximation. For example, replacement of a covalent C–C single bond in a biomolecule with a covalent C–H bond may be appropriate. However, in many other applications, the truncation of a molecular system with a hydrogen atom can lead to errors because of differences in electron density between the real system and the model system. For example, the replacement of a Si–O bond in α-quartz with a Si–H bond may not be appropriate due to the large electronegativity difference between O and H. Special treatment must be also be utilized to account for bond length differences, as

a hydrogen link atom will have a different bond length in the model system than the real atom in the full system. In hybrid methods, this leads to extra complications with geometry optimizations that must be accounted for.[6c]

There is an additional complication from link atom terminations that occurs in many materials systems, particularly for Group IV semiconductors such as silicon or germanium. This can be illustrated using a simple example - the modeling a Si(100) reconstruction with either cluster or periodic boundary condition (PBC) calculations. For any two dimensional PBC model of the Si(100) surface reconstruction and most Si(100) cluster models, truncation of the system leads to two different covalent bonds being broken to the same truncated atom. Using hydrogen atoms for truncation results in two different hydrogen link atoms that represent the same truncated atom, resulting in two atoms being in very close proximity to each other leading to artificial intramolecular H···H interactions. The repulsive forces from these intramolecular interactions cause a buckling on the truncated Si(100) surface and ultimately leads to a failure to produce an accurate model of this common semiconductor.

Improvements to the traditional link atom approach have been proposed in the computational chemistry literature. These methods include hybrid orbital approaches[5b, 8] where localized orbitals are defined from a series of *ab initio* calculations on small test molecules, and later frozen for use at the boundary of a QM/MM calculation. While accurate, they require projection operators and/or parameterization for each specific application. Other methods have been proposed that take an approach similar to the use of hydrogen link atoms, but where effective potentials and/or basis set parameters are fitted to reintroduce electronic effects from portions of the real system that were lost from truncation[9] These methods are simple to implement because the infrastructure is already available in most *ab initio* software packages. However, these methods have only been used for designing monovalent link atoms in truncation of molecular systems. A new method for designing and parameterizing a robust divalent link atom is proposed in this work, along with results displaying their effectiveness for use in *ab initio* calculations.

1.2. Background

Hybrid orbital[5b] and parameterized design-atom[9a, 9d, 9e, 9g, 10] approaches have been suggested as methods for removing the

truncation errors with hybrid methods such as ONIOM. These methods, however, have only been introduced for use in capping single covalent bonds (*vide supra*). Rivail's local self consistent field (LSCF) method,[11] Gao's generalized hybrid orbital method,[8a] and Friesner's frozen orbital method[8b, 12] all belong to the category of frozen orbital methods. These methods are typically implemented for semiemperical or *ab initio* HF calculations but can be adapted for other techniques. It has been shown that the use of hybrid orbitals leads to a satisfactory description of the boundary region, though they require significant theoretical formulation and code development. These methods also require additional parameter fitting that may be system-dependent. However, the more common approach has been to truncate the system in a hybrid method with the use of custom atoms that have similar properties to the molecular region lost due to truncation of the model system. These methods include the pseudobond method of Zhang et al,[9a, 10a, 10b, 10j] quantum capping potential (QCP) of DiLabio and co-workers,[9g, 10e, 10f] effective group potential (EGP) method of Poteau et al,[9e, 10i] and the pseudoatom approach of Taylor et al.[9d] The desired properties are obtained by defining new parameters for basis sets and/or effective core potentials (ECP). The quantum capping potential (QCP) proposed by DiLabio uses a carefully modified ECP by adding shielding and Pauli potentials to a link

atom to create improvements to the hydrogen link atom treatment. Shielding terms are defined as additional terms appended to the standard ECP at the highest angular momentum, which create attractive electronic terms to attempt to bring valence electron density inside the core of the QCP. Pauli potentials are the additional ECP terms added to electrons of angular momenta lower than the maximum angular momentum that attempt to bring electronically repulsive forces between the link atom and its bonded neighbor. For the definition of the QCP, four different sets of parameters were proposed, each with increasing complexity in order to improve its robustness. In the pseudobond method, Zhang *et al.* parameterized an effective core potential for use to replace a methyl group. The ECP consists of a set of shielding and Pauli terms. The custom-defined methyl pseudobond is designed for use with the fluorine 3-21G and 6-31G* basis sets. Further developments have led to the optimization of custom STO-2G basis sets along with their ECP potentials in order to obtain better performance across multiple types of C–C and C–N bonds.[10d, 10j] Wang and Truhlar proposed a method for obtaining link atoms that attempts to reproduce charge transfer to a custom designed link atom called the balanced redistributed charge scheme.[9b, 9c] Fluorine atoms are employed as link atoms, but the core electrons are replaced with the CRENBL ECP and the same basis set as the rest of

the quantum region in the QM/MM calculation. Only two parameters are added to the ECP as a shielding term, one exponent and one coefficient. The exponent value is set to 1 bohr and the coefficient is optimized to recreate the charges of the non-truncated system but in the presence of MM charges. Our divalent pseudoatom is based upon such previous approaches and fitted to obtain results within a target accuracy in electronic structure calculations.

1.3. Method

The analytical form of the nonrelativistic angular momentum-dependent effective core potential[9e] is written as

$$V^{Core}(r) = V_L^{Core}(r) + \sum_{l=0}^{L-1}\sum_{m=-l}^{l}[V_l^{Core}(r) - V_L^{Core}(r)]\sum_m |lm\rangle\langle lm| \quad (1.1)$$

where

$$V_L^{Core}(r) = \sum_k \frac{d_{l,k}e^{-\zeta_{l,k}r^2}}{r^{2-n}} \quad (1.2)$$

and

$$V_l^{Core}(r) - V_L^{Core}(r) = \sum_k \frac{d_{l,k}e^{-\zeta_{l,k}r^2}}{r^{2-n}}, l = 0, \dots, (L-1) \quad (1.3)$$

In Equations (1.1)-(1.3), L is the maximum l beyond which there is little difference in the corresponding effective potentials. For example, L=2 is usually sufficient for silicon though sometimes L=3 is used. ξ and d are parameters, exponent and coefficient, respectively, and n = 0, 1, or 2. The summation over k is typically restricted to l-3 terms. As a replacement of the core electrons of an atom, V^{Core} must ideally satisfy the following conditions:

(1) The pseudo-orbitals must be shape-consistent with the corresponding all-electron valence orbitals;
(2) V^{Core} reproduces the Coulomb and exchange terms coming from the interactions between the core and valence electrons in the all-electron operator;
(3) V^{Core} corrects for the missing nuclear charge due to the loss of the core electrons; and
(4) For l < L, V^{Core} must include Pauli repulsion to prevent collapse of the valence orbitals onto the core.

By adding an additional shielding term (one exponent and coefficient) to the highest angular momentum and two Pauli repulsion (two sets of exponent and coefficient pairs) terms to the two lowest angular momentum correction terms to the ECP, bond angles can be sufficiently represented by controlling the amount of

p character in the pseudoatom's bonding orbitals. If the Pauli term is added under the s projection (the S–F term), the percentage of s character in the bonding orbitals increases when the exponent (ζ) is increased. This trend has been shown using a solid line in the lower box of Figure 1.1. The attractive shielding terms are appended to an existing ECP in an attempt to move electron density from valence electrons towards the core of the pseudoatom. The repulsive Pauli terms are included to create a potential that repels bonded atom neighbors, which in turn adjusts the bond lengths and Mulliken charges of the pseudoatom. DiLabio used a small exponent (ζ=0.539) for the shielding potential to design the silicon QCP.[10f] This was done to minimize the effect of the potential at the Si–Si bond distance, which is roughly 2.35 Å. A similar approach is followed here to determine the exponent of the shielding potential.

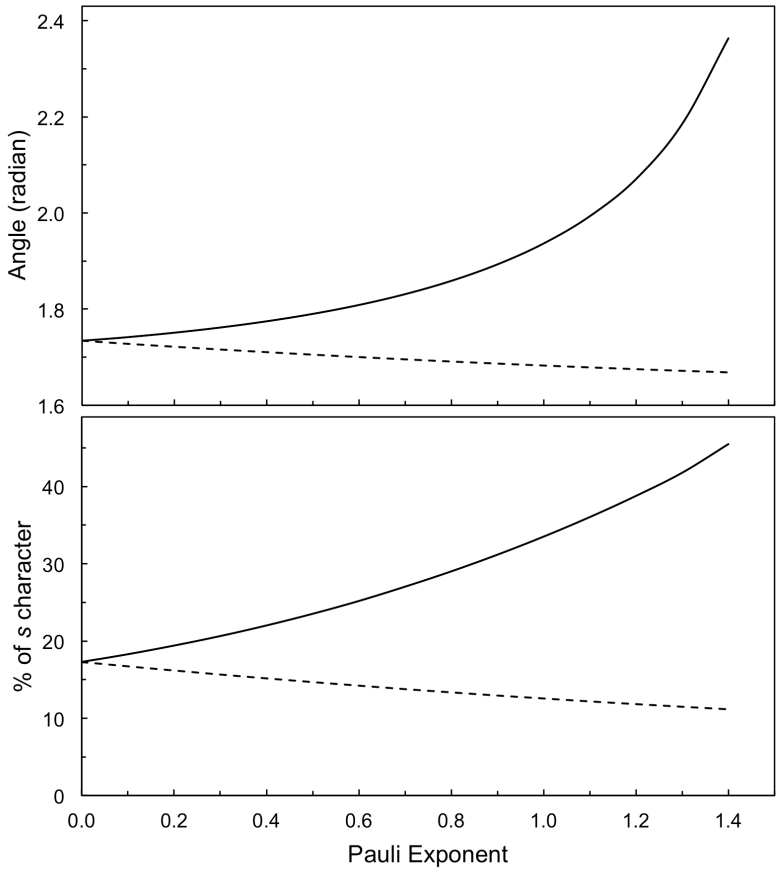

Figure 1.1. Effect of Pauli potentials on the pseudoatom. The change in Pauli coefficient (horizontal axis) affects the hybridization of pseudoatom bonding orbitals as well as the bond angles. The change may take place under S–F projection (solid line) or P–F projection (dashed line).

Different methods can be used for determining optimal parameters for use in a designed pseudopotential. Taylor and co-workers[9d] utilized Equation 1.4 for designing effective core potentials of $-OCH_3$ and $-OCH_2CH_3$ groups. In their work, bond

lengths, bond angles, and dihedral angles were used to fit the ECP parameters where ω_i is a weighing factor and the s_i terms are different internal coordinates (bonds, angles, dihedrals). Pseudobond formalisms[10d, 10j] have used other fitting parameters. ESP charges, gradient norm error, and bond dissociation energies were chosen in these methodologies.

$$f = \sum_i \omega_i (s_i^{fragment} - s_i^{full}) \quad (1.4)$$

In order to develop robust pseudoatoms, designing a method which optimizes ECP parameters that return acceptable results is essential for applications on Si(100) structures where the pseudoatoms are positioned at the boundary of a Si(100) slab or cluster. The ECP parameters, when used with an appropriate basis set and ECP[13] must yield physically meaningful parameters that emulate those from the full system. We have developed a procedure for finding a set of parameters that correspond to a minimum with respect to errors from full calculations on the reference molecules trisilane and disilanol at the B3LYP/6-31G* and M06-2X/6-31G* levels of theory.[14]

Using the intial SDD ECP parameters, bond distances, bond angles, and Mulliken charges of the reference molecules are used to

derive modified ECP parameters via least squares fitting (*vide infra*). The use of bond distances, bond angles, and Mulliken charges, similar to the work of Taylor[9d] is sufficient in our study to obtain good performance for our divalent pseudoatom for its use in Si(100) cluster and slab models. The newly defined ECP parameters for each pseudoatom are used in conjunction with sulfur atoms to represent the divalent silicon pseudoatoms. Sulfur atoms were used because they conserve the total number of electrons in the pseudoatom system and have similar bonding to the fragments they are replacing. In our approach, we attempted to create more flexibility across different bonding environments by utilizing reference molecules that have polar Si–O bonds in combination with Si–Si covalent bonds. Specifically, for the development of silicon divalent pseudoatom, we utilized trisilane and disilanol as reference molecules. Our goal is to derive parameters that yield errors that are typical for standard *ab initio* calculations: 0.02 to 0.04 Å for bond lengths, 2˚ to 5˚ for bond angles, and 0.1 atomic charge for atomic Mulliken population analysis.

The new set of parameters were optimized using the Levenberg-Marquardt linear least squares minimization method implemented in the Octave Optim package.[15] The objective function

f is defined in Equation 1.5, where s_i represents bond lengths, bond angles, and Mulliken charges in the reference molecules with and without the pseudoatom. Similar to Equation 1.4, the weighting factor ω_i is defined as 1.0 for each parameter.

$$f = \sum_i \omega_i \left(s_i^{pseudo} - s_i^{full}\right)^2 \quad (1.5)$$

The generated pseudopotentials for the pseudoatom were tested for their robustness in various bonding environments so they can be used with confidence in truncated Si(100) models. Test sets containing different heteroatomic bonds involving atoms with weak and strong electronegativities and various amounts of ionic character were selected by substitution with functional groups such as, Cl, OH, NH_2. In addition, multiple levels of theory, MP2,[16] B3LYP,[14a-c] M06-2X,[17] PBE,[18] M06-L,[19] and BLYP[14a-c, 20] were used to determine the applicability of the newly designed pseudoatom across a wide spectrum of methods.

1.4. Computational Details

All geometry optimizations were performed with the Gaussian 09 package of programs.[21] The SDD pseudopotential[13, 22] was employed and modified with additional terms for F–up, S–F, and P–F potentials as shown in Table 1.1. The 6-31G(d) basis set[14d-f] was employed uniformly, though all Si pseudoatoms and their full equivalents were treated with 5 pure d-functions (instead of 6 second-order Gaussians as in the standard basis set). The pseudoatom itself uses the polarized split-valence type basis set associated with the silicon SDD pseudopotentials along with a set of d-functions with an exponent value of 0.45.[14d, 22] All atomic charges were derived using Mulliken population analysis.[23]

Type	n	ζ	d
F–up	1	0.284224125	–0.159861722
S–F	2	0.295958462	1.480140911
P–F	2	3.569024533	38.848232626

Table 1.1. The ECP parameters for the silicon divalent pseudoatom.

1.5. Results

Test results for the trisilane (1a) and divalent pseudoatom substituted molecule (1b) are listed in Table 1.2. Bond length, bond angles, and Mulliken charges are computed for the full

molecule as well as for the molecule using the divalent pseudoatom. The difference in the Si–Si bond length between the full and pseudoatom equivalent of trisilane is 0.001 Å and the difference in the Si–Si*–Si angle is 1.1º with the B3LYP functional. Thus we can see that our pseudoatom successfully reproduces the structural parameters of the trisilane molecule. Since the pseudoatom replaces the SiH_2 group in trisilane, we have compared the charge on the pseudoatom with the total charge of the SiH_2 fragment. Results shown in Table 1.2 reveal that the charges on different atomic centers in the model system are in very close agreement with the reference system, with differences less than 0.03 electrons. Similar performance is noted when using the M06-2X and MP2 levels of theory with the 6-31G(d) basis set.

DFT	System	Si–Si*	Si–Si*–Si	Si*–Si–H	q(Si)	q(Si*)
B3LYP	**1a**	2.354	112.9	110.9	0.177	−0.038
	1b	2.353	114.0	108.9	0.147	−0.029
M06-2X	**1a**	2.336	110.5	111.4	0.184	−0.055
	1b	2.351	112.1	109.1	0.143	−0.015
MP2	**1a**	2.342	112.1	110.9	0.417	−0.065
	1b	2.343	108.4	108.6	0.445	−0.167

Table 1.2. Computed bond lengths (Å), bond angles (°) and atomic Mulliken charges (e) of trisilane (**1a**) and SiH_3–Si*–SiH_3 (**1b**) in Figure 1.2 using various methods and 6-31G(d) basis set. For MP2, the Mulliken charges were performed at the HF level of theory. Here, Si* represents a divalent pseudoatom.

While the pseudoatom reproduces bond lengths, bond angles, and charges, of trisilane reasonably well, we have also tested its performance when the pseudoatom is used in disilanol with B3LYP, M06-2X, and MP2. The results of the full atom calculations (2a) and the equivalent pseudoatom calculations (2b) are shown in Table 1.3. Bond lengths for Si–Si bonds across B3LYP, M06-2X, and MP2 all have errors less than 0.015 Å. While the performance with the DFT functionals for more polar Si–O bonds is very good (0.011 Å and 0.016 Å for B3LYP and M06-2X, respectively), MP2 leads to a slightly higher error of 0.033 Å. Bond angles in disilanol are described well with our divalent pseudoatom, with errors across all levels of theory being less than

3.0º. Atomic charges are also in good agreement, particularly with the two density functionals we have selected, as errors are minimized to high accuracy.

We have analyzed the usefulness of the silicon divalent pseudoatom by testing its performance on molecules with various heteronuclear bonds. The molecules are constructed by replacing the terminal SiH_3 group in tetrasilane and trisilane with different simple functional groups. These molecules are listed in Tables 1.4 and 1.5. This testing procedure measures the transferability of the pseudoatom across different chemical environments. Overall, the pseudoatom performs very well across the test sets, as compared to full atom systems with similar conformations. Table 1.4 shows the results for replacing SiH_3–SiH_2–SiH_2–X with SiH_3–Si*–SiH_2–X. In this case, the mean absolute deviation (MAD) for different bond lengths, bond angles, and Mulliken charges with the B3LYP functional for these molecules are well within our ideal errors discussed above, as our mean absolute deviations of the bond lengths, bond angles, and Mulliken charges are 0.007 Å, 1.6º, and 0.029 *e*. This implies that the pseudoatom can be used in different systems with confidence that performance of the atom will behave as expected. The largest unsigned error is also reported. It occurs for the bond angle involving the electronegative Cl atom.

DFT	Sys	Si–Si*	Si*–O	O–Si*–Si	H–O–Si*	q(Si)	q(O)	q(Si*)
B3LYP	**2a**	2.344	1.675	107.4	116.1	0.123	−0.721	0.335
	2b	2.333	1.686	109.7	117.6	0.081	−0.721	0.329
M06-2X	**2a**	2.328	1.668	106.8	116.7	0.121	−0.765	0.362
	2b	2.331	1.684	109.5	117.7	0.085	−0.745	0.334
MP2	**2a**	2.333	1.683	106.5	116.1	0.354	−0.906	0.468
	2b	2.329	1.716	106.2	115	0.423	−0.878	0.335

Table 1.3. Computed bond lengths (Å), bond angles (°) and atomic Mulliken charges (e) of disilanol (**2a**) and HO–Si*–SiH_3 (**2b**) in Figure 1.2 using various methods and 6-31G(d) basis set. For MP2, the Mulliken charges were performed at the HF level of theory. Here, Si* represents a divalent pseudoatom.

X	Bond	AE	Si*	Diff
CH_3	Si–Si*	2.355	2.351	0.004
	Si*– Si^1	2.358	2.365	–0.007
	Si^1–C	1.897	1.887	0.010
NH_2	Si–Si*	2.354	2.349	0.005
	Si*– Si^1	2.369	2.384	–0.015
	Si^1–N	1.745	1.733	0.012
OH	Si–Si*	2.353	2.355	–0.002
	Si*– Si^1	2.348	2.341	0.007
	Si^1–O	1.677	1.669	0.008
SiH_3	Si–Si*	2.354	2.352	0.002
	Si*– Si^1	2.358	2.354	0.004
	Si^1–Si	2.354	2.354	0.000
PH_2	Si–Si*	2.354	2.355	–0.001
	Si*– Si^1	2.357	2.353	0.004
	Si^1–P	2.287	2.283	0.004
SH	Si–Si*	2.354	2.358	–0.004
	Si*– Si^1	2.354	2.340	0.014
	Si^1–S	2.174	2.169	0.005
Cl	Si–Si*	2.354	2.360	–0.006
	Si*– Si^1	2.353	2.337	0.016
	Si^1–Cl	2.095	2.086	0.009
			MAD	0.007
			MAX	0.016

Table 1.4. Computed bond lengths (Å) of SiH_3–SiH_2–Si^1H_2X (AE) and SiH_3–Si*–Si^1H_2X (Si*) at the B3LYP/6-31G(d) level. Here, X represents eight different groups (see the table). Si* represents a divalent pseudo-silicon atom. MAD and MAX are mean absolute deviation and maximum deviation, respectively.

X	Angle	AE	Si*	Diff
CH_3	Si–Si*– Si^1	113.4	114.4	–1.0
	Si*– Si^1–C	112.6	113.1	–0.5
NH_2	Si–Si*– Si^1	112.7	113.8	–1.1
	Si*– Si^1–N	116.9	118.7	–1.8
OH	Si–Si*– Si^1	111.3	112.8	–1.5
	Si*– Si^1–O	105.9	108.0	–2.1
SiH_3	Si–Si*– Si^1	113.0	115.0	–2.0
	Si*– Si^1–Si	113.0	110.7	2.3
PH_2	Si–Si*– Si^1	113.6	114.0	–0.4
	Si*– Si^1–P	110.7	111.5	–0.8
SH	Si–Si*– Si^1	113.6	113.4	0.2
	Si*– Si^1–S	107.7	108.9	–1.2
Cl	Si–Si*– Si^1	113.3	108.2	5.1
	Si*– Si^1–Cl	110.3	113.3	–3.0
			MAD	1.6
			MAX	5.1

Table 1.5. Computed bond angles (°) of SiH_3–SiH_2–Si^1H_2X (AE) and SiH_3–Si*–Si^1H_2X (Si*) at the B3LYP/6-31G(d) level. Here, X represents eight different groups (see the table). Si* represents a divalent pseudo-silicon atom. MAD and MAX are mean absolute deviation and maximum deviation, respectively.

X	Charge	AE	Si*	Diff
CH_3	q(Si*)	−0.060	−0.041	−0.019
	q(Si^1)	0.330	0.273	0.057
NH_2	q(Si*)	−0.102	−0.072	−0.030
	q(Si^1)	0.456	0.377	0.079
	q(N)	−0.855	−0.842	−0.013
OH	q(Si*)	−0.083	−0.051	−0.032
	q(Si^1)	0.546	0.477	0.069
	q(O)	−0.723	−0.709	−0.014
SiH_3	q(Si*)	−0.021	−0.015	−0.006
	q(Si^1)	0.073	0.039	0.034
	q(Si)	0.175	0.191	−0.016
PH_2	q(Si*)	−0.024	−0.015	−0.009
	q(Si^1)	0.165	0.121	0.044
	q(P)	−0.131	−0.120	−0.011
SH	q(Si*)	−0.021	−0.008	−0.013
	q(Si^1)	0.252	0.200	0.052
	q(S)	−0.290	−0.268	−0.022
Cl	q(Si*)	−0.030	−0.036	0.006
	q(Si^1)	0.346	0.290	0.056
	q(Cl)	−0.273	−0.251	−0.022
			MAD	0.029
			MAX	0.079

Table 1.6. Computed atomic Mulliken charges (*e*) of SiH_3−SiH_2−Si^1H_2X (AE) and SiH_3−Si*−Si^1H_2X (Si*) at the B3LYP/6-31G(d) level. Here, X represents eight different groups (see the table). Si* represents a divalent pseudo-silicon atom. MAD and MAX are mean absolute deviation and maximum deviation, respectively.

Table 1.5 presents the performance for replacing SiH_3–SiH_2–X with SiH_3–Si*–X, i.e., where the divalent pseudoatoms are directly bonding to heteroatoms. The results contain larger errors, but that is to be expected because the pseudoatom has to create bonds for a much more diverse set of chemical environments. Mean absolute deviations of bond lengths, bond angles, and Mulliken charges are 0.012 Å, 3.0º, and 0.045*e*, with maximum deviations of 0.047 Å, 6.7º, and 0.128*e*. The largest bond length error occurs for the Si*–C bond. The largest angle error occurs for Si–Si*–N. The largest error in the atomic charge occurs for X=Cl. Overall, the results are acceptable even in such heteroatomic bonds, though larger errors occur in a few cases.

We have mentioned earlier that one of our primary goals is to apply pseudoatoms to solid-state calculations using periodic boundary conditions (PBC). Since PBC calculations with hybrid functionals such as B3LYP are prohibitively expensive, we test how the pseudoatom performs with the BLYP, PBE, and M06-L functionals. Structures considered to represent the H-terminated 2×1 reconstructed Si(100) surface are shown in Figure 1.2. Table 1.6 contains geometrical parameters for optimized structures of periodic silicon surfaces. The surface slab contains one Si–Si dimer

per unit cell terminated with hydrogen atoms. However, using this simple model, a significant problem arises from the capping hydrogen atoms in the lowest layer of the cluster model. The errors originate from the same silicon atom being replaced by two different H-atoms. Such pairs of hydrogen atoms point towards each other in the lowest layer of the slab model, resulting in neighboring hydrogen atoms being closer than the sum of their van der Waals radii. As a result, the ideal, symmetric structure is an unstable saddle point. This leads to an optimized structure yielding a completely unphysical geometry is shown in Figure 1.2. While the structure of the surface Si–Si dimers on the top layer are reproduced fairly well, significant rearrangement of the capping hydrogen atoms are observed in the bottom layers. The capping hydrogen atoms pucker to minimize the repulsive interatomic interactions. Thus, H-capping can cause serious problems for optimizations of the periodic Si(100) surfaces. If the truncation is extended one more layer, the same problem appears in the perpendicular direction, and thus is unavoidable. To circumvent this problem, most periodic calculations use dimerized surface layers at the top and bottom, requiring a fairly large number of intermediate layers to dampen the strain field.

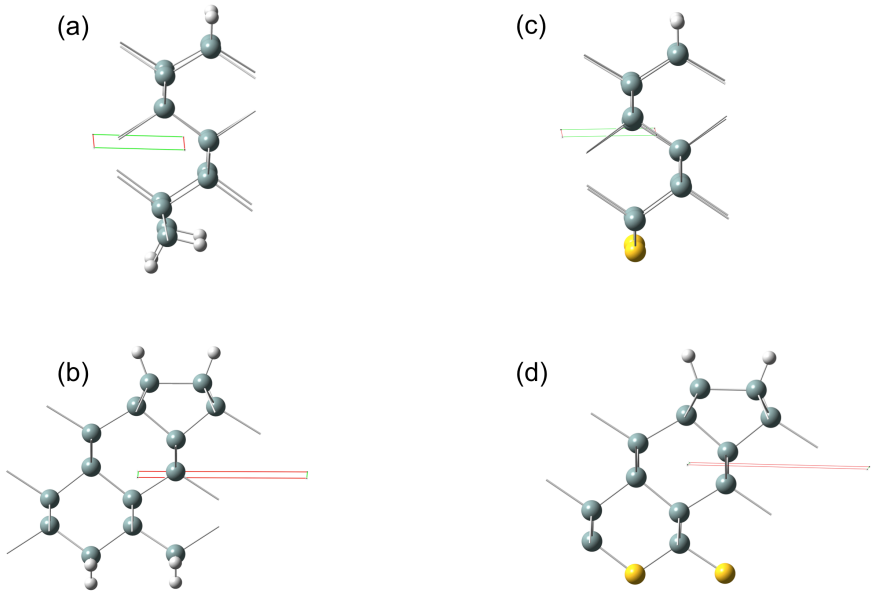

Figure 1.2. Two dimensional PBC optimizations of cluster models representing the hydrogen terminated Si(100) surface. Unphysical distorted structures are obtained from hydrogen link atom truncation in (a) and (b). A physically reasonable symmetric structure is obtained when divalent pseudoatoms are used for capping, as shown in (c) and (d). The perspective of (a) and (c) displays the unit cells from along the surface dimer. The unit cells shown are shown directly towards the direction of the dimer in (b) and (d).

X	Bond	AE	Si*	Diff
CH_3	Si–Si*	2.353	2.337	0.016
	Si*–C	1.897	1.944	−0.047
NH_2	Si–Si*	2.364	2.341	0.023
	Si*–N	1.747	1.736	0.011
OH	Si–Si*	2.344	2.333	0.011
	Si*–O	1.675	1.686	−0.011
SiH_3	Si–Si*	2.354	2.353	0.001
PH_2	Si–Si*	2.351	2.351	0.000
	Si*–P	2.306	2.286	0.020
SH	Si–Si*	2.350	2.350	0.000
	Si*–S	2.173	2.159	0.014
Cl	Si–Si*	2.350	2.343	0.007
	Si*–Cl	2.093	2.094	−0.001
			MAD	0.012
			MAX	0.047

Table 1.7. Computed bond lengths (Å) of SiH_3–SiH_2–X (AE) and SiH_3–Si*–X (Si*) at the B3LYP/6-31G(d) level. Here, X represents eight different groups (see the table). Si* represents a divalent pseudo-silicon atom. MAD and MAX are mean absolute deviation and maximum deviation, respectively.

X	Angle	AE	Si*	Diff
CH_3	Si–Si*–C	112.5	108.7	3.8
	Si*–C–H	110.6	109.5	1.1
NH_2	Si–Si*–N	117.0	110.3	6.7
	Si*–N–H	118.1	123.7	−5.6
OH	Si–Si*–O	107.3	109.7	−2.4
	Si*–O–H	116.2	117.6	−1.4
SiH_3	Si–Si*–Si	112.9	114.0	−1.1
	Si*–Si–H	110.9	108.9	2.0
PH_2	Si–Si*–P	110.7	107.8	2.9
	Si*–P–H	95.0	99.6	−4.6
SH	Si–Si*–S	107.7	111.2	−3.5
	Si*–S–H	96.7	101.0	−4.3
Cl	Si–Si*–Cl	110.2	110.0	0.2
			MAD	3.0
			MAX	6.7

Table 1.8. Computed bond angles (°) of SiH_3–SiH_2–X (AE) and SiH_3–Si*–X (Si*) at the B3LYP/6-31G(d) level. Here, X represents eight different groups (see the table). Si* represents a divalent pseudo-silicon atom. MAD and MAX are mean absolute deviation and maximum deviation, respectively.

X	Charge	AE	Si*	Diff
CH_3	q(Si*)	0.176	0.148	0.028
	q(Si)	0.136	0.103	0.033
	q(C)	−0.655	−0.710	0.055
NH_2	q(Si*)	0.291	0.240	0.051
	q(Si)	0.093	0.080	0.013
	q(N)	−0.854	−0.878	0.024
OH	q(Si*)	0.370	0.329	0.041
	q(Si)	0.123	0.081	0.042
	q(O)	−0.722	−0.721	−0.001
SiH_3	q(Si*)	−0.038	−0.029	−0.009
	q(Si)	0.177	0.147	0.030
PH_2	q(Si*)	0.059	0.012	0.047
	q(Si)	0.183	0.139	0.044
	q(P)	−0.147	−0.115	−0.032
SH	q(Si*)	0.137	0.074	0.063
	q(Si)	0.176	0.133	0.043
	q(S)	−0.288	−0.207	−0.081
Cl	q(Si*)	0.238	0.131	0.107
	q(Si)	0.170	0.133	0.037
	q(Cl)	−0.271	−0.143	−0.128
			MAD	0.045
			MAX	0.128

Table 1.9. Computed atomic Mulliken charges (e) of SiH_3–SiH_2–X (AE) and SiH_3–Si*–X (Si*) at the B3LYP/6-31G(d) level. Here, X represents eight different groups (see the table). Si* represents a divalent pseudo-silicon atom. MAD and MAX are mean absolute deviation and maximum deviation, respectively.

As an alternative, divalent pseudoatoms can be used to replace the SiH_2 groups at the bottom of the surface unit cell. PBC optimization then leads to a regular surface structure, shown in Figure 1.2. The geometric parameters listed in Table 1.6 for the three chosen functionals suggest these models are appropriate for use with our divalent psuedoatoms. This is a unique example that shows how a divalent pseudoatom adequately solves an important problem involving PBC optimization of the Si(100) surface.

Silicon clusters of the Si(100) surface were also truncated to determine the divalent pseudoatom's performance with B3LYP for larger molecular systems. We start with a $Si_{62}H_{52}$ cluster model containing 6 Si–Si dimers (Figure 1.3, top) that is 7 layers deep to avoid the unphysical interactions between hydrogen atoms. We have used pseudoatoms to truncate the cluster at the 4^{th} atomic layer (Figure 1.3, bottom). The dimers on the surface of the Si(100) cluster are insensitive to the truncation employing our divalent pseudoatom, as the dimer bond lengths, dimer Si–H bond lengths, and Si–Si–H bond angles have changed very little compared to the complete $Si_{62}H_{52}$ cluster. This makes the cluster suitable for molecular truncation of clusters, as the geometrical parameters are described well for use with surface reactivity studies, while being computationally efficient. The number of basis functions is

decreased by 315 basis functions from using divalent pseudoatoms in the 4th atomic layer of the cluster.

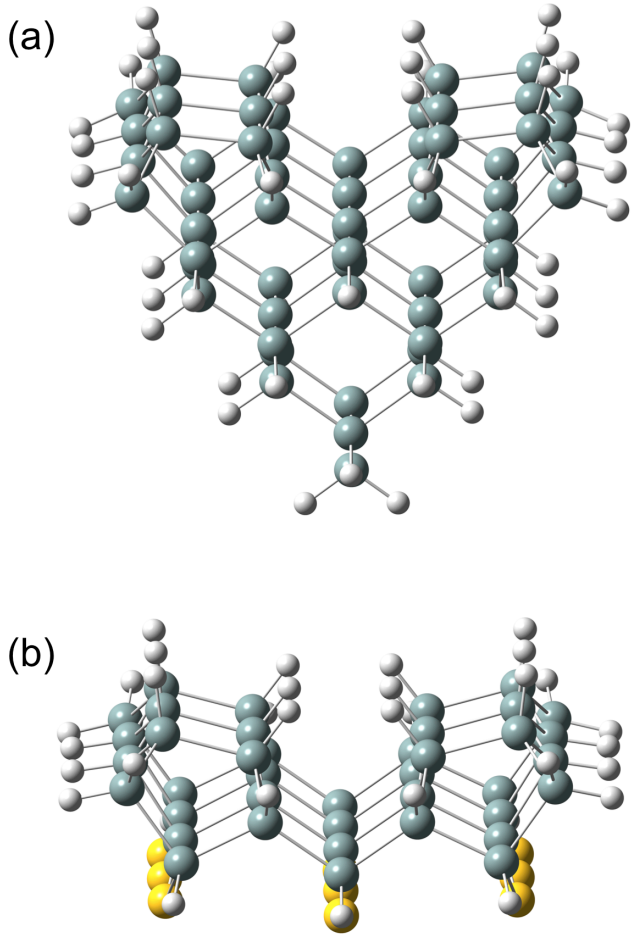

Figure 1.3. Hydrogen terminated Si(100) surface clusters containing six Si–Si dimers. The stoichiometry of the full cluster is $Si_{62}H_{52}$. 3(a) and 3(b) depict the full cluster and truncated cluster at the 4th layer, respectively, at the B3LYP/6-31G(d) level of theory.

Parameter	Si-Si Dimer	1^{st}-2^{nd} Layer Si-Si	2^{nd}-3^{rd} Layer Si-Si
BLYP Si* Truncated	2.445	2.407	2.393
BLYP H Truncated	2.447	2.412	2.393
Absolute Deviation	0.002	0.005	0.000
M06-L Si* Truncated	2.394	2.354	2.342
M06-L H Truncated	2.396	2.359	2.342
Absolute Deviation	0.002	0.005	0.000
PBE Si* Truncated	2.419	2.379	2.370
PBE H Truncated	2.419	2.384	2.369
Absolute Deviation	0.000	0.005	0.001

Table 1.10. Computed bond lengths (Å) of 7-layer Si(100) slabs using BLYP, M06-L, and PBE with the 6-31G(d) basis set. Here, Si* represents a divalent pseudoatom.

To demonstrate that the divalent pseudoatom is robust for truncation of cluster and does not affect chemical processes on the surfaces of Si clusters, reactivity studies were performed on Si*

truncated clusters. We have studied two small adsorbate reactions, dissociation of water, and hydrogenation of a surface dimer, on Si_9H_{12} clusters, and with an equivalent Si* truncated cluster where the divalent pseudoatom is attached to the 3rd atomic layer. The first reaction on this cluster model is the dissociation of water[24] using B3LYP/6-31G(d). In Figures 1.4 and 1.5, the reaction energy profile and the individual structures and energies along the reaction pathway are shown. There are negligible differences in the transition state barrier height (0.1 kcal/mol) and relative energies of the products (0.6 kcal/mol). Overall, negligible changes occurred to the geometries and energies of reaction pathways compared to the standard Si_9H_{12} cluster model with the same model chemistry.

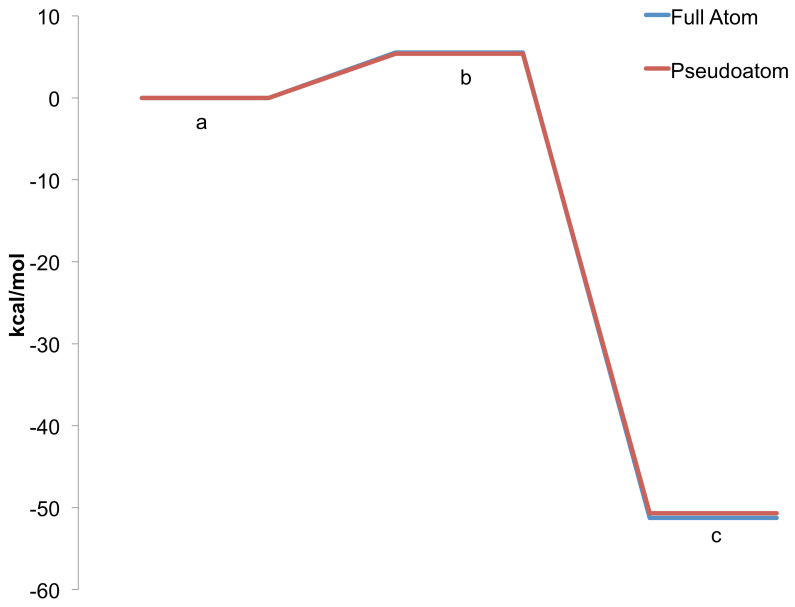

Figure 1.4. The reaction energy profile for dissociation of water on a Si_9H_{12} cluster and equivalent pseudoatom truncated cluster.

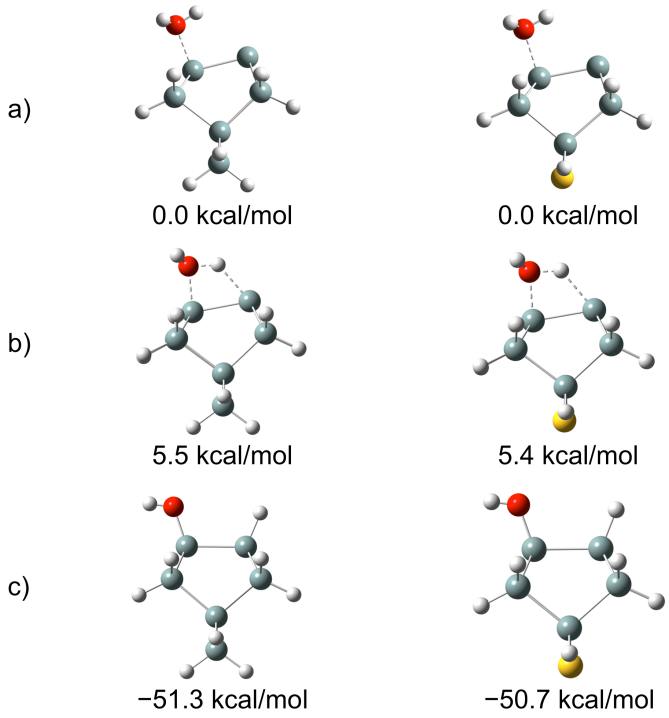

Figure 1.5. The full atom structures, pseudoatom structures and relative energies corresponding to the water dissociation pathway presented in Figure 1.6.

The second reaction studied is the hydrogenation of the silicon dimer by molecular hydrogen[25] and subsequent monohydride and dihydride species formation on the Si_9H_{12} cluster using B3LYP/6-31G(d). The relative energies in the reaction pathway are shown in Figure 1.6. In Figure 1.7, the structures and relative energies of the reactants, transition states, and products

are reported. All relative energy differences between the two cluster models were within 1.4 kcal/mol. The structural parameters and energies are in agreement between the standard Si_9H_{12} model and the truncated pseudoatom model with the same model chemistry, despite the breaking of the dimer Si–Si bond during the dihydride formation.

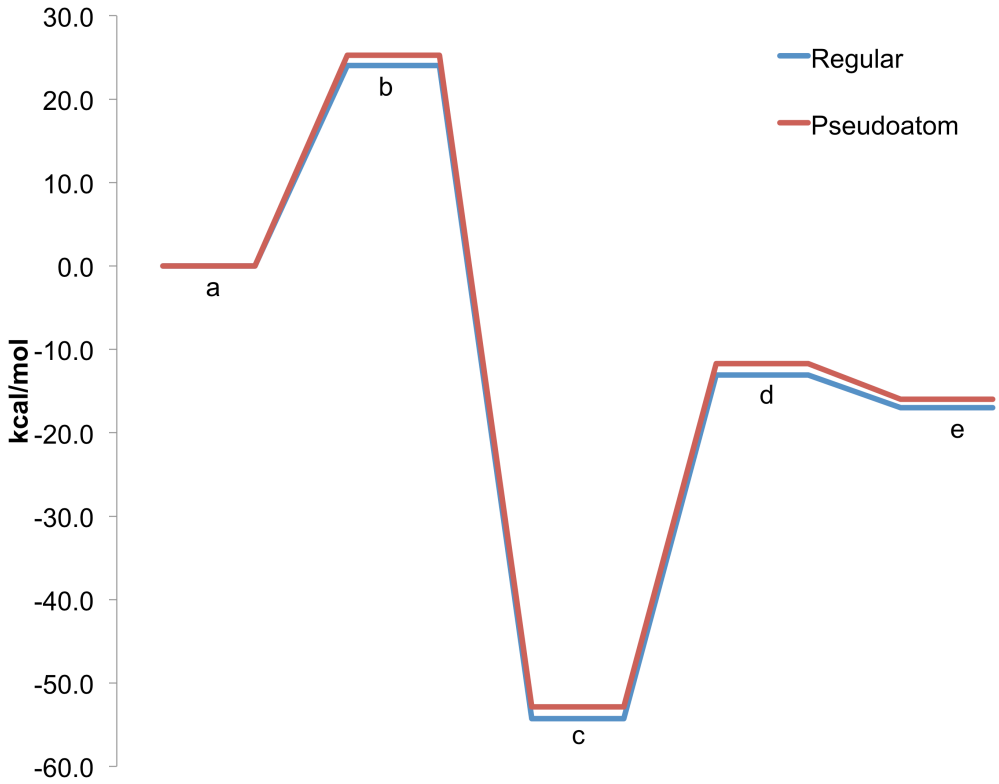

Figure 1.6. The reaction energy profile for the hydrogenation and subsequent formation of monohydride and dihydride species on a Si_9H_{12} cluster and equivalent pseudoatom truncated cluster.

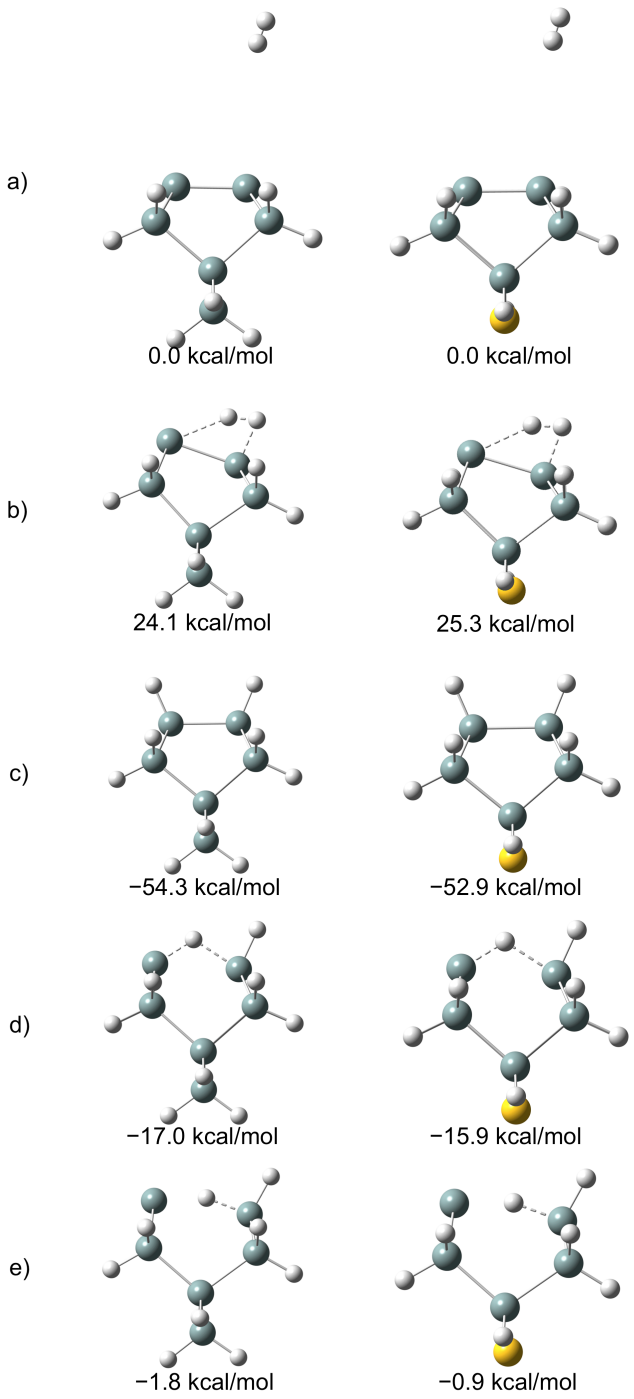

Figure 1.7. The full atom structures, pseudoatom structures and relative energies corresponding to the hydrogenation and subsequent formation of monohydride and dihydride species pathway presented in Figure 1.6.

1.6. Conclusions

In summary, the design-atom approach has been extended to divalent silicon, making it applicable to important problems related to Si(100) surface chemistry. The ECP parameters of our design-atoms are obtained by fitting to information on both Si–Si and Si–O bonds. Thus, we have attempted to derive a single set of parameters that are applicable for both systems and for a range of other bonding situations. This has been reasonably successful and thus we call our design-atom a divalent *pseudoatom*. We demonstrated their applications on building efficient cluster models for the Si(100) surface and illustrated their importance in describing surface chemical reactions.

Although the divalent silicon pseudoatom developed here performs reasonably well for small molecules and surface cluster models, they have some deficiencies. They have a tendency to yield larger errors with structures containing electronegative groups near a pseudoatom. The transferability of the pseudoatom is also important. In our investigations, we found that the pseudoatoms can be used with the B3LYP functional, M06-2X functional and MP2 for cluster calculations. For slab models, the BLYP functional, M06-L functional, and PBE functional can be used with slab calculations.

However, the transferability with respect to basis set has not been explored. At this point, if we desire to use different basis sets, for example 3-21G, to treat the valence electrons of the pseudoatom, the effective core parameters need to be refitted. Future work will focus on making pseudoatoms less basis set dependent, more transferable, and more widely applicable.

1.7. References

1. Boeyens, J. C. A.; Comba, P., Molecular mechanics: theoretical basis, rules, scope and limits. *Coordination Chemistry Reviews* **2001,** *212* (1), 3-10.

2. Dewar, M. J. S.; Zoebisch, E. G.; Healy, E. F.; Stewart, J. J. P., Development and use of quantum mechanical molecular models. 76. AM1: a new general purpose quantum mechanical molecular model. *J. Am. Chem. Soc.* **1985,** *107* (13), 3902-3909.

3. Stewart, J. P., Optimization of parameters for semiempirical methods V: Modification of NDDO approximations and application to 70 elements. *J. Mol. Model.* **2007,** *13* (12), 1173-1213.

4. (a) Humbel, S.; Sieber, S.; Morokuma, K., The IMOMO method: Integration of different levels of molecular orbital approximations for geometry optimization of large systems: Test for n-butane conformation and S_N2 reaction: $RCl+Cl^-$ *J. Chem. Phys.* **1996,** *105* (5), 1959-1967; (b) Parandekar, P. V.; Hratchian, H. P.; Raghavachari, K., Applications and assessment of QM:QM electronic embedding using generalized asymmetric Mulliken atomic charges. *J. Chem. Phys.* **2008,** *129* (14), 145101-10.

5. (a) Maseras, F.; Morokuma, K., IMOMM: A new integrated ab initio + molecular mechanics geometry optimization scheme of

equilibrium structures and transition states. *J. Comput. Chem.* **1995,** *16* (9), 1170-1179; (b) Kairys, V.; Jensen, J. H., QM/MM Boundaries Across Covalent Bonds: A Frozen Localized Molecular Orbital-Based Approach for the Effective Fragment Potential Method. *J. Phys. Chem. A* **2000,** *104* (28), 6656-6665; (c) Warshel, A.; Levitt, M., Theoretical studies of enzymic reactions: Dielectric, electrostatic and steric stabilization of the carbonium ion in the reaction of lysozyme. *Journal of Molecular Biology* **1976,** *103* (2), 227-249.

6. (a) Svensson, M.; Humbel, S.; Froese, R. D. J.; Matsubara, T.; Sieber, S.; Morokuma, K., ONIOM: A Multilayered Integrated MO + MM Method for Geometry Optimizations and Single Point Energy Predictions. A Test for Diels–Alder Reactions and $Pt(P(t\text{-}Bu)_3)_2 + H_2$ Oxidative Addition. *J. Phys. Chem.* **1996,** *100* (50), 19357-19363; (b) Vreven, T.; Byun, K. S.; Komáromi, I.; Dapprich, S.; Montgomery, J. A.; Morokuma, K.; Frisch, M. J., Combining Quantum Mechanics Methods with Molecular Mechanics Methods in ONIOM. *J. Chem. Theory and Comput.* **2006,** *2* (3), 815-826; (c) Vreven, T.; Morokuma, K.; Farkas, Ö.; Schlegel, H. B.; Frisch, M. J., Geometry optimization with QM/MM, ONIOM, and other combined methods. I. Microiterations and constraints. *J. Comput. Chem.* **2003,** *24* (6), 760-769.

7. Halls, M. D.; Raghavachari, K., Importance of Steric Effects in Cluster Models of Silicon Surface Chemistry: ONIOM Studies of the

Atomic Layer Deposition (ALD) of Al_2O_3 on H/Si(111). *J. Phys. Chem. A* **2004,** *108* (15), 2982-2987.

8. (a) Gao, J.; Amara, P.; Alhambra, C.; Field, M. J., A Generalized Hybrid Orbital (GHO) Method for the Treatment of Boundary Atoms in Combined QM/MM Calculations. *J. Phys. Chem. A* **1998,** *102* (24), 4714-4721; (b) Murphy, R. B.; Philipp, D. M.; Friesner, R. A., A mixed quantum mechanics/molecular mechanics (QM/MM) method for large-scale modeling of chemistry in protein environments. *J. Comput. Chem.* **2000,** *21* (16), 1442-1457.

9. (a) Zhang, Y.; Lee, T.-S.; Yang, W., A pseudobond approach to combining quantum mechanical and molecular mechanical methods. *J. Chem. Phys.* **1999,** *110* (1), 46-54; (b) Wang, B.; Truhlar, D. G., Geometry optimization using tuned and balanced redistributed charge schemes for combined quantum mechanical and molecular mechanical calculations. *PCCP* **2011,** *13* (22), 10556-10564; (c) Wang, B.; Truhlar, D. G., Combined Quantum Mechanical and Molecular Mechanical Methods for Calculating Potential Energy Surfaces: Tuned and Balanced Redistributed-Charge Algorithm. *J. Chem. Theory and Comput.* **2010,** *6* (2), 359-369; (d) Taylor, D. E.; Bunte, S. W.; Runge, K., A Pseudoatom Approach to Molecular Truncation: Application in ab Initio MBPT Methods. *J. Phys. Chem. A* **2006,** *110* (19), 6279-6284; (e) Poteau, R.; Ortega, I.; Alary, F.; Solis, A. R.; Barthelat, J.-C.; Daudey, J.-P., Effective Group Potentials. 1. Method. *J. Phys. Chem. A* **2000,** *105* (1), 198-205; (f) Lewin, J. L.; Cramer, C. J., Modified Carbon Pseudopotential for Use in ONIOM

Calculations of Alkyl-Substituted Metallocenes. *J. Phys. Chem. A* **2008,** *112* (50), 12754-12760; (g) DiLabio, G. A.; Hurley, M. M.; Christiansen, P. A., Simple one-electron quantum capping potentials for use in hybrid QM/MM studies of biological molecules. *J. Chem. Phys.* **2002,** *116* (22), 9578-9584.

10. (a) Zhang, Y., Improved pseudobonds for combined ab initio quantum mechanical/molecular mechanical methods. *J. Chem. Phys.* **2005,** *122* (2), 024114-7; (b) Zhang, Y., Pseudobond ab initio QM/MM approach and its applications to enzyme reactions. *Theor. Chem. Acc.* **2006,** *116* (1-3), 43-50; (c) Xiao, C.; Zhang, Y., Design-atom approach for the quantum mechanical/molecular mechanical covalent boundary: A design-carbon atom with five valence electrons. *J. Chem. Phys.* **2007,** *127* (12), 124102-9; (d) Parks, J. M.; Hu, H.; Cohen, A. J.; Yang, W., A pseudobond parametrization for improved electrostatics in quantum mechanical/molecular mechanical simulations of enzymes. *J. Chem. Phys.* **2008,** *129* (15), 154106-6; (e) DiLabio, G. A.; Dogel, S. A.; Wolkow, R. A., A simple and accurate approach for calculating the vibration spectra of molecules on surfaces: Comparisons to high resolution electron energy loss data for ethylene on silicon. *Surf. Sci.* **2006,** *600* (16), L209-L213; (f) DiLabio, G. A.; Wolkow, R. A.; Johnson, E. R., Efficient silicon surface and cluster modeling using quantum capping potentials. *J. Chem. Phys.* **2005,** *122* (4), 044708-5; (g) Ohnishi, Y.-y.; Nakao, Y.; Sato, H.; Sakaki, S., Frontier Orbital Consistent Quantum Capping Potential (FOC-QCP) for Bulky Ligand of Transition Metal Complexes. *J. Phys. Chem. A* **2008,** *112* (9), 1946-1955; (h) Jardillier,

N.; Goursot, A., One-electron quantum capping potential for hybrid QM/MM studies of silicate molecules and solids. *Chem. Phys. Lett.* **2008,** *454* (1–3), 65-69; (i) Poteau, R.; Alary, F.; Abou El Makarim, H.; Heully, J.-L.; Barthelat, J.-C.; Daudey, J.-P., Effective Group Potentials. 2. Extraction and Transferability for Chemical Groups Involved in Covalent or Donor–Acceptor Bonds. *J. Phys. Chem. A* **2000,** *105* (1), 206-214; (j) Chaudret, R.; Parks, J. M.; Yang, W., Pseudobond parameters for QM/MM studies involving nucleosides, nucleotides, and their analogs. *J. Chem. Phys.* **2013,** *138* (4), 045102-7.

11. (a) Assfeld, X.; Rivail, J.-L., Quantum chemical computations on parts of large molecules: the ab initio local self consistent field method. *Chem. Phys. Lett.* **1996,** *263* (1–2), 100-106; (b) Monard, G.; Loos, M.; Théry, V.; Baka, K.; Rivail, J.-L., Hybrid classical quantum force field for modeling very large molecules. *International Journal of Quantum Chemistry* **1996,** *58* (2), 153-159; (c) Théry, V.; Rinaldi, D.; Rivail, J.-L.; Maigret, B.; Ferenczy, G. G., Quantum mechanical computations on very large molecular systems: The local self-consistent field method. *J. Comput. Chem.* **1994,** *15* (3), 269-282.

12. Philipp, D. M.; Friesner, R. A., Mixed ab initio QM/MM modeling using frozen orbitals and tests with alanine dipeptide and tetrapeptide. *J. Comput. Chem.* **1999,** *20* (14), 1468-1494.

13. Dolg, M.; Wedig, U.; Stoll, H.; Preuss, H., Energy-adjusted ab initio pseudopotentials for the first row transition elements. *J. Chem. Phys.* **1987,** *86* (2), 866.

14. (a) Becke, A. D., Density-functional exchange-energy approximation with correct asymptotic behavior. *Phys. Rev. A* **1988,** *38* (6), 3098-3100; (b) Becke, A. D., Density-functional thermochemistry. III. The role of exact exchange. *J. Chem. Phys.* **1993,** *98* (7), 5648-5652; (c) Lee, C.; Yang, W.; Parr, R. G., Development of the Colle-Salvetti correlation-energy formula into a functional of the electron density. *Phys. Rev. B* **1988,** *37* (2), 785-789; (d) Francl, M. M.; Pietro, W. J.; Hehre, W. J.; Binkley, J. S.; Gordon, M. S.; DeFrees, D. J.; Pople, J. A., Self-consistent molecular orbital methods. XXIII. A polarization-type basis set for second-row elements. *J. Chem. Phys.* **1982,** *77* (7), 3654-3665; (e) Hariharan, P. C.; Pople, J. A., The influence of polarization functions on molecular orbital hydrogenation energies. *Theoretica chimica acta* **1973,** *28* (3), 213-222; (f) Krishnan, R.; Binkley, J. S.; Seeger, R.; Pople, J. A., Self-consistent molecular orbital methods. XX. A basis set for correlated wave functions. *J. Chem. Phys.* **1980,** *72* (1), 650.

15. Eaton, J. W.; Bateman, D.; Hauberg, S., *GNU Octave Manual Version 3*. Network Theory Limited: 2008.

16. Møller, C.; Plesset, M. S., Note on an Approximation Treatment for Many-Electron Systems. *Physical Review* **1934,** *46* (7), 618-622.

17. Zhao, Y.; Truhlar, D. G., The M06 suite of density functionals for main group thermochemistry, thermochemical kinetics, noncovalent interactions, excited states, and transition elements: two new functionals and systematic testing of four M06-class functionals and 12 other functionals. *Theor. Chem. Acc.* **2007,** *120* (1-3), 215-241.

18. Perdew, J. P.; Burke, K.; Ernzerhof, M., Generalized Gradient Approximation Made Simple [Phys. Rev. Lett. 77, 3865 (1996)]. *Phys. Rev. Lett.* **1997,** *78* (7), 1396-1396.

19. Zhao, Y.; Truhlar, D. G., A new local density functional for main-group thermochemistry, transition metal bonding, thermochemical kinetics, and noncovalent interactions. *J. Chem. Phys.* **2006,** *125* (19), 194101-18.

20. Miehlich, B.; Savin, A.; Stoll, H.; Preuss, H., Results obtained with the correlation energy density functionals of Becke and Lee, Yang and Parr. *Chem. Phys. Lett.* **1989,** *157* (3), 200-206.

21. Frisch, M. J.; Trucks, G. W.; Schlegel, H. B.; Scuseria, G. E.; Robb, M. A.; Cheeseman, J. R.; Scalmani, G.; Barone, V.; Mennucci, B.; Petersson, G. A.; Nakatsuji, H.; Caricato, M.; Li, X.; Hratchian, H. P.; Izmaylov, A. F.; Bloino, J.; Zheng, G.; Sonnenberg, J. L.; Hada, M.; Ehara, M.; Toyota, K.; Fukuda, R.; Hasegawa, J.; Ishida, M.; Nakajima, T.; Honda, Y.; Kitao, O.; Nakai, H.; Vreven, T.; Montgomery, J. A.; Peralta, J. E.; Ogliaro, F.; Bearpark, M.; Heyd, J. J.; Brothers, E.; Kudin,

K. N.; Staroverov, V. N.; Kobayashi, R.; Normand, J.; Raghavachari, K.; Rendell, A.; Burant, J. C.; Iyengar, S. S.; Tomasi, J.; Cossi, M.; Rega, N.; Millam, J. M.; Klene, M.; Knox, J. E.; Cross, J. B.; Bakken, V.; Adamo, C.; Jaramillo, J.; Gomperts, R.; Stratmann, R. E.; Yazyev, O.; Austin, A. J.; Cammi, R.; Pomelli, C.; Ochterski, J. W.; Martin, R. L.; Morokuma, K.; Zakrzewski, V. G.; Voth, G. A.; Salvador, P.; Dannenberg, J. J.; Dapprich, S.; Daniels, A. D.; Farkas; Foresman, J. B.; Ortiz, J. V.; Cioslowski, J.; Fox, D. J. *Gaussian 09, Revision C.01*, Wallingford CT, 2009.

22. Igel-Mann, G.; Stoll, H.; Preuss, H., Pseudopotentials for main group elements (IIIa through VIIa). *Mol. Phys.* **1988,** *65* (6), 1321-1328.

23. Mulliken, R. S., Electronic Population Analysis on LCAOMO Molecular Wave Functions. I. *J. Chem. Phys.* **1955,** *23* (10), 1833.

24. Konecny, R.; Doren, D. J., Adsorption of water on Si(100)-(2 x 1): A study with density functional theory. *J. Chem. Phys.* **1997,** *106* (6), 2426-2435.

25. (a) Wu, C. J.; Ionova, I. V.; Carter, E. A., Ab initio H2 desorption pathways for H/Si(100): the role of SiH2(a). *Surf. Sci.* **1993,** *295* (1–2), 64-78; (b) Jing, Z.; Whitten, J. L., Pathway of H_{2} desorption from dihydride Si(100). *Phys. Rev. B* **1993,** *48* (23), 17296-17300; (c) Vittadini, A.; Selloni, A., Density functional study

of H2 desorption from monohydride and dihydride Si(100) surfaces. *Chem. Phys. Lett.* **1995,** *235* (3–4), 334-340.

Chapter Two

Modeling Non-Periodic Adsorption on Periodic Surfaces: A Composite Energy Approach for Low-Coverage Limits

2.1. Introduction

The study of adsorbate/surface interactions is of fundamental importance in materials science. Such interactions determine many key aspects of surface-reactivity such as the binding site, adsorption geometry, and coverage dependence. Understanding and modeling such phenomena can therefore greatly help aid in the design of useful materials that could be influential across the fields of surface science, catalysis, nanotechnology and the semiconductor industry.[1]

There are two common approaches to the theoretical study of the structures and properties of adsorbate/surface interactions. In the *slab approach*, periodic boundary conditions (PBC) are imposed to perform calculations on the extended surface with full periodicity, typically using density functional techniques. It yields an accurate representation of the entire surface structure without any boundary effects, and provides an excellent description of problems such as surface reconstructions.[2] In the case of

adsorbate/surface interactions, the adsorbate will be included in the unit cell, providing an accurate description of surfaces with complete monolayer coverage. However, the description of lower adsorbate coverages may result in potential problems since significant unphysical adsorbate/adsorbate interactions (that are inherently present due to the required replication of the unit cells) may be present unless large unit cells are chosen.

In the alternative *cluster approach*, quantum chemical calculations are performed on a cluster representing the local region of interest in the surface under investigation.[3] The cluster approach is suitable for describing the local structure around an adsorbate and for investigating problems such as defects on surfaces. However, the cluster approach introduces inherent errors due to truncation effects, boundary effects resulting from the loss of symmetry, and unphysical geometrical distortions unless constraints are imposed. It is perhaps most suited for an isolated adsorbate but can have deficiencies for adsorbate/surface interactions at higher coverages.[4]

Stability of silicon surfaces is a key factor in many electronic and semiconductor applications. In order to bring kinetic and thermodynamic stability to the surface, functional groups can be

utilized. In particular, hydrogen passivated Si(111) surfaces[5] can be modified by functionalization reactions to yield alkyl terminated surfaces.[6] Such organic functional groups on the Si(111) surface provide stability since the relatively strong Si–C bond is resilient to further chemical modification due to its inherently low polarity.[7] Similarly, diamond surfaces have been known for their exceptional structural hardness, thermal conductivity, and chemical inertness.[8] Many of the same ideas on silicon surface chemistry can be considered on diamond surfaces as well.[9]

In this chapter, we develop a broadly applicable composite approach that has the full advantage of a PBC treatment but can be applied to model a local adsorbate in the low coverage regime. The proposed method uses an extrapolated energy expression to cancel the adsorbate/adsorbate interactions while still including the influence of the periodic surface on a single adsorbate. We apply the method to investigate adsorbates on Si(111) and C(111) surfaces to illustrate the effectiveness of the new approach.

2.2. Method

The typical PBC calculation of an adsorption process involves an initial selection of an appropriate unit cell with which the

adsorbate molecule interacts. The geometry of the composite adsorbate/surface system is then optimized via energy minimization (assuming one adsorbate per unit cell). Density functional theory is normally employed in such PBC calculations though hybrid methods such as MP2:DFT can also be used.[10] The adsorption energy is then computed as Equation 2.1,

$$\Delta E_{int} = E^*_{ads/sur} - E^*_{sur} - E_{ads} \quad (2.1)$$

where $E^*_{ads/sur}$ is the energy of the combined adsorbate/surface, E^*_{sur} is the energy of the surface, and E_{ads} is the energy of the adsorbate molecule.[11] The first two energies are obtained using PBC calculations (as denoted by the asterisk) whereas the energy of the adsorbate is obtained as a free molecule. In the limit of low coverage, this can cause serious errors for small unit cells due to the spurious adsorbate/adsorbate interactions that are present in the $E^*_{ads/sur}$ supercell calculation that are not present in the real system. Choosing larger unit cells where the adsorbate/adsorbate interaction is negligible is a general solution to this problem. However, this increases the computational cost of the calculation as well as the number of optimization steps before convergence of the unit cell, and may not be feasible in many cases.

One way to assess the quality of the chosen unit cell is to evaluate the lateral interaction energies of the adsorbate molecules. This can be done by using a PBC calculation with a monolayer of adsorbate molecules at the same geometry of the composite adsorbate/surface system.[12] If the adsorbate/adsorbate interaction energy is small with respect to the adsorbate/surface interaction energy, the interaction strength is considered to be reliably obtained.

However, there can be a more serious potential problem. If the adsorbate/adsorbate interactions are not small, the geometry obtained for the $E^*_{ads/sur}$ composite system may not be reliable in the first place. Using this geometry to understand the adsorption process or to correct for the adsorbate/adsorbate interactions may introduce additional errors. Clearly, it is important to obtain the geometry in the presence/absence of interactions that are appropriate for the real system. In addition, it will be useful to have a method where the same unit cell that is used for the surface can also be used for the composite $E^*_{ads/sur}$ system at both high and low coverage limits.

We propose a composite energy expression for the adsorbate/surface system where the lateral adsorbate/adsorbate

interaction energy is cancelled by extrapolation, similar in spirit to that used in the ONIOM[13] technique and other hybrid methods where more accurate descriptions of adsorbates can be achieved.[14] In our composite energy model at the low-coverage limit, we have

$$E^*_{ads/sur}(LC) = E^*_{ads/sur} - E^*_{ads} + E_{ads} \qquad (2.2)$$

Here LC represents the low-coverage limit. Our procedure is represented schematically in Figure 2.1. $E^*_{ads/sur}$ represents the total energy of the slab-based adsorbate-surface calculation. This energy is equivalent to a standard periodic calculation of an adsorbate at full coverage. Similarly, E^*_{ads} is defined as the total energy of a slab calculation that only contains adsorbates such that the calculation properly describes lateral adsorbate-adsorbate interactions. The third term on the right hand side of Equation 2.2 is the energy of a non-periodically described single adsorbate, E_{ads}.

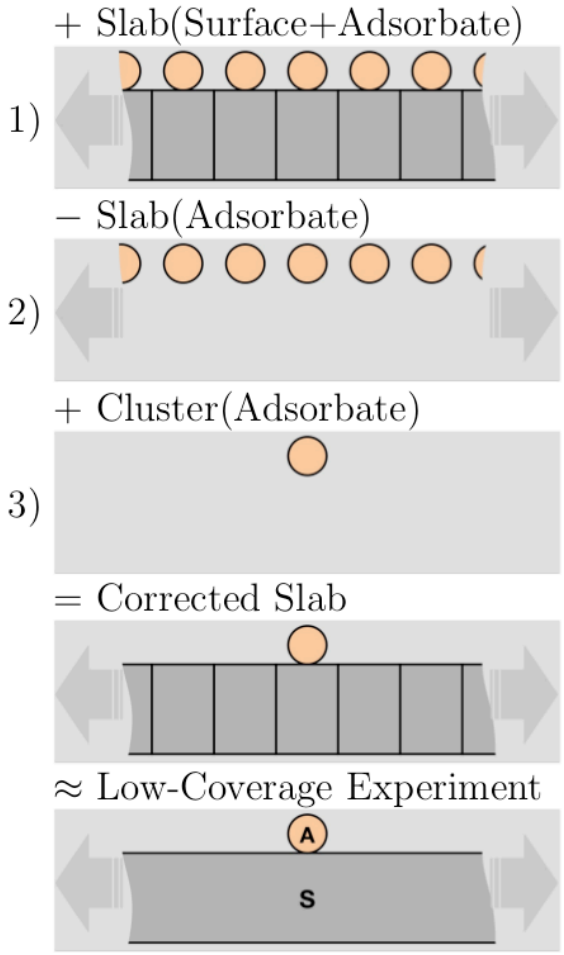

Figure 2.1. Schematic representation of the PBC-LC methodology. Orange circles represent the adsorbate. Gray regions represent the surface or surface unit cells.

Equation 2.2 can be considered effectively as the low-coverage energy for the adsorbate/surface system where the lateral adsorbate/adsorbate interactions are cancelled by the last two terms on the right hand side. We not only quantify the extent to

which adsorbate/adsorbate interactions affect the overall binding energy, but also focus our attention on the *geometric effects of such lateral interactions. Thus geometry optimizations are performed with the minimization of the composite energy expression in (2), providing a correction to the entire potential energy surface.*

Overall, the low-coverage energy in our method is obtained from three independent calculations: a full PBC surface/adsorbate calculation, a PBC adsorbate calculation, and a molecular adsorbate calculation. Since the composite energy is a simple sum of three independent energy evaluations, the energy gradients are also a summation,

$$\partial/\partial q\, E_{low\text{-}cover} = \partial/\partial q\, E^*_{ads/sur} - \partial/\partial q\, E^*_{ads} + \partial/\partial q\, E_{ads} \qquad (2.3)$$

where q represents one of the coordinates corresponding to the geometrical degrees of freedom of the molecular system. In our implementation, we compute the gradients with respect to the Cartesian coordinates defined for the molecular system. Analytical gradients are determined for each of the three independent energy calculations on the right hand side of Equation 2.3 and summed to obtain our corrected gradient term on the left hand side.

We use these energy and gradients from Equations 2.2 and 2.3 to explore *the potential energy surface of the composite energy model* described in Fig. 1 to obtain geometries of adsorbed molecules on Si(111) and C(111) surfaces at the low-coverage limit. The overall method will be labeled as PBC-LC where LC denotes low-coverage.

As mentioned earlier, our PBC-LC method uses concepts similar in spirit to the ONIOM method.[13] They both use an extrapolated energy expression that is a sum of three independent energy evaluations. In a normal "two-layer" ONIOM calculation, the interactions lost from truncating the "real" system into the "model" system at the high level of theory are evaluated at a lower level of theory to perform an effective extrapolation. Instead, our approach attempts to cancel the effects of adsorbate/adsorbate interactions to investigate periodic systems at low surface coverage. However, unlike ONIOM, only one level of theory is used for all regions of the system. Equivalently, our method can be considered as addition of the presence of a periodic surface to a single adsorbate.

The two independent calculations that correspond to the last two terms of Equations 2.2 and 2.3 must be treated with care. For a typical adsorbate forming a covalent bond with the surface (e.g.,

methyl-terminated Si(111) surface), chemical bonds will be broken when performing electronic structure calculations on the periodic adsorbate or single adsorbate calculations. In order to model the adsorbate in its adsorbed state, we replace the surface/adsorbate bond with a hydrogen “link atom”/adsorbate bond. As is customary with such link atom calculations, we employ a scale factor that describes the relationship between the new and old bonds. For example, to reflect the fact that the length of the C–Si bond (~ 1.89 Å) is longer than that of the C–H link atom bond (~ 1.08 Å) when describing a methyl group on the Si(111) surface, we choose a scale factor of 0.573 (i.e., the ratio between the bond lengths) to allow the link atom bond to be described in an appropriate manner. This scale factor is not only effective for the individual calculations, but it also provides a way to project forces and energies from the link atom onto the adsorbate and surface atoms.[15]

Overall, our method is general and can be used with many basis sets and levels of theory. The method can be used to obtain a meaningful energy and gradient from any method of choice where analytical gradients are available. In this work, we have used density functional theory using the gradient-corrected M06L functional[16] and the atom-centered standard 6-31G(d) basis set to explore the applicability of the method. The use of hybrid density

functionals that include exact exchange is also possible though the computational cost will be higher for PBC calculations with such functionals.

2.3. Computational Details

Geometry optimizations on all the systems were performed at the M06L/6-31G(d)[17] level of theory. C(111) and Si(111) 4-layer surface models with small unit cells were initially optimized without constraints (standard PBC) and subsequent optimizations were performed with adsorbates at low-coverage with our PBC-LC method. The same unit cell translation vectors were used in both calculations to isolate the geometric changes due to adsorbate-adsorbate interactions. Cluster models were also performed at the M06L/6-31G(d) level of theory. Rigid scans involving dihedral angle rotations were performed from the optimized geometries to evaluate the potential energy surfaces. All calculations were performed using the Gaussian 09 suite of programs.[18] Hydrogen link atom scale factors of 0.573, 0.700, and 0.600 were used for C–Si (replaced by C–H), C–C (replaced by C–H), and O–Si (replaced by O–H), respectively.

2.4. Results and Discussion

2.4.1. Si(111)/methyl group.

The methyl-terminated silicon surface is an interesting system where the interactions between the neighboring methyl groups play a key role in determining the adsorbate geometry that depends on the surface coverage. Experimentally, the complete monolayer methyl-terminated Si(111) surface has been prepared and investigated by several groups.[19] All methyl groups are equivalent on a completely terminated surface. *However, their orientation with respect to each other depends on the surface coverage*; the key geometrical parameter in this case is the dihedral angle of the methyl groups with respect to each other. For an isolated methyl group on the Si(111) surface, we expect a staggered conformation with respect to the next layer that is typical for silicon or carbon (H–C–Si–Si dihedral angle of 60°, the three-fold symmetry-equivalent value of 180°).[20] The dihedral angle for an isolated methyl group on a Si(111) surface has been investigated with a cluster model containing seven surface sites where the central site contains a methyl group and the remaining sites are terminated with hydrogen atoms. The optimized structure is shown in Figure 2.2(a). As expected, the calculated optimized dihedral

angle is 60°. The Si–C–H bond angle in the cluster with the M06L/6-31G(d) level (111°), close to the expected tetrahedral value.

At high methyl coverage, however, a staggered conformation is not preferred since it orients hydrogen atoms on adjacent methyl groups toward each other. The distance between the nearest non-bonded hydrogen atoms for this staggered conformation (~ 2.0 Å) is significantly smaller than the sum of their van der Waals radii (2.4 Å), resulting in steric repulsions. Methyl group rotations away from the staggered conformation decrease this repulsion that is minimized at a dihedral angle of 30°. Thus the optimized dihedral angle at high coverage is expected to lie between 30° and 60°. Previous results obtained by Goddard and coworkers[21,22] (38° using PBE functional and a plane wave basis set) and by Ferguson and Raghavachari[23] (41° using BLYP/6-31G(d) and 38° with HSE/6-31G(d)) are all consistent with this analysis. Our optimized value in this study using the M06L/6-31G(d) level of theory (37°) is also similar, as expected. The inter-adsorbate H···H distance at the M06L/6-31G(d) level has a value of 2.325 Å, suggesting that van der Waals repulsions have been diminished substantially. Figure 2.2(b) presents the optimized geometry of this system.

We have determined the optimized geometry at the low-coverage limit for the periodic system with the proposed PBC-LC model. We started the optimization from the dihedral angle (37°) obtained in the completely interacting case. The final optimized dihedral angle is 60°, clearly demonstrating the appropriate cancellation of the repulsive adsorbate-adsorbate interactions as shown in Figure 2.2(c). The Si–C–H bond angle also has a value very similar to that in the cluster model. The "inter-adsorbate" nonbonding H···H distance now has a smaller value of 2.077 Å, because the hydrogen atoms are no longer in the presence of the steric repulsion. Geometric parameters for the systems shown in Figure 2.2 are listed in Table 2.1.

The potential energy surface corresponding to the methyl dihedral angle rotation has been determined for the regular PBC as well as with PBC-LC. The results obtained using a rigid scan (i.e., changing the dihedral angle but keeping the other parameters constant) are shown in Figure 2.3. The standard PBC calculated energies reveal a minimum at a dihedral angle of 38° though the structure at 60° is only slightly higher in energy. The rigid scan also shows a barrier of 2.2 kcal/mol at the dihedral angle of 0° that corresponds to an eclipsed conformation. Our new method

provides an energy minimum at 60° and a rotation barrier of 1.7 kcal/mol at 0°. The results are similar to the those obtained previously with the BLYP functional.[23]

	PBC	PBC-LC	Cluster
Si–Si–C–H Dihedral	37.0	60.0	60.0
H···H Distance	2.325	2.077	---
C–Si Bond Distance	1.911	1.907	1.896
C–H Bond Distance	1.097	1.097	1.097
Si–Si–C Bond Angle	108.6	109.1	109.9
H–C–H Bond Angle	107.4	107.5	107.7
Si–C–H Bond Angle	111.3	111.5	111.2

Table 2.1. M06L/6-31G(d) geometrical parameters of a methyl group adsorbed Si(111) surface. Bond angles and dihedral angles are in degrees. Bond distances are reported in angstroms.

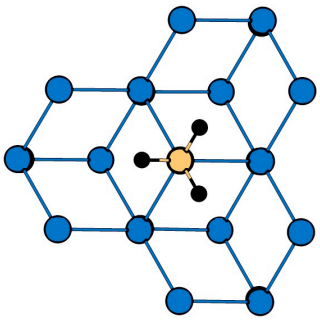

(a)

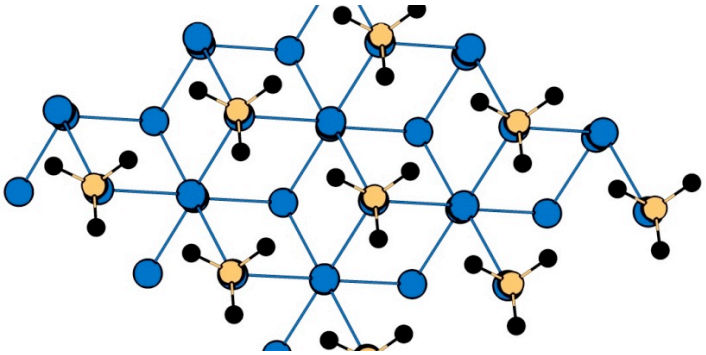

(b)

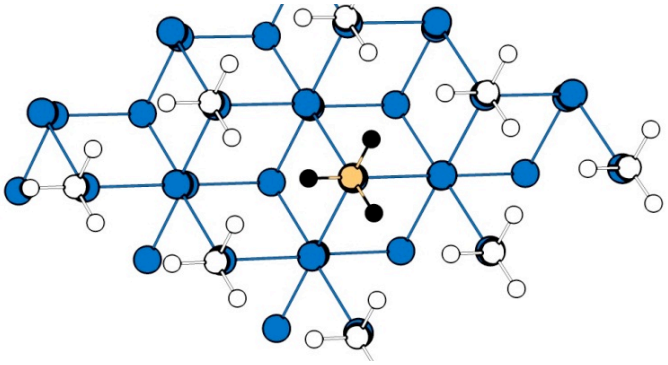

(c)

Figure 2.2 M06L/6-31G(d) geometries for methyl on Si(111) for (a) Cluster model (b) PBC, and (c) PBC-LC. Si atoms shown in dark blue, C atoms in yellow, and H atoms in black.

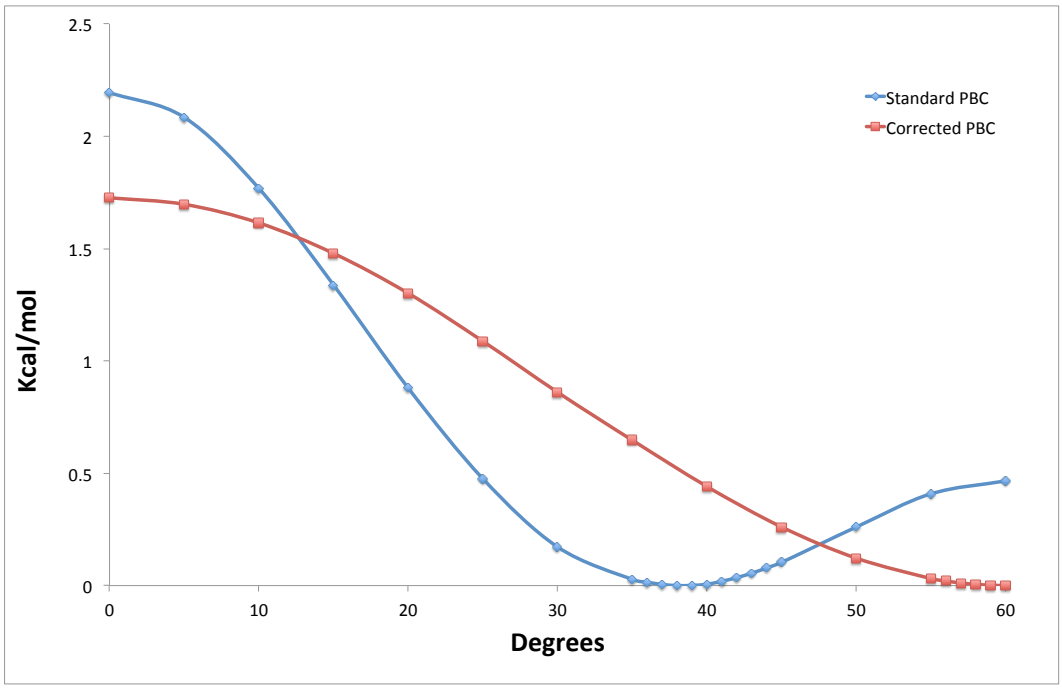

Figure 2.3. Scan of the relative energy (vertical axis, kcal/mol) *vs.* Si–Si–C–H dihedral angle (horizontal axis, degrees) for PBC (blue) and PBC-LC (red) for methyl on Si(111). Energies were evaluated with M06L/6-31G(d).

2.4.2. Si(111)/ethyl group.

We have first used a cluster model to study an isolated ethyl group adsorbed on a Si(111) surface. The optimized geometric values, along with the analogous PBC obtained geometric values are reported in Table 2.2. The expected staggered configuration is obtained as shown in Figure 2.4(a) with a Si–C–C angle of 115˚,

slightly larger than the tetrahedral angle. At higher coverages of the ethyl group, however, substantially larger steric repulsions are present. When this system is modeled at 100% coverage using standard PBC at the M06L/6-31G(d) level, severe angle strain occurs on the adsorbates due to the limited volume available to accommodate the bulkier group, as shown in Figure 2.4(b). For example, the Si–C–C angle increases to 130° from the expected value of ~ 110° to decrease the adsorbate-adsorbate distance and the consequent steric repulsions. This is similar to the value of 131° reported by Nemanick *et al.* at 100% coverage using the PBE functional.[21] In order to avoid large adsorbate-adsorbate repulsions, the surface Si–C bond tilts significantly from the surface normal, with the three distinct Si–Si–C angles ranging from 95° to 123°. The ethyl groups are oriented to minimize the repulsive interactions with a Si–Si–C–C dihedral angle of 154°. The minimum H···H distance between adjacent ethyl groups is 2.14 Å.

	PBC	PBC-LC	Cluster
Si–Si–C–C Dihedral	−154.0	−177.8	−178.4
Si–C–C Bond Angle	130.2	114.7	114.9
Si–Si–C Bond Angle	95.0	108.3	106.8
Si′–Si–C Bond Angle	123.8	112.1	111.1
Si″–Si–C Bond Angle	109.4	107.7	111.9
H···H Distance	2.143	0.756	---
C–Si Bond Distance	1.934	1.913	1.905

Table 2.2. M06L/6-31G(d) geometrical parameters of an ethyl adsorbate on the Si(111) surface. Bond angles and dihedral angles are in degrees. Bond distances are reported in angstroms.

The optimizations carried out with the PBC-LC method lead to a significantly less strained geometry as shown in Figure 2.4(c). For example, the Si–C–C angle has a value of 115°, in agreement with the corresponding angle obtained with an isolated Si(111) cluster model shown in Figure 2.4(a). The Si–Si–C angles (108°) are very close to the tetrahedral angle. If we replicate the ethyl geometry to the neighboring unit cell, the minimum H···H distance occurs at 0.76 Å, though this interaction is not felt due to the cancellation of the adsorbate-adsorbate interactions in our model.

However, even in this case, our results are robust enough to allow for an accurate description of the low-coverage limit using a periodic surface.

Previous work has shown that due to the strong steric repulsions, 100% ethyl coverage cannot be obtained experimentally and that coverages up to 75-80% maybe possible.[24] At such lower coverages, reasonable bond angles can be maintained without unduly increasing the steric interactions.[6a, 25]

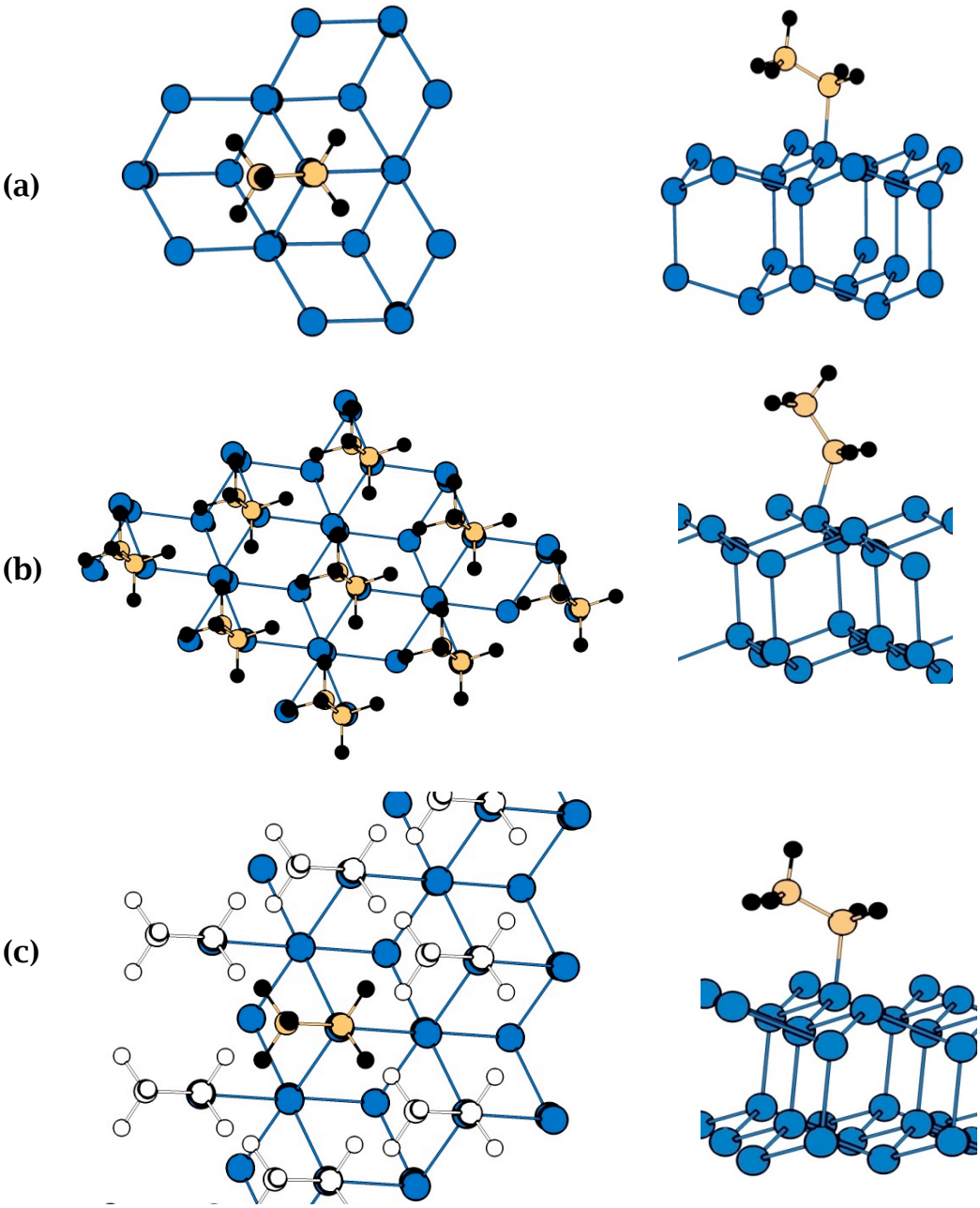

Figure 2.4. M06L/6-31G(d) geometries for ethyl on Si(111) for (a) Cluster model (b) PBC, and (c) PBC-LC. Top view (left) and side view (right). Si atoms shown in dark blue, C atoms in yellow, and H atoms in black.

2.4.3. Si(111)/methoxy group.

The isolated methoxy group geometry has been investigated with the cluster model (Figure 2.5(a)). The Si–O–C angle has a value of 120° with a staggered conformation for the methyl group (Si–Si–O–C dihedral angle of 180°). The interactions between neighboring methoxy groups are smaller than those between neighboring ethyl groups.[26] Thus, using standard PBC optimization (Figure 2.5(b)), the Si–O–C angle opens out only moderately to 127°, which is in agreement with previous studies.[27] Also, there is an accompanying slight twist of the dihedral angle to 160° at the M06L/6-31G(d) level of theory. The optimized geometry shows very little neighboring group interactions. The closest H···H contact is 2.43 Å indicating very little steric repulsion, and the closest OH distance is 2.48 Å indicating that any hydrogen bonding interaction is also weak.

As in the previous cases, the optimization using our proposed PBC-LC method (Figure 2.5(c)) yields geometries very close to that from the isolated cluster. The Si–O–C angle is 121° while the dihedral angle is 178°. The interactions resulting from neighboring groups are clearly cancelled out by our method, resulting in a shorter intercell H···H distance of 2.06 Å and a non-bonded O–H distance of 2.00 Å.

	PBC	PBC-LC	Cluster
Si–Si–O–C Dihedral	−160.2	−178.0	−180.0
Si–O–C Bond Angle	126.7	121.4	120.5
Si–Si–O Bond Angle	99.9	103.8	102.0
Si′–Si–O Bond Angle	112.1	110.7	112.0
Si″–S–O Bond Angle	113.3	111.4	112.0
H···H Distance	2.432	2.064	---
O–Si Bond Distance	1.683	1.686	1.686
H···O Distance	2.480	1.995	---
C–H Bond Distance 1	1.098	1.105	1.103
C–H Bond Distance 2	1.099	1.104	1.103
C–H Bond Distance 3	1.099	1.097	1.095

Table 2.3. M06L/6-31G(d) geometrical parameters of a methoxy adsorbate on the Si(111) surface. Bond angles and dihedral angles are in degrees. Bond distances are reported in angstroms.

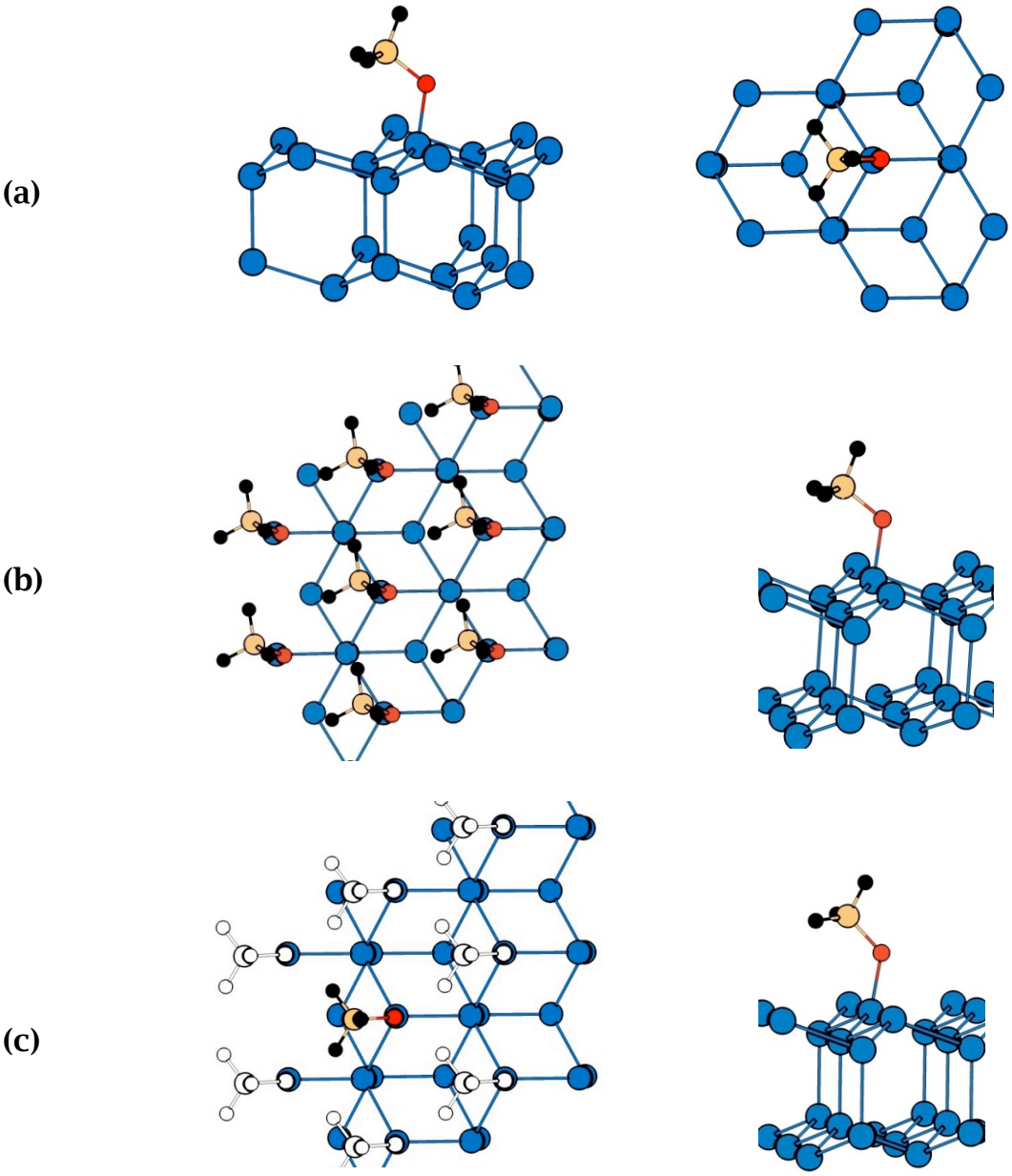

Figure 2.5. M06L/6-31G(d) geometries for methoxy on Si(111) for (a) Cluster model (b) PBC, and (c) PBC-LC. Top view (left) and side view (right). Si atoms shown in dark blue, C atoms in yellow, and H atoms in black.

2.4.4. C(111)/methyl group.

In order to consider a challenging case to test our method for extreme steric repulsion, we have considered the methyl adsorption on the diamond C(111) surface. Geometric parameters are reported in Table 2.4. Since the C–C distances are much smaller than the Si–Si distances, complete monolayer methyl coverage places the neighboring non-bonded methyl hydrogen atoms in close proximity (~ 0.7 Å) resulting in dramatically large van der Waals repulsions. Such a situation is unlikely to be realized under experimental conditions though it can be studied using computational methods.

In this case, an isolated methyl group using a cluster model (Figure 2.6(a)) yields the expected perpendicular attachment of the adsorbate, a staggered geometry (H–C–C–C = 60°), along with reasonable bond lengths and angles. As expected, the regular PBC optimization at the full coverage limit (Figure 2.6(b)) shows strong distortions due to the steric repulsions. In particular, the optimization results in tilting of the methyl groups to increase the non-bonded H···H distances and decrease in the unfavorable steric repulsions (within the limited unit cell size of the surface). In

addition, the optimized dihedral angle (H–C–C–C) has a value of 26°, close to the value expected when lateral adsorbate-adsorbate repulsions dominate. The nearest H···H non-bonded distance is 1.61 Å indicating that substantially unfavorable interactions are still present.

C(111)/CH_3	PBC	PBC-LC	Cluster
C–C–C–H Dihedral	26.0	60.2	60.3
H···H Distance	1.612	0.747	---
C–C Bond Distance	1.535	1.512	1.538
C–H Bond Distance	1.036	1.101	1.093
C–C–C Bond Angle	98.9	109.7	110.3
C′–C–C Bond Angle	108.1	109.7	110.3
C″–C–C Bond Angle	118.5	110.1	110.3
H–C–H Bond Angle	101.3	106.9	106.5
C–C–H Bond Angle	106.0	111.9	112.3

Table 2.4. M06L/6-31G(d) geometrical parameters of a methyl adsorbate on the C(111) surface. Bond angles and dihedral angles are in degrees. Bond distances are reported in angstroms.

We have optimized the geometry at the low-coverage limit by employing our PBC-LC method. Starting from a PBC dihedral angle of 26°, the resulting optimized dihedral angle with the PBC-LC model is 60° as seen in the case of the isolated cluster model. This result suggests that the unfavorable interactions are cancelled out even in this extreme case where the shortest inter-adsorbate H···H non-bonded distance is only 0.75 Å. In particular, PBC-LC yields a stable, minimized geometry where the adsorbed methyl group is correctly oriented perpendicular to the Si(111) surface. The geometry does not suffer from distortions caused by steric interactions among the nearby adsorbates that result when standard PBC methods are employed.

Overall, our method recovers the geometry obtained with the cluster model for these simple surfaces. However, we emphasize that, unlike the cluster model, the complete environment of the periodic surface is felt by the adsorbate in our composite model without any boundary or truncation effects. This will be important in systems with more complex surface reconstructions or, more importantly, for the investigation of chemical reactions occurring at surfaces where boundary effects can play a key role, e.g., for the study of radical-initiated chain reactions on Si(100) surfaces.[28]

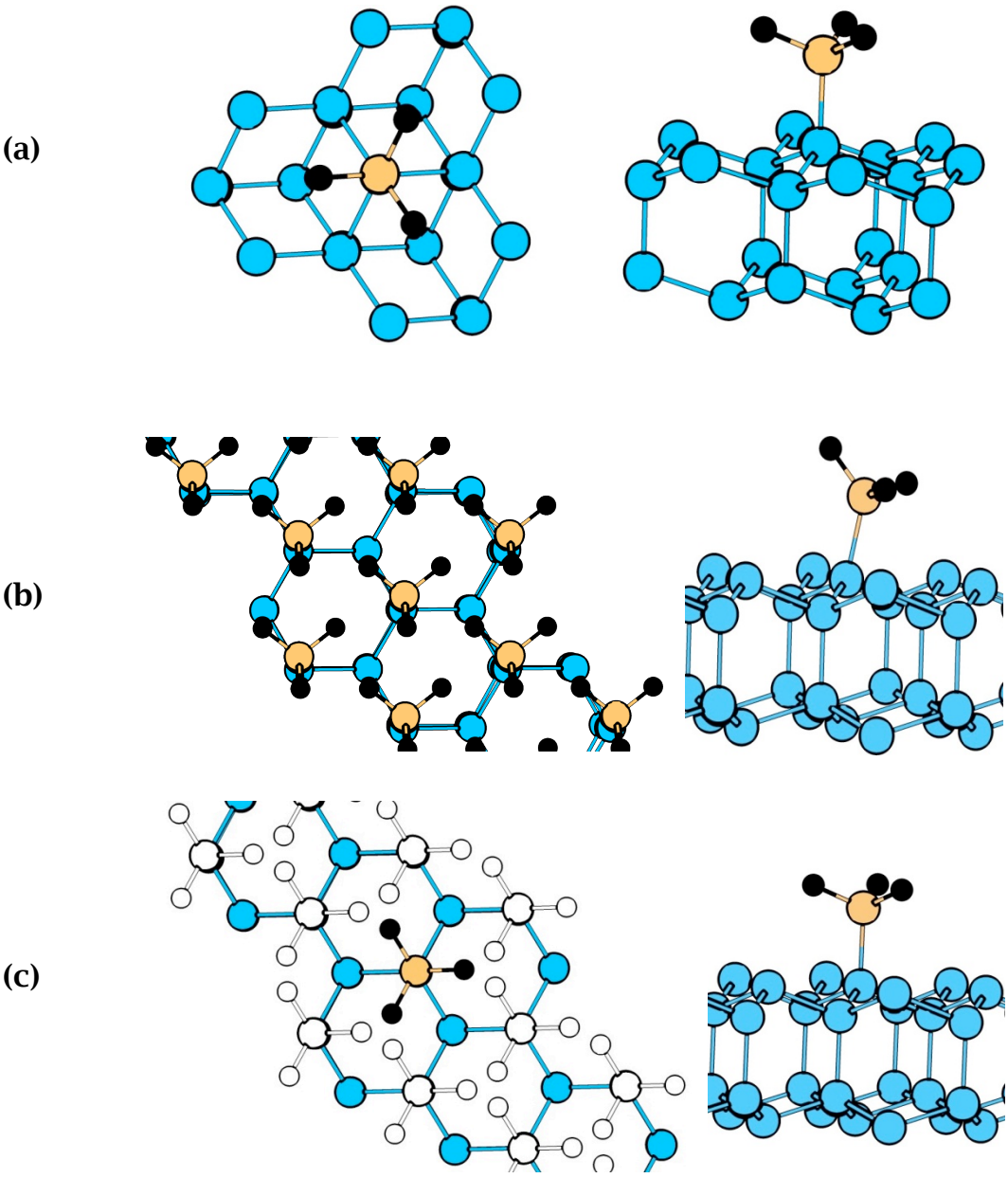

Figure 2.6. M06L/6-31G(d) geometries for methyl on C(111) for (a) Cluster model (b) PBC, and (c) PBC-LC. Top view (left) and side view (right). Surface C atoms shown in light blue, adsorbate C atoms in yellow, and H atoms in black.

2.5. Conclusions

We have formulated the PBC-LC method for the simulation of adsorbates on periodic surfaces at the low-coverage limit. In this method, we use an ONIOM-like extrapolation to cancel inter-cell adsorbate-adsorbate interactions. Our method provides a good description of the entire potential energy surface, and enables the use of small unit cells to study geometrical relaxations associated with adsorption processes at low coverages. The geometries from our test examples show the effectiveness of this method for the Si(111) and C(111) surfaces. This method can to be widely employed to study low-coverage adsorptions as well as chemical reactions on surfaces.

2.6. References

1. Somorjai, G. A.; Li, Y., *Introduction to Surface Chemistry and Catalysis*. Wiley: New Jersey, 2010.

2. Ihm, J.; Cohen, M. L.; Chadi, D. J., (2 × 1) reconstructed Si(001) surface: Self-consistent calculations of dimer models. *Physical Review B* **1980,** *21* (10), 4592-4599.

3. Raghavachari, K.; Halls, M. D., Quantum chemical studies of semiconductor surface chemistry using cluster models. *Molecular Physics* **2004,** *102* (4), 381-393.

4. Ferguson, G. A.; Raghavachari, K., The emergence of collective vibrations in cluster models: Quantum chemical study of the methyl-terminated Si(111) surface. *The Journal of Chemical Physics* **2006,** *125* (15), 154708-8.

5. Higashi, G. S.; Chabal, Y. J.; Trucks, G. W.; Raghavachari, K., Ideal hydrogen termination of the Si (111) surface. *Applied Physics Letters* **1990,** *56* (7), 656-658.

6. (a) Yu, H.; Webb, L. J.; Solares, S. D.; Cao, P.; Goddard, W. A.; Heath, J. R.; Lewis, N. S., Scanning Tunneling Microscopy of

Ethylated Si(111) Surfaces Prepared by a Chlorination/Alkylation Process. *The Journal of Physical Chemistry B* **2006,** *110* (47), 23898-23903; (b) Yamada, T.; Inoue, T.; Yamada, K.; Takano, N.; Osaka, T.; Harada, H.; Nishiyama, K.; Taniguchi, I., Detection of C−Si Covalent Bond in CH3 Adsorbate Formed by Chemical Reaction of CH3MgBr and H:Si(111). *Journal of the American Chemical Society* **2003,** *125* (26), 8039-8042; (c) Barrelet, C. J.; Robinson, D. B.; Cheng, J.; Hunt, T. P.; Quate, C. F.; Chidsey, C. E. D., Surface Characterization and Electrochemical Properties of Alkyl, Fluorinated Alkyl, and Alkoxy Monolayers on Silicon. *Langmuir* **2001,** *17* (11), 3460-3465; (d) Cai, W.; Lin, Z.; Strother, T.; Smith, L. M.; Hamers, R. J., Chemical Modification and Patterning of Iodine-Terminated Silicon Surfaces Using Visible Light. *The Journal of Physical Chemistry B* **2002,** *106* (10), 2656-2664; (e) He, J.; Patitsas, S. N.; Preston, K. F.; Wolkow, R. A.; Wayner, D. D. M., Covalent bonding of thiophenes to Si(111) by a halogenation/thienylation route. *Chemical Physics Letters* **1998,** *286* (5–6), 508-514; (f) Rohde, R. D.; Agnew, H. D.; Yeo, W.-S.; Bailey, R. C.; Heath, J. R., A Non-Oxidative Approach toward Chemically and Electrochemically Functionalizing Si(111). *Journal of the American Chemical Society* **2006,** *128* (29), 9518-9525.

7. Buriak, J. M., Organometallic Chemistry on Silicon and Germanium Surfaces. *Chemical Reviews* **2002,** *102* (5), 1271-1308.

8. Ekimov, E. A.; Sidorov, V. A.; Bauer, E. D.; Mel'nik, N. N.; Curro, N. J.; Thompson, J. D.; Stishov, S. M., Superconductivity in Diamond. *Nature* **2004,** *428*, 542-545.

9. Nichols, B. M.; Butler, J. E.; Russell, J. J. N.; Hamers, R. J., Photochemical Functionalization fo Hydrogen-Terminated Diamond Surfaces: A Structural and Mechanisitic Study. *J. Phys. Chem. B* **2005,** *109*, 20938-20947.

10. (a) Hansen, N.; Kerber, T.; Sauer, J.; Bell, A. T.; Keil, F. J., Quantum Chemical Modeling of Benzene Ethylation over H-ZSM-5 Approaching Chemical Accuracy: A Hybrid MP2:DFT Study. *Journal of the American Chemical Society* **2010,** *132* (33), 11525-11538; (b) Svelle, S.; Tuma, C.; Rozanska, X.; Kerber, T.; Sauer, J., Quantum Chemical Modeling of Zeolite-Catalyzed Methylation Reactions: Toward Chemical Accuracy for Barriers. *Journal of the American Chemical Society* **2008,** *131* (2), 816-825.

11. Valenzano, L.; Civalleri, B.; Sillar, K.; Sauer, J., Heats of Adsorption of CO and CO2 in Metal–Organic Frameworks: Quantum Mechanical Study of CPO-27-M (M = Mg, Ni, Zn). *The Journal of Physical Chemistry C* **2011,** *115* (44), 21777-21784.

12. Labat, F. d. r.; Ciofini, I.; Hratchian, H. P.; Frisch, M.; Raghavachari, K.; Adamo, C., First Principles Modeling of Eosin-Loaded ZnO Films: A Step toward the Understanding of Dye-Sensitized Solar Cell Performances. *Journal of the American Chemical Society* **2009,** *131* (40), 14290-14298.

13. (a) Svensson, M.; Humbel, S.; Morokuma, K., Energetics using the single point IMOMO (integrated molecular orbital+molecular orbital) calculations: Choices of computational levels and model system. *Journal of Chemical Physics* **1996,** *105* (9), 3654-3661; (b) Svensson, M.; Humbel, S.; Froese, R. D. J.; Matsubara, T.; Sieber, S.; Morokuma, K., ONIOM: A Multilayered Integrated MO + MM Method for Geometry Optimizations and Single Point Energy Predictions. A Test for Diels−Alder Reactions and Pt(P(t-Bu)3)2 + H2 Oxidative Addition. *The Journal of Physical Chemistry* **1996,** *100* (50), 19357-19363; (c) Vreven, T.; Morokuma, K.; Farkas, Ö.; Schlegel, H. B.; Frisch, M. J., Geometry optimization with QM/MM, ONIOM, and other combined methods. I. Microiterations and constraints. *Journal of Computational Chemistry* **2003,** *24* (6), 760-769.

14. (a) Tosoni, S.; Sauer, J., Accurate quantum chemical energies for the interaction of hydrocarbons with oxide surfaces: CH4/MgO(001). *Physical Chemistry Chemical Physics* **2010,** *12* (42);

(b) Tuma, C.; Sauer, J., A hybrid MP2/planewave-DFT scheme for large chemical systems: proton jumps in zeolites. *Chemical Physics Letters* **2004,** *387* (4–6), 388-394; (c) Eichler, U.; Kölmel, C. M.; Sauer, J., Combining ab initio techniques with analytical potential functions for structure predictions of large systems: Method and application to crystalline silica polymorphs. *Journal of Computational Chemistry* **1997,** *18* (4), 463-477.

15. Vreven, T.; Byun, K. S.; Komáromi, I.; Dapprich, S.; Montgomery, J. A.; Morokuma, K.; Frisch, M. J., Combining Quantum Mechanics Methods with Molecular Mechanics Methods in ONIOM. *Journal of Chemical Theory and Computation* **2006,** *2* (3), 815-826.

16. Zhao, Y.; Truhlar, D. G., A New Local Density Functional for Main-Group Thermochemistry, Transition Metal Bonding, Thermochemical Kinetics and Noncovalent Interactions. *J. Chem. Phys.* **2006,** *125*, 194101.

17. (a) Francl, M. M.; Pietro, W. J.; Hehre, W. J.; Binkley, J. S.; Gordon, M. S.; DeFrees, D. J.; Pople, J. A., Self-consistent Molecular Orbital Methods. XXII. A Polarization-type Basis Set for Second-row Elements. *J. Chem. Phys.* **1982,** *77* (7), 3654-3666; (b) Hariharan, P. C.; Pople, J. A., The Influence of Polarization Functions on

Molecular Orbital Hydrogenation Energies. *Theoret. chim. Acta* **1973,** *28*, 213-222.

18. Frisch, M. J.; Trucks, G. W.; Schlegel, H. B.; Scuseria, G. E.; Robb, M. A.; Cheeseman, J. R.; Scalmani, G.; Barone, V.; Mennucci, B.; Petersson, G. A.; Nakatsuji, H.; Caricato, M.; Li, X.; Hratchian, H. P.; Izmaylov, A. F.; Bloino, J.; Zheng, G.; Sonnenberg, J. L.; Hada, M.; Ehara, M.; Toyota, K.; Fukuda, R.; Hasegawa, J.; Ishida, M.; Nakajima, T.; Honda, Y.; Kitao, O.; Nakai, H.; Vreven, T.; Montgomery, J. J. A.; Peralta, J. E.; Ogliaro, F.; Bearpark, M.; Heyd, J. J.; Brothers, E.; Kudin, K. N.; Staroverov, V. N.; Kobayashi, R.; Normand, J.; Raghavachari, K.; Rendell, A.; Burant, J. C.; Iyengar, S. S.; Tomasi, J.; Cossi, M.; Rega, N.; Millam, J. M.; Klene, M.; Knox, J. E.; Cross, J. B.; Bakken, V.; Adamo, C.; Jaramillo, J.; Gomperts, R.; Stratmann, R. E.; Yazyev, O.; Austin, A. J.; Cammi, R.; Pomelli, C.; Ochterski, J. W.; Martin, R. L.; Morokuma, K.; Zakrzewski, V. G.; Voth, G. A.; Salvador, P.; Dannenberg, J. J.; Dapprich, S.; Daniels, A. D.; Farkas, Ö.; Foresman, J. B.; Ortiz, J. V.; Cioslowski, J.; Fox, D. J. Gaussia1 09 Revision A.1.

19. (a) Fidélis, A.; Ozanam, F.; Chazalviel, J. N., Fully methylated, atomically flat (111) silicon surface. *Surface Science* **2000,** *444* (1–3), L7-L10; (b) Aliano, A.; Li, Y.; Cicero, G.; Galli, G., Structural and

Electronic Properties of the Methyl-Terminated Si(111) Surface. *The Journal of Physical Chemistry C* **2010,** *114* (27), 11898-11902.

20. Yu, H.; Webb, L. J.; Ries, R. S.; Solares, S. D.; Goddard, W. A.; Heath, J. R.; Lewis, N. S., Low-Temperature STM Images of Methyl-Terminated Si(111) Surfaces. *The Journal of Physical Chemistry B* **2004,** *109* (2), 671-674.

21. Nemanick, E. J.; Hurley, P. T.; Webb, L. J.; Knapp, D. W.; Michalak, D. J.; Brunschwig, B. S.; Lewis, N. S., Chemical and electrical passivation of single-crystal silicon(100) surfaces through a two-step chlorination/alkylation process. *Journal of Physical Chemistry B* **2006,** *110* (30), 14770-14778.

22. Solares, S. D.; Yu, H.; Webb, L. J.; Lewis, N. S.; Heath, J. R.; Goddard, W. A., Chlorination–Methylation of the Hydrogen-Terminated Silicon(111) Surface Can Induce a Stacking Fault in the Presence of Etch Pits. *Journal of the American Chemical Society* **2006,** *128* (12), 3850-3851.

23. Ferguson, G. A.; Raghavachari, K., The emergence of collective vibrations in cluster models: Quantum chemical study of the methyl-terminated Si(111) surface. *Journal of Chemical Physics* **2006,** *125*, 154708.

24. Jaeckel, B.; Hunger, R.; Webb, L. J.; Jaegermann, W.; Lewis, N. S., High-Resolution Synchrotron Photoemission Studies of the Electronic Structure and Thermal Stability of CH3- and C2H5-Functionalized Si(111) Surfaces. *The Journal of Physical Chemistry C* **2007,** *111* (49), 18204-18213.

25. (a) Johansson, E.; Hurley, P. T.; Brunschwig, B. S.; Lewis, N. S., Infrared Vibrational Spectroscopy of Isotopically Labeled Ethyl-Terminated Si(111) Surfaces Prepared Using a Two-Step Chlorination/Alkylation Procedure. *The Journal of Physical Chemistry C* **2009,** *113* (34), 15239-15245; (b) Webb, L. J.; Rivillon, S.; Michalak, D. J.; Chabal, Y. J.; Lewis, N. S., Transmission Infrared Spectroscopy of Methyl- and Ethyl-Terminated Silicon(111) Surfaces. *The Journal of Physical Chemistry B* **2006,** *110* (14), 7349-7356.

26. Solares, S. D.; Michalak, D. J.; Goddard, W. A.; Lewis, N. S., Theoretical Investigation of the Structure and Coverage of the Si(111)–OCH3 Surface. *The Journal of Physical Chemistry B* **2006,** *110* (16), 8171-8175.

27. Michalak, D. J.; Rivillon, S.; Chabal, Y. J.; Estève, A.; Lewis, N. S., Infrared Spectroscopic Investigation of the Reaction of

Hydrogen-Terminated, (111)-Oriented, Silicon Surfaces with Liquid Methanol. *The Journal of Physical Chemistry B* **2006,** *110* (41), 20426-20434.

28. Ferguson, G. A.; Than, C. T.-L.; Raghavachari, K., Extending Molecular Lines on the Si(100)-2 × 1 Surface: A Theoretical Study of the Effect of Allylic Mercaptan Adsorbates on Radical Chain Reactions. *The Journal of Physical Chemistry Letters* **2010,** *1* (4), 679-685.

Chapter Three

Composite Energy Methods to Selectively Remove Intramolecular Interactions

3.1. Introduction

A large portion of useful chemical and biochemical transformations have their origins not only in covalent bonding networks but also in weak interactions such as hydrogen bonding, electrostatic interactions and dispersion interactions. From applications such as protein folding,[13] ionic solvents,[14] anion/cation binding,[15] etc., a significant amount of structural stability is due to such nonbonding interactions, typically involving energies less than 15 kcal/mol. Dipole-dipole, dipole-induced dipole, and other weak intermolecular forces often dictate chemical reactivity as well. Therefore, such weak interactions are of major interest to the chemistry community at large. Theoretical tools that can investigate and quantify the behavior of non-bonded interactions can lead to new breakthroughs in understanding, design, and prediction of novel, important chemistry.

The composite methods described in this work are designed to identify specific non-bonded atom-atom interactions and effectively cancel them in a manner related to previous models. ONIOM,[6] one of the most common hybrid energy schemes, utilizes multiple levels of theory to achieve high accuracy calculations for large molecular systems at a significantly reduced computational cost. Composite energy schemes can also be utilized to incorporate additional energetic contributions to a model, such as the work of Sauer et al.,[16] where PBC (periodic boundary conditions) energies of an extended system using DFT were integrated with high accuracy MP2 calculations to describe adsorption.

There have been several previous approaches to derive the energetic contributions of weak interactions. The simplest method to in a molecular complex is to calculate the energetic difference between a hydrogen bonded dimer and its non-interacting monomers. However, this method is limited to intermolecular interactions. Another rigorous method that can analyze intermolecular interactions, Symmetry Adapted Perturbation Theory (SAPT),[17] can decompose interactions into four basic components: electrostatic, induction, dispersion, and exchange. Some methods include electron density and the Laplacian of the electron density to attempt to determine the strength of the

hydrogen bond. Atoms in Molecules (AIM)[18] can be used to define hydrogen bond critical points (HBCPs) that can be located and analyzed to derive information about the energetic stability of a hydrogen bond.[19]

Weak interactions are important to consider in studies of silicon surfaces. Silicon has been the primary material for the semiconductor and electronics industries, and extensive research is being carried out on functionalized silicon surfaces for potential applications in many areas of technology. The two most important systems for silicon surface chemistry are the Si(100) and Si(111) surfaces. The Si(111) surface, when hydrogenated or etched under mild conditions, creates an atomically flat surface.[1] The Si(100) surface reconstructs to form dimer rows that are preserved upon hydrogen termination. Both of these surfaces can be modified for reactivity studies by creating a localized radical site, e.g., through the use of an STM tip.[2] Many adsorption studies have been performed experimentally[2-3] and theoretically[4] for understanding functionalized silicon surfaces.

Computational investigations of silicon surface chemistry are commonly carried out either using a slab approach (periodic boundary conditions) or the alternative cluster approach. For

localized chemistry, cluster models that provide an accurate description of the local region of interaction and its immediate environment are an appropriate choice.[5] The basic cluster model is first defined from a bulk structure and the surface reactive site. The dangling bonds resulting from any broken bulk Si–Si bonds are then terminated with hydrogen "link" atoms to avoid any artifacts due to excess spin or charge. Additionally, constraints may be applied to make the cluster model have more appropriate boundary effects. Cluster models are advantageous for use in many surface reactivity studies because they can be treated exactly like a finite molecule, unlike slab calculations, where methods that calculate exact exchange, such has HF, MP2, or B3LYP, are prohibitively expensive for large unit cells. Computationally, cluster models are significantly more efficient for surface reactivity studies because sufficiently large unit cells must be employed to ignore intercell adsorbate interactions.

The focus in this work is on silicon surface models of importance in microelectronics. Cluster models that model the Si(100) surface require a finite truncation, and when appropriately chosen, can lead to reactivity and behavior in agreement with experimental results. However, without careful treatment, the standard cluster methods for modeling the Si(100) surface can

potentially lead to significant problems. This is particularly true for larger clusters that contain multiple surface dimers along and across dimer rows.

3.2. A Composite Energy Treatment for Sterically Hindered Cluster Models for the Si(100) Surface

3.2.1 Background

The potential problems for the Si(100) surface can be illustrated with the model shown in Figure 3.1. The surface shown has two dimers in adjacent rows that can describe chemical reactions (*vide infra*) when interactions between neighboring dimers are significant. The ideal surface is shown on the left and a truncated cluster model that is terminated at the fourth layer is shown on the right. The main reason for the problem is that truncation of the bonds between two layers of a Si(100) surface leads to *two covalent bonds being severed to the same atom* in the lower layer. If both broken bonds are terminated with hydrogen atoms, the two capping hydrogen atoms (that both represent the same original silicon atom) will be ~ 1.4-1.5 Å apart, resulting in repulsive H···H interactions, as the two atoms are significantly closer than the sum of their van der Waals radii (2.4 Å). Such an

interaction is clearly unphysical, arising only because of truncation. If such a terminated structure is optimized without constraints, substantial geometrical distortions occur, as the hydrogen atoms optimize to a H···H distance of 2.475 Å at the B3LYP/6-31G(d,p) level.

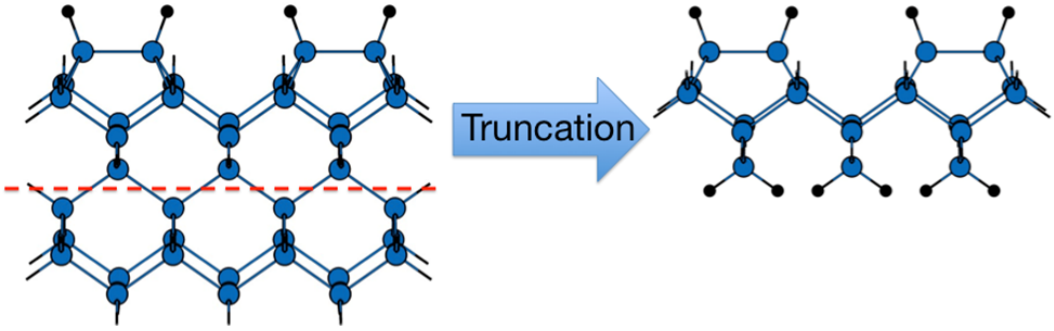

Figure 3.1. Starting from a model representing the reconstructed Si(100) surface (left), truncation of the surface at the fourth layer using a standard hydrogen link atom termination leads to the cluster model (right). Silicon atoms are in blue and hydrogen atoms are in black.

There are several potential solutions to this problem. The cluster can be extended to deeper layers leading to a tapered structure that avoids such interactions, at the expense of larger computational cost. A second solution is to truncate with divalent "pseudoatoms" instead of monovalent hydrogen atoms, which will be discussed in more detail in chapter 3. A more common solution

is to sidestep the problem by freezing the atoms of the lower layers in performing geometry optimizations to avoid the unphysical artifacts that could lead to distorted geometries.

Here, a new composite method is proposed that allows for the selective removal of the effects of the unphysical steric interaction. It uses concepts similar in spirit to the ONIOM[6] method that uses a hybrid potential energy surface. However, instead of combining multiple levels of theory in different regions as in standard ONIOM, we define a hybrid energy in our method that purposefully attempts to remove the relevant interactions by cancelling them via a series of independent calculations at a fixed level of theory. The hybrid potential energy can be minimized with respect to geometrical parameters to find meaningful structures, minima that reflect how a system would behave without the presence of the forces that would otherwise exist in a standard calculation.

To overcome this unphysical distortion due to truncation in the Si(100) surface, a hybrid energy scheme is defined as shown in Figure 3.2. In this composite energy, undesirable interactions present in the full system (**A**) are missing from the interaction energy between excised fragments defined from the full system (**B**)

and replaced by the individual non-interacting equivalent fragments (**C**). In a similar manner to the composite energy defined in our PBC-LC method[7], as a starting point the composite energy can be defined in Equation 3.1 as:

$$E(\text{composite}) = E_{full} - E_{model,interacting} + \Sigma E_{model,noninteracting} \quad (3.1)$$

In this particular example, such a composite energy expression requires five separate subsystem calculations, all of which are dependent upon the geometry of the full cluster at each energy evaluation. In other words, each individual subsystem has a geometry (e.g., cartesian coordinates) that is derived from the coordinates of the full molecular system at the current optimization step. Apart from the full molecular system calculation (E_{full}), the remaining four subsystem calculations are performed on the smaller models (derived from the full system) and add very little overhead to the overall computational expense. Note that link atom terminations are used for each of the subsystems that involve broken covalent bonds. The link atoms (hydrogens) replace the corresponding silicon atoms, but bond lengths are shortened by a constant scale factor (0.61) to reflect the fact that Si–H bonds are much shorter than Si–Si bonds.

However, there can be a potential problem when applying Equation 3.1 to geometry optimizations. This is due to a possible imbalance between the repulsive interactions in the full system and the model system, as they may not cancel exactly since they represent similar, but not identical, structural entities. This may cause a deficiency in representing the energy and gradient of the molecular system at certain geometries where $E_{model,interacting}$ strongly dominates as a highly repulsive term (e.g., by portions of the model system coming in close proximity to each other). Since $E_{model,interacting}$ is included with a negative sign, E(composite) is lowered, and this may lead to a collapse of the hydrogens towards each other. To avoid this, we have included a fitted van der Waals-type repulsive term that prevents such non-bonded hydrogens from getting too close. Thus we define a final modified composite energy expression defined in Equation 3.2.

$$E(\text{composite}) = E_{full} - E_{model,interacting} - \Sigma E_{model,noninteracting} + \Sigma E_{H\cdots H\ Correction} \quad (3.2)$$

In Equation 3.2, an additional term, $\Sigma E_{H\cdots H\ Correction}$, is added to energy of the full molecular system. This correction (Figure 3.3 (**d**)), which adds a (fitted) repulsive van der Waals interaction between nonbonded H···H pairs in the model system, is a key component for obtaining reasonable chemical structures. In the case of the

Si(100) cluster at the B3LYP/6-31G(d,p) level, we implemented this by replacing the Lennard-Jones parameters of the Dreiding force field[8] with new parameters (R_0 = 4.0 Å, D_0 = 1×10^{-6} kcal/mol). The parameters were adjusted to yield a reasonably shaped potential curve (i.e., relaxed scan) as a function of the H···H distance with a single minimum at a value close to the expected value of 1.4-1.5 Å.

Since the composite energy is the sum of the energies of independent sub-calculations, the corresponding gradients required for geometry optimization can also be defined in a similar manner, requiring only independent sub-calculations. Additionally, since the spurious interaction has been omitted in the composite energy, unconstrained optimization of the transition state and ground state geometries on this new composite potential energy surface are well-defined and can be performed with a standard geometry optimizer. In the case of the Si(100) surface, the optimized geometry for the cluster without any constraints yields the structure shown in the top portion of Figure 3.4 The structure is distorted strongly at the bottom layer due to the unfavorable steric repulsions and is clearly not representative of the real surface. Using the expression in Equation 3.2, the cluster is described quite well (Figure 3.4, bottom). The geometry relaxes,

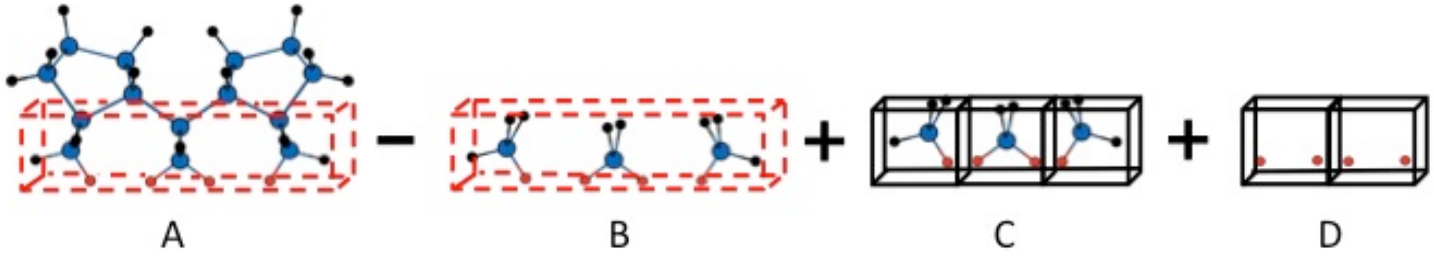

Figure 3.2. The hybrid energy scheme proposed for removing spurious repulsive intramolecular hydrogen interactions. The composite energy and gradient are evaluated as a sum of the energy and forces of each subsystem. Appropriate link atom scale factors must be used to terminate the broken bonds. Silicon atoms are in blue and hydrogen atoms are in black and red. Red hydrogen atoms contribute to the unphysical repulsive interactions of the silicon cluster.

allowing for H···H distances of 1.454 Å that is very close to the expected value. The corresponding potential energy curve is given as Figure 3.3. At the optimized geometry, the bottom layer is quite flat while the curvature of the surface is considerably minimized. The Si–Si dimers located at the reconstruction of the Si(100) cluster are slightly tilted inwards across dimer rows. Despite these small differences from an ideal Si(100) reconstructed surface, this model can be used to analyze important surface chemistry without the application of any constraints.

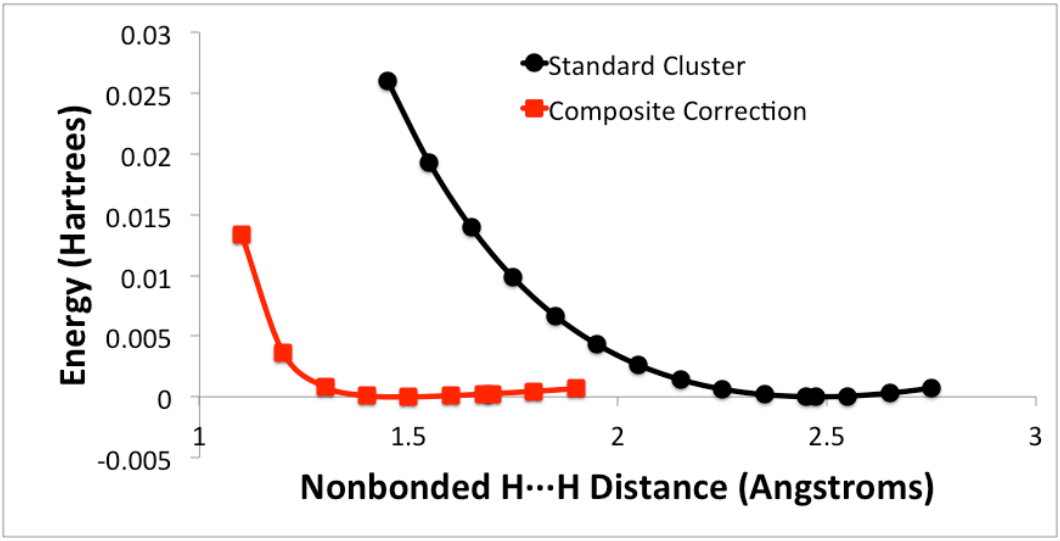

Figure 3.3. Relaxed scan of the non-bonded H···H distance on the bottom layer of the $Si_{21}H_{28}$ cluster. Energies were calculated at the B3LYP/6-31G(d,p) level of theory. The standard cluster has a minimum at 2.475 Å while our composite correction has a minimum at 1.454 Å.

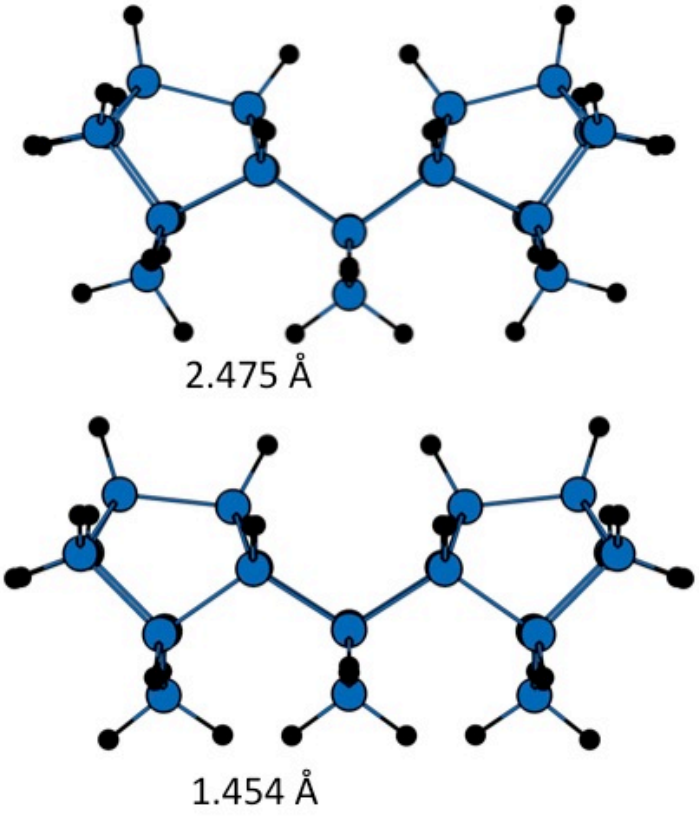

Figure 3.4. Optimized Si(100) cluster geometries at the B3LYP/6-31G(d,p) level of theory. Silicon atoms are in blue and hydrogen atoms are in black. A standard geometry optimization (top) leads to geometrical distortions, with bottom layer H···H distances at 2.475 Å. Geometry optimization utilizing our proposed composite energy scheme (bottom) has a minimum with bottom layer H···H distances at 1.454 Å.

3.2.2. Computational Details

All calculations were performed using the Gaussian Development Version[9] program package. The level of theory used in all the optimization of Si(100) clusters was B3LYP[10a, 10b, 10c/6-31G(d,p){Francl, 1982 #6, 10d, 10e]. A scale factor of 0.61 was used to determine the bond lengths involving link atoms (i.e., ratio of the bond lengths Si–H / Si–Si = 0.61).

3.2.3. Results and Discussion

Patterned line growth of allylic mercaptan (ALM) on the Si(100) surface has been of considerable interest in the silicon semiconductor surface community.[11] The line growth reactions result from radical-initiated chain reactions and have been investigated for many adsorbates. While many adsorbates undergo chain reactions *along* dimer rows, ALM reacts *across* dimer rows, leading to novel patterns on the Si(100) surface. We demonstrate the robustness of our method by efficiently using it to study surface reactions concerning such mechanisms.

In previous work, Ferguson, Than and Raghavachari[12] have used cluster models to theoretically investigate possible

mechanisms for radical initiated line growth across silicon dimer rows. The cluster models that were used to study these geometries required freezing the coordinates of all of the silicon atoms except for the top two layers in the model; this is a dramatically large constraint. However, such freezing of atoms was employed to ensure that large and unphysical geometric distortions are avoided. Our interaction deletion method provides an efficient alternative to overcome such severe unphysical constraints.

The first step in the line growth process across the Si dimers is the adsorption of ALM on a Si(100) surface at a localized radical site. Two products are possible at this step: one with a primary carbon radical (labeled "branched") and another with a secondary carbon radical (labeled "linear"). We have optimized the two possible initial adsorption products from the interaction of ALM with a surface radical site (Figure 3.5). Reasonable geometries are obtained for both structures with our composite energy approach.

Further, our method is useful for studying transition states as well. In the complete reaction mechanism, the carbon radical (branched or linear) rearranges to a sulfur radical (not shown). This is followed by an important step involved in the line growth, *viz.* a hydrogen atom abstraction reaction involving an interdimer

transition state. It involves the sulfur radical, in either a linear or branched structure, capturing a hydrogen atom from the neighboring dimer, breaking the Si–H bond, and creating a silicon radical localized on the adjacent dimer. The reactant, transition state, and product, obtained for both the branched and linear reaction pathways, are shown in (Figure 3.6). In all cases, our composite energy model has been employed to obtain the optimized geometries.

Since our composite energy method effectively cancels the unphysical hydrogen-hydrogen interactions, reasonable adsorbate geometries are obtained in all cases, including the transition states. The large buckling obtained in the unconstrained model is avoided for all the structures. The stretched S···H and H···Si distances are described appropriately in our model with minimal distortion from the bottom layer of the 4-layer Si(100) cluster model. This suggests that our Lennard-Jones-type parameters are transferable across the potential energy surface.

Energetically, our method is in agreement with the previous work of Ferguson *et al.*[12a] A 5.7 kcal/mol difference is obtained between the branched and linear initial adsorbates (**Fig. 4**), with the linear structure being preferred. This is very close to the value

obtained previously with the constrained model (5.4 kcal/mol) as well as that with an unconstrained cluster (5.7 kcal/mol). The close agreement between the different models is consistent with the fact that the structures all occur within a single dimer and may not be sensitive to the presence of surface strain.

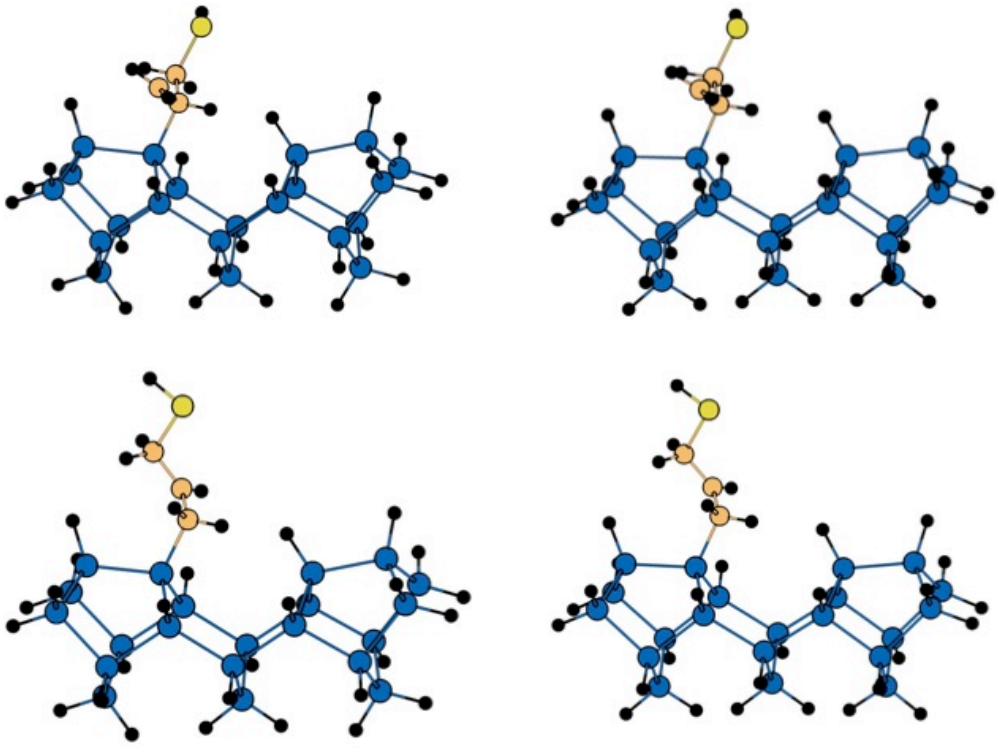

Figure 3.5. Optimized branched (top) and linear (bottom) allylic mercaptan adsorbate on Si(100) using a standard optimization procedure (left) and our defined hybrid energy method (right. Sulfur, carbon, silicon, and hydrogen are shown in yellow, orange, blue and black, respectively.

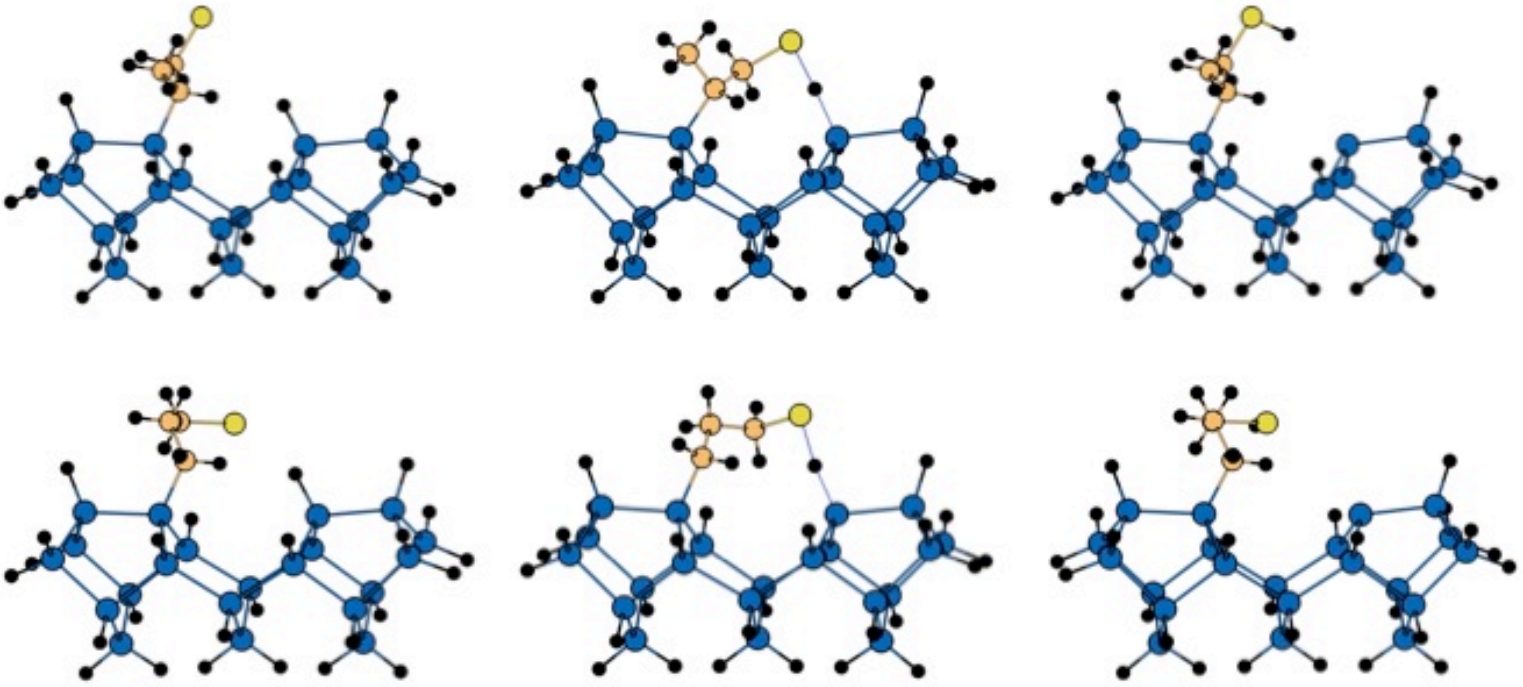

Figure 3.6. Optimized reactant (left), transition state (middle), and product (right), along a hydrogen abstraction coordinate with branched (top) and linear (bottom) allylic 1 mercaptan adsorbate on Si(100) using our defined hybrid method. Sulfur, silicon, and hydrogen are shown in yellow, blue, and black, respectively.

The transition state barrier height for the hydrogen abstraction process from an initial branched adsorbate (Figure 3.6) is 5.8 kcal/mol. This is within 1 kcal/mol of the value reported with the constrained cluster model (6.6 kcal/mol). Similarly, the linear adsorbate leads to a barrier height of 3.6 kcal/mol, and is in reasonable agreement with the 2.2 kcal/mol calculated from the constrained cluster model. However, the relative energy barrier between the branched and linear adsorbate structures changes significantly from 2.2 kcal/mol (current model) to 4.4 kcal/mol (constrained model). Interestingly, the unconstrained cluster model calculations predict barrier heights (5.0 kcal/mol and 3.3 kcal/mol, respectively, for branched and linear adsorbates) that are quite close to our new model. While the current results suggest that the previous models perform satisfactorily for this system, larger differences between the different models are likely to be seen for more complex reactions involving direct bridge bonds between adjacent dimers. In general, much larger cluster models which avoid such unphysical interactions would be needed to get reliable results for such complex systems. However, we can efficiently obtain results which should be comparable in accuracy to such more expensive calculations using our novel composite method.

3.3. Interaction Deletion: A Composite Energy Method for the Optimization of Molecular Systems Selectively Removing Specific Non-Bonded Interactions

3.3.1. Background

Weak interactions caused by intermolecular and intramolecular forces affect the equilibrium positions of the nuclei contained in the chemical model. The total perturbation in the geometrical structure can be quantified by invoking the concept of strain energy. Previous efforts have attempted to determine the amount of strain energy in complete and select portions of a molecular system.[20] In this work, we will describe a simple way to measure the strain energy contributed from user-selected groups of atoms through the use of geometry optimizations.

Our approach is to use composite energy models that minimize geometrical parameters without selected non-covalent interactions. In previous work, we have suggested a composite PBC-LC model (periodic boundary condition at low coverage) to study chemical reactions of adsorbates on surfaces by removing intercell adsorbate-adsorbate interactions on Si(111) surfaces.[7] We have also suggested a method that reduces major geometrical

distortions Si(100) clusters caused by the artificial truncation of bulk Si–Si bonds.[21] With a novel scheme defined below, we suggest a general way of defining a composite method to essentially remove atom-atom interactions such as hydrogen bonds from an ab-initio or DFT based calculation. Geometry optimizations with such a composite energy are illustrative in understanding the nature of such weak interactions and their structural consequences.

3.3.2. Method

To effectively cancel specified non-covalent interactions, the energies and forces from the complete molecular system of choice must be appropriately altered. We illustrate the implementation of our method by using 1,6-hexanediol, containing an intramolecular hydrogen bond, as an example. We want to define a composite energy that has the specific interaction energy removed (Equation 3.3).

$$E(\text{composite}) = E(\text{full}) - E(\text{interaction}) \qquad (3.3)$$

E(interaction) itself can be defined in terms of truncated subsystems that contain the specified interaction. The simplest

scheme will be to truncate at the location of the two oxygen atoms, i.e., excise the O–C bonds and replace them with O–H bonds using hydrogen link atoms (*vide infra*). Then, the interaction energy for 1,6-hexanediol can be defined as the difference in energy between the interacting system (water dimer) and the two non-interacting systems (water monomers). Each calculation utilizes the coordinates of the full system.

While the above scheme is well-defined and simple, it is likely to be inadequate to represent the interaction energy accurately. The selected interactions contained in the full molecular system and the truncated fragments are not balanced since their chemical environments are very different. This imbalance can be corrected by including parts of the backbone in each truncated system. For example, if the first neighbor effects are included, this will yield a methanol dimer as the model interacting system, and two methanol monomers as the non-interacting analogues. In a similar manner, other progressively more complete model systems can be defined. If an increasing part of the backbone is included in each truncated fragment, the monomers begin to overlap, and this has to be taken into account to avoid overcounting. In the general case, the interaction energy can be defined as Equation 3.3:

$$E(\text{interaction}) = E(D \cup A) - E(D) - E(A) + E(D \cap A) \quad (3.3)$$

where D and A stand for the truncated donor and acceptor model systems, and ∪ and ∩ stand for union and intersection operators, respectively. If the complete backbone is included for the donor as well as the acceptor, E[D∪A] is the same as E(full), and we can define a composite hybrid energy scheme as below:

The most straightforward hybrid energy scheme can be defined as below in Equation (3.4):

$$E(\text{composite}) = E_{\text{OH Donor, Backbone}} + E_{\text{OH Acceptor, Backbone}} - E_{\text{Backbone}} \quad (3.4)$$

where $E_{\text{OH Donor, Backbone}}$ is the energy of a fragment defined from the total system geometry that contains the intramolecular hydrogen bond acceptor and the common backbone of the molecule, which in the example of 1,6-hexanediol would be hexanol. , Similarly, $E_{\text{OH Donor, Backbone}}$ would contain the intramolecular hydrogen bond acceptor and the common backbone and E_{Backbone} is the system without any hydroxyl groups. The composite energy is defined similarly to what is defined in the Connectivity Based Heirarchy, where double counting of overlapping fragments are cancelled to preserve bonding between atoms.[22] An example is illustrated in Figure 3.7. Each calculation utilizes the coordinates of the full system that is

excised appropriately to describe the relevant interactions. Whenever covalent bonds are broken, the unsatisfied valences are terminated with hydrogen link atoms.[23] The link atoms utilize scale factors to give an appropriate bonding description, as in the standard ONIOM method. The required gradients are also a sum of the gradients for each sub-calculation. The link atom gradients are projected onto the host and supporting atoms, as in the standard ONIOM approach.

The energies and gradients from this composite energy expression can then be employed to perform geometry optimizations. Every calculation is performed with the same basis set and method. This creates a simple implementation for existing electronic structure software to perform energy evaluations and geometry optimizations. Therefore, our novel method can explore the energetic and geometric consequences of non-covalent interactions (such as hydrogen bonding) or defined fragments atoms. The method is general, and can be used with any ab-initio or density functional approach.

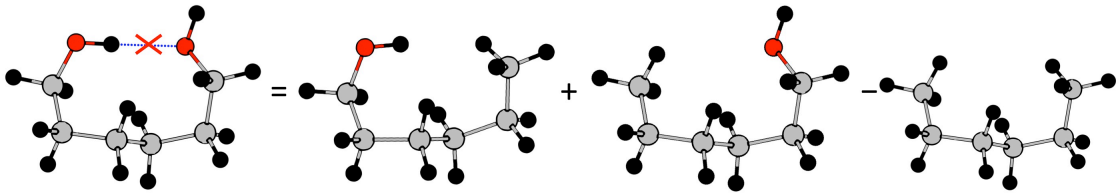

Figure 3.7. Pictorial representation of the proposed composite energy scheme. In this example, three user-defined, independent calculations are formed such that the difference of energies leads to the forces and energy of the hydrogen bond being removed from the total system. Link atoms are used to cap the severed covalent bonds.

3.3.3. Computational Details

All ab-initio calculations were performed at the MP2/6-31+G(d,p) level of theory[10d, 10e, 24] using the Gaussian 09 set of programs.[9] For each system being investigated (*vide infra*), the geometries were initially optimized to minimize the traditional MP2 energy. These structures were then used for single point evaluations with our new composite energy to evaluate the strength of the hydrogen bonding interaction at this geometry. More importantly, we perform geometry optimizations *to minimize the composite energy* discussed above. This will provide the preferred

geometry for the system where the chosen interaction is “turned off” while keeping the rest of the molecular interactions intact.

We illustrate the applicability of our method using the following three examples:

(1) First, we consider two conformations of 1,6-hexanediol, one with a strong intramolecular hydrogen bond, and the other without any intramolecular hydrogen bond.[25] The first conformation is the $tG^{+}G^{+}TG^{+}G^{+}g^{-}$ form shown in Figure 3.8(a). We use the standard notation[25] where t, g denote the trans or gauche nature of the terminal hydroxyl group, while T, G denote the trans and gauche orientation of the carbon-carbon bonds. G^{+} denotes a dihedral angle around -60°, while G^{-} denotes a dihedral angle around $+60^{\circ}$. This structure has a strong intramolecular hydrogen bond that will be investigated by our approach. We compare it with a second all-trans conformation, shown in Figure 3.8(b), where there is no possibility of a hydrogen bond.

(2) Second, we consider two conformations of 1,4-cyclohexanediol. Again, the first conformation, based on a disubstituted twist-boat conformation of cyclohexane shown in Figure 3.10(a), has a strong intramolecular hydrogen bond.[26] The composite method optimization of the twist-

boat conformation leads to structures that reflect a lack of hydrogen bonding in the model. We compare it with a second conformation, based on a disubstituted chair conformation of cyclohexane shown in Figure 3.10(b), that does not have a intramolecular hydrogen bond.

(3) Third, we demonstrate the applicability of our method for a larger problem involving a dissociative adsorption of ammonia on a Si(100) surface, shown in Figure 3.12. The adsorption of NH_3 on two adjacent dimer sites can give rise to inter-dimer hydrogen bond between two adjacent NH_2 groups that will be analyzed with our approach.

3.3.4. Results and Discussion

3.3.4.1. 1,6-Hexanediol

As mentioned above, for 1,6-hexanediol, hydrogen bonding can occur in the $tG^+G^+TG^+G^+g^-$ conformation, Figure 3.8.(a), while the fully trans conformation, Figure 3.8.(b), cannot have intramolecular hydrogen bonds. The hydrogen bonding distance in the standard MP2 optimized structure for Figure 3.8.(a) is 2.023 Å. This is in the range of typical OH···O distances seen in water clusters, 1.8–2.0 Å, indicating a strong hydrogen bond. In fact, the presence of this hydrogen bond makes this conformation to be more stable than the

all-trans conformation by 2.9 kcal/mol at the MP2/6-31+G(d,p) level, reversing the order seen for the parent hexane where the trans conformation is more stable by 1.2 kcal/mol. While larger basis sets may be needed to calculate definitive relative energies for such conformations, the key physically important points can all be seen in our results.

A particularly important point here is that there is significant strain in Figure 3.8.(a) since it has to adopt a structure conducive to the formation of the hydrogen bond. Consequentially, the backbone of Figure 3.8.(a) has to distort sufficiently to allow the atoms involved in the hydrogen bond to point towards each other at a close enough distance to interact in a stabilizing manner. This may be roughly considered as a “preparation energy”, an energy penalty that partially offsets the stabilization energy due to the formation of the hydrogen bond. Our interaction deletion method allows a clear, quantitative understanding of the different factors involved.

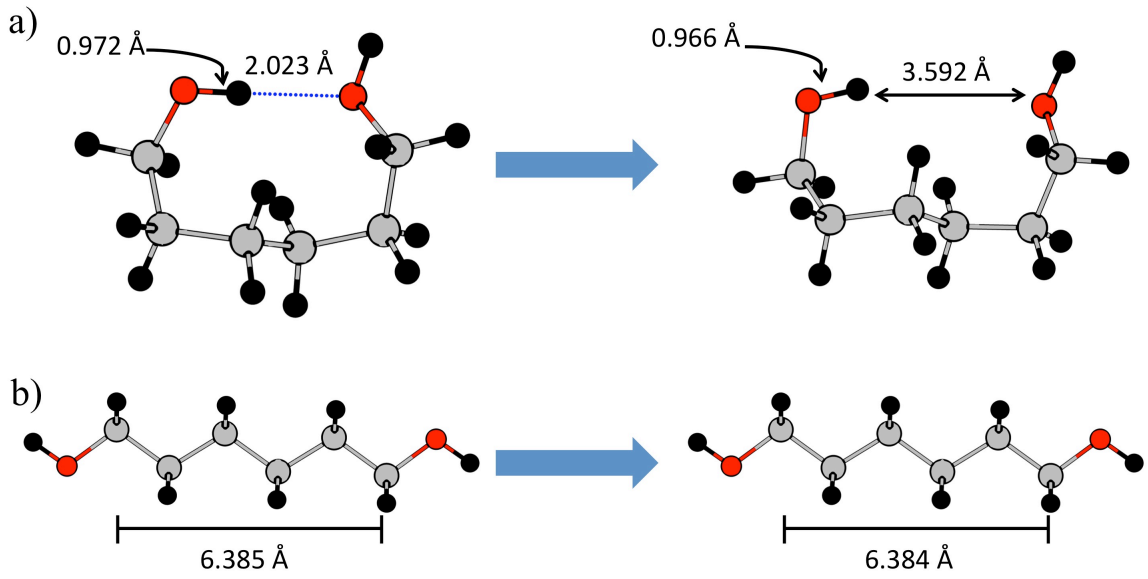

Figure 3.8. The structures of optimized (a) 1,6-(tG$^+$G$^+$TG$^+$G$^+$g$^-$)-hexanediol and (b) 1,6-(tTTTt)-hexanediol with two different methods. Structures positioned on the left side of (a) and (b) were optimized using standard MP2/6-31+G(d,p). Structures on the right side of (a) and (b) were optimized using the composite energy scheme proposed with MP2/6-31+G(d,p).

The interaction between the two hydroxyl groups can be analyzed in terms of some key geometrical parameters. The O···O distance is 2.995 Å, indicating a nearly linear hydrogen bond. The most useful geometrical parameter that illustrates the nature of the backbone distortion is the $C_1 \cdots C_6$ distance. The standard MP2

geometry optimization of Figure 3.8.(a) results in the $C_1 \cdots C_6$ distance of 4.416 Å. For comparison, the corresponding $C_1 \cdots C_6$ distance in the *same conformation of the parent hexane* (G^+TG^+) is 5.073 Å. It is clear that hydrogen bonding does cause a distortion of the backbone of the molecule to obtain the stability provided from the interaction.

Now we can consider the effect of using our composite model to turn off the hydrogen bonding interaction. Using a full *geometry optimization* with our composite energy method leads to a $C_1 \cdots C_6$ distance of 5.073 Å, in agreement with the parent hexane (5.073 Å) where the carbon backbone is in the same conformation, but without any hydrogen bonds. More interestingly, the relaxation of the backbone causes the OH···O distance to increase to 3.592 Å, a clear consequence of the cancellation of the interaction between the two groups. The OH bond distance of the hydrogen donating hydroxyl group decreases from 0.972 to 0.966 Å, consistent with the lack of a hydrogen bond. While the other distances and angles change somewhat, the most dramatic effect is observed on the hydrogen bonding atoms.

In contrast to the intramolecular hydrogen bonding case of Figure 3.8.(a), the fully trans conformation of 1,6-hexanediol does

not distort or change with the use of our composite energy method. The standard MP2 geometry optimization creates a head to tail $C_1 \cdots C_6$ distance of 6.385 Å. This is in agreement to our composite energy optimization when removing the OH···OH interaction, with a distance of 6.384 Å. For comparison, the corresponding parent hexane conformation (TTT) has a very similar $C_1 \cdots C_6$ distance of 6.419 Å at the same MP2/6-31+G(d,p) level of theory. Therefore, our method is robust and can describe the appropriate physics of the molecular system even when omitting interactions.

The energetic effects of our method can also be considered, as represented in Figure 3.9. As expected, there is a negligible energy difference (0.0 kcal/mol) for Figure 3.8.(b). For Figure 3.8.(a), the difference between the standard MP2 energy and our composite energy at the respective *optimized geometries* is 3.2 kcal/mol, the latter being higher in energy due to the effective removal of the hydrogen bond. The total 3.2 kcal/mol of instability from the loss of hydrogen bonding can be elucidated further by taking the difference between the standard MP2 energy and the composite model *single point energy* with the MP2 optimized structure. This leads to a value of 5.6 kcal/mol, quantifying the loss of the stabilizing effect of the hydrogen bond in the absence of

any geometric relaxation. To investigate the contribution of geometry relaxation in Figure 3.8.(a), the difference between the single point composite energy and the fully optimized composite energy leads to a value of 2.4 kcal/mol. The total energy of the hydrogen bond is thus the difference of the two components, leading to a value of 3.6 kcal/mol, as seen above.

The discussion above suggests that the preparation energy penalty is 2.4 kcal/mol. To consider if this is meaningful, we performed calculations on the *parent hexane* to compute the energy difference between the optimized structure and that evaluated at the optimized structure for Figure 3.8.(a), after replacing the two hydroxyl groups with hydrogen atoms. This yields the energy penalty on distorting the backbone hydrocarbon skeleton in preparing Figure 3.8.(a) for hydrogen bonding. The resulting energy difference for hexane is 2.7 kcal/mol, very close to the value derived for 1,6-hexanediol of 2.4 kcal/mol. While the good agreement suggests a good performance for our method, the important point is that the energy from the composite method has been derived from the full molecule after effectively omitting specific hydrogen bonding interactions.

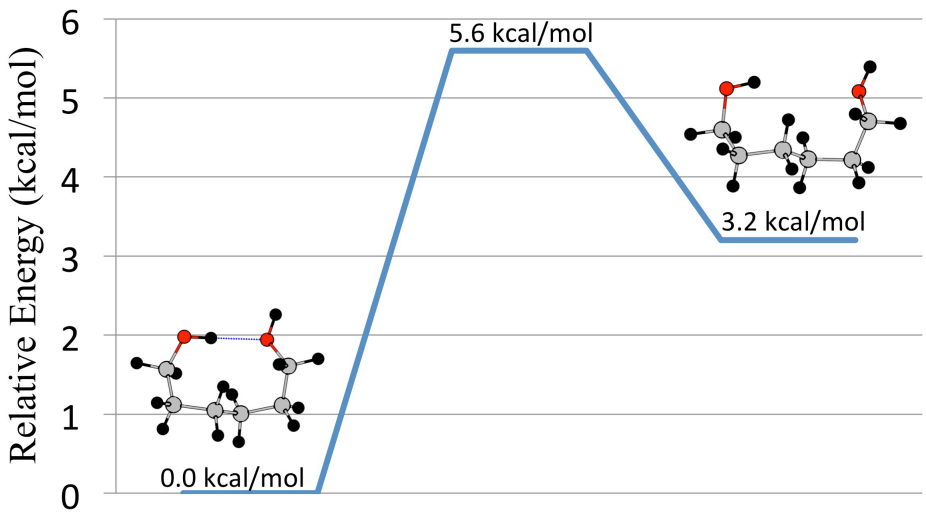

Figure 3.9. Energy profile of 1,6-(tG^{+}G^{+}TG^{+}G^{+}g^{-})-hexanediol obtained from comparisons between the standard MP2 energy and geometries with those obtained from a single point energy (Figure 3.8.(a), left) with the composite energy scheme (5.6 kcal/mol) and optimized geometry (Figure 3.8.(a), right) with the composite energy scheme (3.2 kcal/mol).

3.3.4.2. 1,4-Cyclohexanediol

The second example is a twist-boat conformation of cis-1,4-cyclohexanediol that allows an intramolecular hydrogen bond across the ring system. At the fully optimized geometry at the

MP2/6-31+G(d,p) level, the hydrogen bond distance is 1.922 Å, even shorter than the value of 2.023 Å seen earlier for 1,6-hexanediol. Again, the hydrogen bonded conformation will be compared with a different conformation (chair form) where hydrogen bonding is not possible. While the basic concepts used in the analysis are analgous to those for 1,6-hexanediol, the results will lead to a description of molecular relaxation unique to what was described for a linear system containing a intramolecular hydrogen bond.

When our composite energy is employed for geometry optimizations on the chair isomer (Figure 3.10(b)), there are completely negligible differences between our newly obtained geometries and those from the standard MP2 optimization. This suggests that very little hydrogen bonding interactions are occurring in the system, as expected. However, when cis-1,4-cyclohexanediol is in the twist-boat conformer, hydrogen bonding occurs when the hydroxyl groups are appropriately pointed towards each other. The structures of the twist-boat conformer are shown in Figure 3.10(a). In this case, some dramatic changes occur between results for geometry optimizations between traditional MP2 and our novel composite method. Most notably, the OH···O distance *increases* from the value of 1.922 Å to 1.995 Å.

The explanation for this behavior comes from the ring constraint present in this example. In the fully optimized structure, the carbon atoms that are bonded to the two functional groups are at a distance of 2.831 Å. It should be noted that this distance is longer than the distance found in the parent hydrocarbon cyclohexane in the same twist-boat conformation (2.755 Å), i.e., the ring system accommodated the hydrogen bond by causing significant geometric strain (i.e., expansion) on the ring itself, as without this geometric change, the two hydroxyl groups would have been too close to create an optimal hydrogen bond. When the hydrogen bond is not present, the hydroxyl groups relax closer to its optimal geometry, and the 1,4-distance shortens to 2.822 Å. In turn, this causes the hydroxyl groups to obtain a conformation where hydrogen bonding does not occur, consistent with the natural bond and dihedral angles for the system. Thus, the observations can be attributed to the relaxation in the ring system.

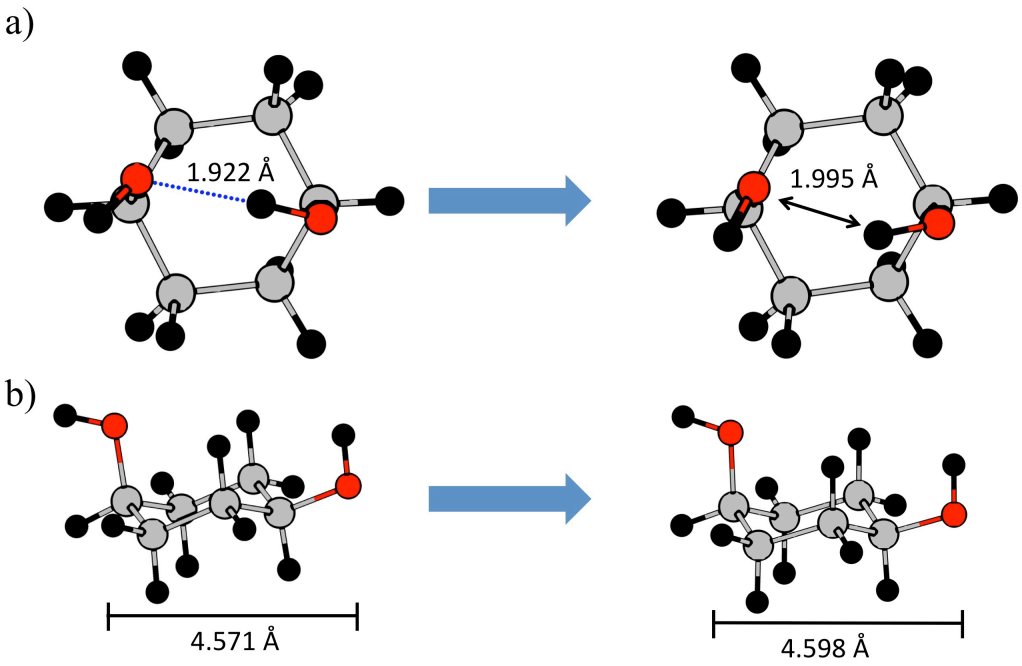

Figure 3.10. The structures of optimized cis-1,4-cyclohexane with two different methods. The left structures in the twist-boat (a) and chair (b) conformations were optimized using standard MP2/6-31+G(d,p). The right structures were optimized using the composite energy scheme with MP2/6-31+G(d,p).

The energetic consequences from removing the intramolecular hydrogen bond in cis-1,4-cyclohexanediol were also considered. The relative energies and associated geometries are reported in Figure 3.11. For Figure 3.10.(a), the difference between the standard MP2 energy and our composite energy at the respective *optimized geometries* is 3.9 kcal/mol. This is in agreement with the value of 3.2 kcal/mol seen earlier in 1,6-

hexanediol, Figure 3.8.(a). The difference between the standard MP2 energy and the composite model *single point energy* with the MP2 optimized structure for Figure 3.10.(a) yields a value of 4.4 kcal/mol, indicating the strength of the hydrogen bond in the absence of any geometric relaxation. The difference between the two values seen for Figure 3.10.(a), yields a preparation energy of 0.5 kcal/mol. For comparison, we performed calculations on the *parent cyclohexane* to compute the energy difference between the optimized structure and that evaluated at the optimized structure for Figure 3.10.(a), after replacing the two hydroxyl groups with hydrogen atoms. The resulting energy penalty for distorting the backbone for cyclohexane is 1.3 kcal/mol, reasonably close to the previous value of 0.5 kcal/mol. The difference may reflect the fact that the composite method reflects the full molecule rather than just the parent hydrocarbon.

Traditional MP2/6-31+G(d,p) optimizations of the chair and twist-boat conformations of cyclohexane predict a 6.5 kcal/mol preference for the chair structure, in agreement with a previously reported MP2 relative energies with a double-zeta basis set with d polarization functions.[27] Comparison of this energetic preference to our cyclohexane

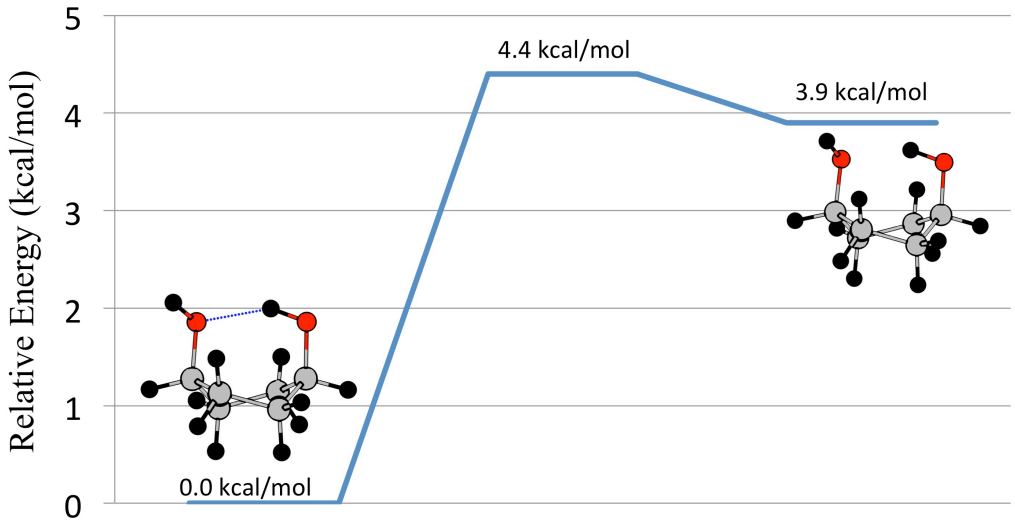

Figure 3.11. Energy profile of cis-1,4-cyclohexanediol obtained from comparisons between the standard MP2 energy and geometries with those obtained from a single point energy (Figure 3.10.(a), left) with the composite energy scheme (3.9 kcal/mol) and optimized geometry (Figure 3.10.(a), right) with the composite energy scheme (1.9 kcal/mol).

diol systems are illustrative. In the presence of hydrogen bonding, the preference for the chair structure decreases to 2.6 kcal/mol. Our analysis shows that part of this decrease (0.5 kcal/mol) comes from hydrogen bonding while the rest comes from the substitution itself. For cis-1,4-dimethylcyclohexane, a system which contains substituent effects without intramolecular hydrogen bonds, has a 5.2 kcal/mol preference for the chair conformation. The substituent effects, therefore, play a role in the geometric

relaxation of cis-1,4-cyclohexanediol. In fact, for 2,5-dimethyl 1,4-cyclohexanediol, the intramolecularly hydrogen-bonded twist-boat conformation appears to be comparable in stability to the chair conformation.[26a] The energetic preference for the chair structure is only 0.3 kcal/mol at the MP2/6-31G(d,p) level of theory.

3.3.4.3 Ammonia adsorption on Si(100)

Larger systems can also be studied with our composite energy method. To demonstrate its capability as to tool to elucidate weak interactions on surface models, we modeled the dissociation products of ammonia molecules on a fully relaxed $Si_{15}H_{16}$ cluster model representing two adjacent dimers on the Si(100) surface. Coverage dependence has been experimentally shown to be associated with shifts of the Si–H stretching frequencies of the dissociated ammonia.[28] We use this molecular system as an example of how our composite energy method can be used to quantify and describe the energetic changes and geometric distortions that occur as nearby adsorbates interact at higher coverages.

When two ammonia adsorbates dissociate on neighboring dimers in a Si(100) dimer row, one hydrogen bond is formed. At

the MP2/6-31G+(d,p) level, the hydrogen bond length is 2.382 Å. Performing a geometry optimization at the MP2/6-31+G(d,p) level using our composite energy method shows a relaxation of the geometry without the presence of the interdimer hydrogen bond. The distance between the two adsorbates, the NH···N distance, has increased in length to 2.754 Å. Geometries are reported in Figure 3.12. The strain energy in the adsorbate is now decreased in the absence of any stability from the formation of a hydrogen bond.

In order to understand the results from the calculation are reasonable, we compare the geometry optimization of the cluster model of 2 dissociated NH_3 on Si(100) with our composite energy scheme with a single NH_3 dissociated on a fully relaxed $Si_{15}H_{16}$ cluster with a standard geometry optimization using MP2/6-31+G(d,p). Figure 3.13 contains the optimized geometries of these two systems. The structures determined from these two calculations describe NH_2 functional groups that do not contain hydrogen bonds, as evident by their agreement in geometrical parameters. The Si–N–H bond angles, which describe the distortion of the amine group is 119.1° for our composite energy optimized geometry and 115.2° for a single dissociated ammonia on a hydrogen terminated si(100) surface, indicating that the results from our novel method are in agreement with a system that can

not contain hydrogen bonding. A second notable geometric parameter is the N–H bond distance, with values of 1.012 and 1.017 Å for the composite optimized and standard MP2 optimized systems, respectively. These values confirm the validity of our newly determined geometrical parameters describe a system where the weak hydrogen bond interaction has been excluded, as the standard hydrogen bond donor N–H bond distance is 1.018, slightly longer than those reported for the cases where this interaction does not exist.

The relative energies and associated geometries from the composite and standard MP2 optimized geometries are reported in Figure 3.14. For two dissociated ammonia on Si(100) at high coverage, the total interaction energy, including geometric and hydrogen bonding interactions is 2.0 kcal/mol. The strength of the hydrogen bond at the standard MP2 is calculated as 2.5 kcal/mol. The preparation energy of this system is 0.5 kcal/mol. This outcome is reasonable, as the silicon cluster did not have to undergo a large geometric distortion in order for they hydrogen bond to stabilize the total energy of the system.

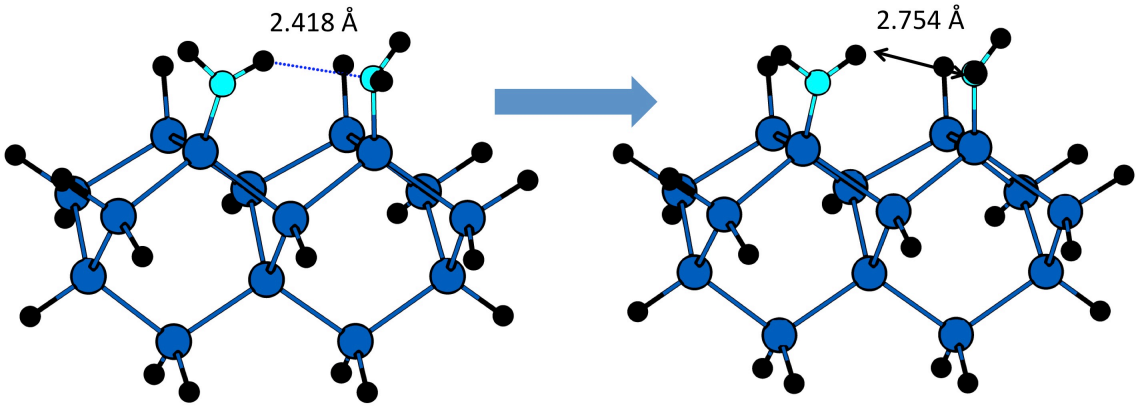

Figure 3.12. The optimized structures of two ammonia adsorbates dissociated on a $Si_{15}H_{16}$ cluster using two different methods: (left) standard geometry optimization using MP2/6-31+G(d,p) and (right) composite energy scheme using MP2/6-31+G(d,p).

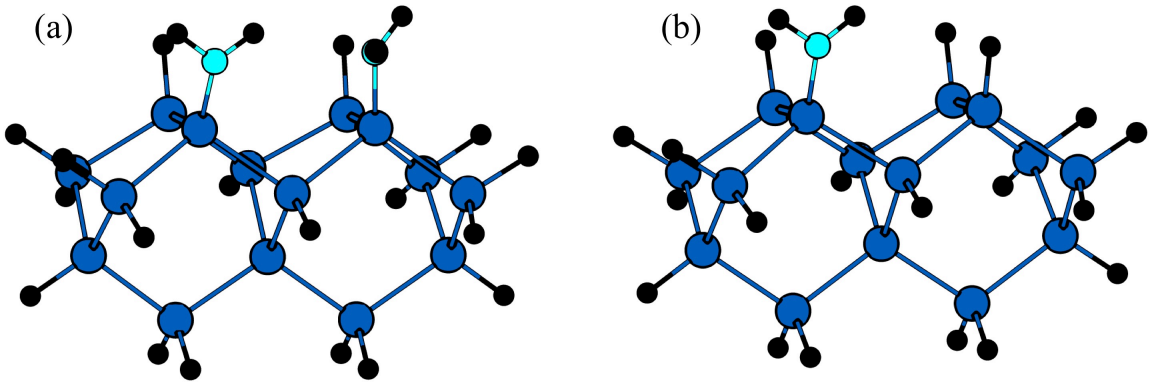

Figure 3.13. Comparison of our Interaction Deletion obtained geometry of two dissociated ammonia adsorbates with a singly dissociated ammonia and H-passivated $Si_{15}H_{16}$ cluster.

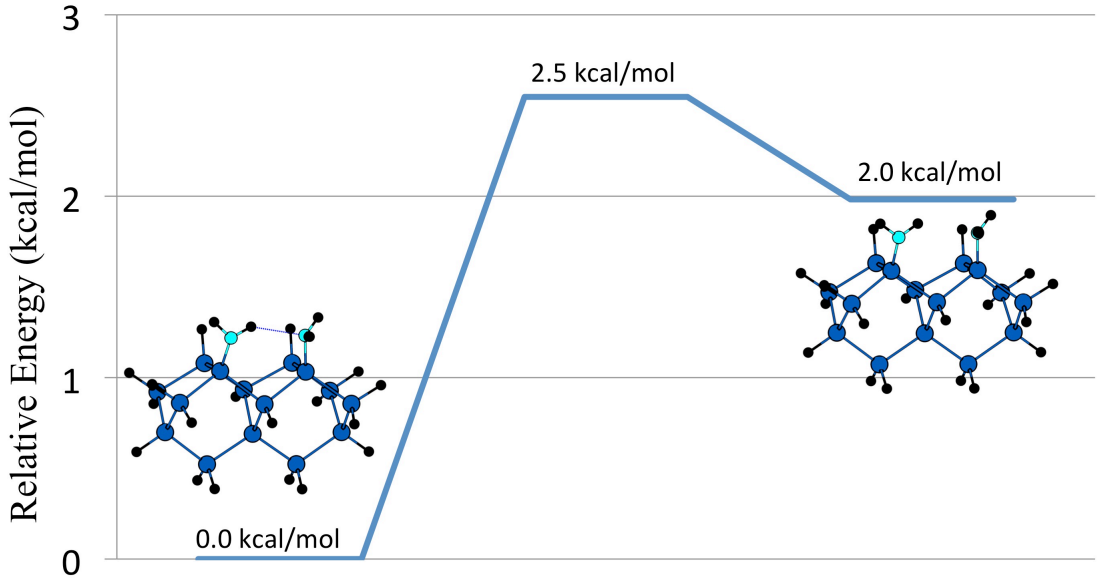

Figure 3.14. Energy profile of two dissociated ammonia on Si(100) obtained from comparisons between the standard MP2 energy and geometries with those obtained from a single point energy (6, left) with the composite energy scheme (3.6 kcal/mol) and optimized geometry (6, right) with the composite energy scheme (3.0 kcal/mol).

3.4. Conclusions

We have defined two composite methods with which we can optimize the geometrical parameters. A hybrid scheme was defined for a sterically hindered cluster model representing the Si(100) surface. The hybrid energy effectively cancels the unphysical intramolecular H···H interactions due to truncation of the reconstructed silicon surface. The located minima obtained for the initial interaction of allylic mercaptan on the Si(100) surface as well as some of the key transition states are described well with our new model. Overall, our composite energy method should be useful for many future applications involving chemistry on the Si(100) surface. However, this method is not the only composite method that can be generalized to solve the problem of selectively removing weak interactions from a molecular system. Non-periodic systems can also contain interactions that can have geometric consequences. A general composite energy method was described that can be used to selectively remove all interactions between any two atoms or fragments in a finite molecular system.

We have proposed a novel hybrid scheme that can be utilized to gain understanding into the energetics of weak interactions such as hydrogen bonds and their contributions to the associated strain

energies in molecular systems. The specific atom-atom interactions can be user-defined and the method is general for any ab-initio or density functional method. Energies and forces are easily obtained with this composite approach, allowing geometry optimizations that lead to chemically meaningful structures that describe how the canceled interactions contribute to the local geometrical minima. We illustrate the application of our new hybrid scheme by computing the influence of intramolecular hydrogen bonding interactions in two small molecules, 1,6-($tG^+G^+TG^+G^+g^-$)-hexanediol and cis-1,4-cyclohexanediol. We demonstrate that the composite method can be extended to larger molecular systems by showing its application on a Si(100) surface model containing interactions between dissociated ammonia on adjacent surface dimers. The method is robust and should be applicable for other large molecular studies, such as those in materials systems and biomolecules.

3.5. References

1. Higashi, G. S.; Chabal, Y. J.; Trucks, G. W.; Raghavachari, K., Ideal hydrogen termination of the Si (111) surface. *Applied Physics Letters* **1990,** *56* (7), 656-658.

2. Buriak, J. M., Organometallic Chemistry on Silicon and Germanium Surfaces. *Chemical Reviews* **2002,** *102* (5), 1271-1308.

3. Neergaard Waltenburg, H.; Yates, J. T., Surface Chemistry of Silicon. *Chemical Reviews* **1995,** *95* (5), 1589-1673.

4. (a) Solares, S. D.; Michalak, D. J.; Goddard, W. A.; Lewis, N. S., Theoretical Investigation of the Structure and Coverage of the Si(111)–OCH3 Surface. *The Journal of Physical Chemistry B* **2006,** *110* (16), 8171-8175; (b) Solares, S. D.; Yu, H.; Webb, L. J.; Lewis, N. S.; Heath, J. R.; Goddard, W. A., Chlorination–Methylation of the Hydrogen-Terminated Silicon(111) Surface Can Induce a Stacking Fault in the Presence of Etch Pits. *Journal of the American Chemical Society* **2006,** *128* (12), 3850-3851; (c) Yu, H.; Webb, L. J.; Solares, S. D.; Cao, P.; Goddard, W. A.; Heath, J. R.; Lewis, N. S., Scanning Tunneling Microscopy of Ethylated Si(111) Surfaces Prepared by a

Chlorination/Alkylation Process. *The Journal of Physical Chemistry B* **2006,** *110* (47), 23898-23903.

5. Raghavachari, K.; Halls, M. D., Quantum chemical studies of semiconductor surface chemistry using cluster models. *Molecular Physics* **2004,** *102* (4), 381-393.

6. (a) Svensson, M.; Humbel, S.; Froese, R. D. J.; Matsubara, T.; Sieber, S.; Morokuma, K., ONIOM: A Multilayered Integrated MO + MM Method for Geometry Optimizations and Single Point Energy Predictions. A Test for Diels–Alder Reactions and $Pt(P(t\text{-}Bu)_3)_2 + H_2$ Oxidative Addition. *The Journal of Physical Chemistry* **1996,** *100* (50), 19357-19363; (b) Vreven, T.; Byun, K. S.; Komáromi, I.; Dapprich, S.; Montgomery, J. A.; Morokuma, K.; Frisch, M. J., Combining Quantum Mechanics Methods with Molecular Mechanics Methods in ONIOM. *Journal of Chemical Theory and Computation* **2006,** *2* (3), 815-826; (c) Vreven, T.; Morokuma, K.; Farkas, Ö.; Schlegel, H. B.; Frisch, M. J., Geometry optimization with QM/MM, ONIOM, and other combined methods. I. Microiterations and constraints. *Journal of Computational Chemistry* **2003,** *24* (6), 760-769.

7. Gamoke, B. C.; Mayhall, N. J.; Raghavachari, K., Modeling Nonperiodic Adsorption on Periodic Surfaces: A Composite Energy Approach for Low-Coverage Limits. *The Journal of Physical Chemistry C* **2012,** *116* (22), 12048-12054.

8. Mayo, S. L.; Olafson, B. D.; Goddard, W. A., DREIDING: a generic force field for molecular simulations. *The Journal of Physical Chemistry* **1990,** *94* (26), 8897-8909.

9. Frisch, M. J.; Trucks, G. W.; Schlegel, H. B.; Scuseria, G. E.; Robb, M. A.; Cheeseman, J. R.; Scalmani, G.; Barone, V.; Mennucci, B.; Petersson, G. A.; Nakatsuji, H.; Caricato, M.; Li, X.; Hratchian, H. P.; Izmaylov, A. F.; Bloino, J.; Zheng, G.; Sonnenberg, J. L.; Hada, M.; Ehara, M.; Toyota, K.; Fukuda, R.; Hasegawa, J.; Ishida, M.; Nakajima, T.; Honda, Y.; Kitao, O.; Nakai, H.; Vreven, T.; Montgomery, J. A.; Peralta, J. E.; Ogliaro, F.; Bearpark, M.; Heyd, J. J.; Brothers, E.; Kudin, K. N.; Staroverov, V. N.; Kobayashi, R.; Normand, J.; Raghavachari, K.; Rendell, A.; Burant, J. C.; Iyengar, S. S.; Tomasi, J.; Cossi, M.; Rega, N.; Millam, J. M.; Klene, M.; Knox, J. E.; Cross, J. B.; Bakken, V.; Adamo, C.; Jaramillo, J.; Gomperts, R.; Stratmann, R. E.; Yazyev, O.; Austin, A. J.; Cammi, R.; Pomelli, C.; Ochterski, J. W.; Martin, R. L.; Morokuma, K.; Zakrzewski, V. G.; Voth, G. A.; Salvador, P.; Dannenberg, J. J.; Dapprich, S.; Daniels, A. D.; Farkas; Foresman, J.

B.; Ortiz, J. V.; Cioslowski, J.; Fox, D. J. *Gaussian 09, Revision C.01*, Wallingford CT, 2009.

10. (a) Becke, A., Density-functional exchange-energy approximation with correct asymptotic behavior. *Physical Review A* **1988,** *38* (6), 3098-3100; (b) Becke, A. D., Density - functional thermochemistry. III. The role of exact exchange. *The Journal of Chemical Physics* **1993,** *98* (7), 5648-5652; (c) Lee, C.; Yang, W.; Parr, R., Development of the Colle-Salvetti correlation-energy formula into a functional of the electron density. *Physical Review B* **1988,** *37* (2), 785-789; (d) Hariharan, P. C.; Pople, J. A., The influence of polarization functions on molecular orbital hydrogenation energies. *Theoret. Chim. Acta* **1973,** *28* (3), 213-222; (e) Krishnan, R.; Binkley, J. S.; Seeger, R.; Pople, J. A., Self - consistent molecular orbital methods. XX. A basis set for correlated wave functions. *The Journal of Chemical Physics* **1980,** *72* (1), 650-654.

11. (a) Hossain, M. Z.; Kato, H. S.; Kawai, M., Fabrication of Interconnected 1D Molecular Lines along and across the Dimer Rows on the Si(100)–(2 × 1)–H Surface through the Radical Chain Reaction. *The Journal of Physical Chemistry B* **2005,** *109* (49), 23129-23133; (b) Hossain, M. Z.; Kato, H. S.; Kawai, M., Self-Directed Chain Reaction by Small Ketones with the Dangling Bond Site on

the Si(100)-(2 × 1)-H Surface: Acetophenone, A Unique Example. *Journal of the American Chemical Society* **2008,** *130* (34), 11518-11523; (c) Hossain, M. Z.; Kato, H. S.; Kawai, M., Valence States of One-Dimensional Molecular Assembly Formed by Ketone Molecules on the Si(100)-(2 × 1)-H Surface. *The Journal of Physical Chemistry C* **2009,** *113* (24), 10751-10754.

12. (a) Ferguson, G. A.; Than, C. T.-L.; Raghavachari, K., Line Growth on the H/Si(100)-2 × 1 Surface: Density Functional Study of Allylic Mercaptan Reaction Mechanisms. *The Journal of Physical Chemistry C* **2009,** *113* (43), 18817-18822; (b) Ferguson, G. A.; Than, C. T.-L.; Raghavachari, K., Extending Molecular Lines on the Si(100)-2 × 1 Surface: A Theoretical Study of the Effect of Allylic Mercaptan Adsorbates on Radical Chain Reactions. *The Journal of Physical Chemistry Letters* **2010,** *1* (4), 679-685.

13. (a) Dill, K. A., Dominant forces in protein folding. *Biochemistry* **1990,** *29* (31), 7133-7155; (b) Dill, K. A.; MacCallum, J. L., The Protein-Folding Problem, 50 Years On. *Science* **2012,** *338* (6110), 1042-1046.

14. (a) Aparicio, S.; Atilhan, M.; Karadas, F., Thermophysical Properties of Pure Ionic Liquids: Review of Present Situation.

Industrial & Engineering Chemistry Research **2010,** *49* (20), 9580-9595; (b) Marsh, K. N.; Boxall, J. A.; Lichtenthaler, R., Room temperature ionic liquids and their mixtures—a review. *Fluid Phase Equilibria* **2004,** *219* (1), 93-98; (c) Niedermeyer, H.; Hallett, J. P.; Villar-Garcia, I. J.; Hunt, P. A.; Welton, T., Mixtures of ionic liquids. *Chemical Society Reviews* **2012,** *41* (23), 7780-7802.

15. (a) Ballester, P., Anion binding in covalent and self-assembled molecular capsules. *Chemical Society Reviews* **2010,** *39* (10), 3810-3830; (b) Li, Y.; Pink, M.; Karty, J. A.; Flood, A. H., Dipole-Promoted and Size-Dependent Cooperativity between Pyridyl-Containing Triazolophanes and Halides Leads to Persistent Sandwich Complexes with Iodide. *Journal of the American Chemical Society* **2008,** *130* (51), 17293-17295; (c) Srinivasan, A.; Ishizuka, T.; Osuka, A.; Furuta, H., Doubly N-Confused Hexaphyrin: A Novel Aromatic Expanded Porphyrin that Complexes Bis-metals in the Core. *Journal of the American Chemical Society* **2003,** *125* (4), 878-879.

16. Tuma, C.; Sauer, J., A hybrid MP2/planewave-DFT scheme for large chemical systems: proton jumps in zeolites. *Chemical Physics Letters* **2004,** *387* (4–6), 388-394.

17. (a) Jeziorski, B.; Moszynski, R.; Szalewicz, K., Perturbation Theory Approach to Intermolecular Potential Energy Surfaces of van der Waals Complexes. *Chemical Reviews* **1994,** *94* (7), 1887-1930; (b) Misquitta, A. J.; Podeszwa, R.; Jeziorski, B.; Szalewicz, K., Intermolecular potentials based on symmetry-adapted perturbation theory with dispersion energies from time-dependent density-functional calculations. *The Journal of Chemical Physics* **2005,** *123* (21), -.

18. Bader, R. F. W., A quantum theory of molecular structure and its applications. *Chemical Reviews* **1991,** *91* (5), 893-928.

19. (a) Parthasarathi, R.; Subramanian, V.; Sathyamurthy, N., Hydrogen Bonding without Borders: An Atoms-in-Molecules Perspective. *The Journal of Physical Chemistry A* **2006,** *110* (10), 3349-3351; (b) Espinosa, E.; Molins, E.; Lecomte, C., Hydrogen bond strengths revealed by topological analyses of experimentally observed electron densities. *Chemical Physics Letters* **1998,** *285* (3–4), 170-173.

20. (a) Grimme, S., Theoretical Bond and Strain Energies of Molecules Derived from Properties of the Charge Density at Bond Critical Points. *Journal of the American Chemical Society* **1996,** *118*

(6), 1529-1534; (b) Liebman, J. F.; Greenberg, A., A survey of strained organic molecules. *Chemical Reviews* **1976,** *76* (3), 311-365.

21. Gamoke, B. C.; Mayhall, N. J.; Raghavachari, K., A Composite Energy Treatment for Sterically Hindered Cluster Models for the Si(100) Surface. *Journal of Chemical Theory and Computation* **2012,** *8* (12), 5132-5136.

22. (a) Ramabhadran, R. O.; Raghavachari, K., Theoretical Thermochemistry for Organic Molecules: Development of the Generalized Connectivity-Based Hierarchy. *Journal of Chemical Theory and Computation* **2011,** *7* (7), 2094-2103; (b) Ramabhadran, R. O.; Raghavachari, K., Connectivity-Based Hierarchy for Theoretical Thermochemistry: Assessment Using Wave Function-Based Methods. *The Journal of Physical Chemistry A* **2012,** *116* (28), 7531-7537.

23. Chung, L. W.; Hirao, H.; Li, X.; Morokuma, K., The ONIOM method: its foundation and applications to metalloenzymes and photobiology. *Wiley Interdisciplinary Reviews: Computational Molecular Science* **2012,** *2* (2), 327-350.

24. (a) Møller, C.; Plesset, M. S., Note on an Approximation Treatment for Many-Electron Systems. *Physical Review* **1934,** *46* (7), 618-622; (b) Francl, M. M.; Pietro, W. J.; Hehre, W. J.; Binkley, J. S.; Gordon, M. S.; DeFrees, D. J.; Pople, J. A., Self - consistent molecular orbital methods. XXIII. A polarization - type basis set for second - row elements. *The Journal of Chemical Physics* **1982,** *77* (7), 3654-3665.

25. Chen, H.-Y.; Cheng, Y.-L.; Takahashi, K., Theoretical Calculation of the OH Vibrational Overtone Spectra of 1,5-Pentanediol and 1,6-Hexanediol. *The Journal of Physical Chemistry A* **2011,** *115* (50), 14315-14324.

26. (a) Stolow, R. D., Intramolecular Hydrogen Bonding in Non-chair Conformations of Cis-1,4-cyclohexanediols. *Journal of the American Chemical Society* **1961,** *83* (11), 2592-2593; (b) Shikata, T.; Okuzono, M., Hydration/Dehydration Behavior of Polyalcoholic Compounds Governed by Development of Intramolecular Hydrogen Bonds. *The Journal of Physical Chemistry B* **2013,** *117* (9), 2782-2788.

27. Dixon, D. A.; Komornicki, A., Ab initio conformational analysis of cyclohexane. *The Journal of Physical Chemistry* **1990,** *94* (14), 5630-5636.

28. (a) Queeney, K. T.; Chabal, Y. J.; Raghavachari, K., Role of Interdimer Interactions in NH_{3} Dissociation on Si(100)-(2×1). *Physical Review Letters* **2001,** *86* (6), 1046-1049; (b) Bischoff, J. L.; Kubler, L.; Bolmont, D.; Sébenne, C. A.; Lacharme, J. P.; Bonnet, J. E.; Hricovini, K., A photoemission study of ammonia adsorption on Si(100)2 × 1 and Si(111)2 × 1 surfaces. *Surface Science* **1993,** *293* (1–2), 35-40; (c) Hlil, E. K.; Kubler, L.; Bischoff, J. L.; Bolmont, D., Photoemission study of ammonia dissociation on Si(100) below 700 K. *Physical Review B* **1987,** *35* (11), 5913-5916; (d) Smedarchina, Z.; Zgierski, M., Model, First-Principle Calculation of Ammonia Dissociation on Si(100) Surface. Importance of Proton Tunneling. *International Journal of Molecular Sciences* **2003,** *4* (7), 445-459; (e) Widjaja, Y.; Mysinger, M. M.; Musgrave, C. B., Ab Initio Study of Adsorption and Decomposition of NH_3 on Si(100)-(2×1). *The Journal of Physical Chemistry B* **2000,** *104* (11), 2527-2533.

Chapter Four

Modelling X-ray Photoelectron Spectra with Ab-initio Techniques

4.1. Introduction

Small molecule functionalized silicon surfaces are of large importance to the semiconductor community. Understanding such adsorbate-surface interactions can lead to the further development of catalysts, thin film formation, and molecular electronics. Controlled reactions on crystal substrates can dictate nano-patterning processes that are highly ordered, and therefore can functionalize surfaces with specific properties and geometric configurations.[1] For example, water completely dissociates on the Si(100) surface, creating a OH and H terminated surface with 100% coverage.[2] On the etched Si(111) surface, a complete and ordered monolayer of hydrogen[3] or methyl[4] groups can occur. These functionalized surfaces can be easily determined using experimental techniques such as x-ray photoelectron spectroscopy (XPS),[5] ultraviolet photoelectron spectroscopy (UPS),[6] scanning tunneling microscopy (STM),[7] high-resolution electron energy loss spectroscopy (HREELS),[8] and infrared spectroscopy (IR).[9] However, as functionalized surfaces become more complex, which can occur from the structure of an adsorbate, the reactions that an adsorbate

undergoes, or inhomogeneity of the bonding environments intrinsic to surface increases, it becomes increasingly difficult to elucidate surface features merely with experimental data.

X-ray photoelectron spectroscopy (XPS) is a useful technique for obtaining structural and electronic information of a molecule or bulk material. It is a common technique used for identification of chemical composition and bonding environments. Because of its utility as a spectroscopic technique, it is also frequently referred to as ESCA, Electron Spectroscopy for Chemical Analysis, as coined by Kai Siegbahn.[10] Provided with enough system information, this procedure can be used to elucidate structural information with great sensitivity, as small, local defect sites can be probed, as well as general structural features common to the system of interest.

Computational approaches provide an additional tool that can be useful in assigning peaks or with providing predictive guidance for experimental data. In the case of XPS, various methods are currently available but many are not appropriate for use in surface science applications, as calculated core electron binding energy (CEBE) shifts need to have an error typically less than 0.2 eV in order to be useful in assigning experimental spectra while having an appropriate memory requirements and scaling of

computational operations with respect to the number of basis functions and electrons of the larger systems required to describe surface reactivity. The most cost effective method available that is based from ab-initio calculations is Koopman's theorm. However, this method is inappropriate for determining CEBEs because it lacks correlation and relaxation effects, which are required to accurately describe ionization from a core molecular orbital. EOM-IP-CCSD and EOM-IP-CISD[11] can be used to obtain core ionizations with a large computational cost, as the scaling of $O(N^6)$ and $O(N^5)$, respectively. Electron propagator techniques,[12] OVGF, P3, and ΔMBPT(2)[13] scale as $O(ov^4)$, $O(o^2v^3)$, and $O(N^5)$, respectively.

However, the TOEP2[12d, 15] method, proposed by Ortiz et al., is a second-order perturbation correction to the transition orbital method. The transition orbital method uses Janak's theorem, shown in Equation 1, where the ionization energy is defined to be an integral of the ionized orbital from an occupation number of zero to one.

$$E_{N-1} - E_N = \int_0^1 \epsilon_i(n)dn \qquad (1)$$

Ortiz suggests using a one-point quadrature where the occupation of the ionized orbital is equal to 0.5, as shown in Equation 2.

$$\int_0^1 \epsilon_i(n)dn \approx \epsilon_i\left(\frac{1}{2}\right)(1-0) = \epsilon_i\left(\frac{1}{2}\right) \quad (2)$$

The optimized SCF wavefunction with the two-electron operator modified for the ionized orbital leads to a set of new orbital eigenvalues that differ from the standard SCF orbitals where the ionized orbital has an eigenvalue equal to an approximate ionization energy that is accurate to second order. This set of orbitals is then used as an initial guess for a second-order electron propagator, as shown in Equation 3.

$$\omega_k = \epsilon_k + \sum_{q,s<t} \frac{|\langle kq||st\rangle|^2 N_{qst}}{\omega_k + \epsilon_q - \epsilon_s - \epsilon_t}, \; N_{qst} = n_q(1 - n_s - n_t) + n_s n_t \quad (3)$$

With Equation 3, it is clear that only a partial molecular orbital transformation is required, as the first index in all the electron repulsion integrals only depend upon the ionized orbital k. The transition operator method[14] corrected with a second order perturbation (TOEP2) has a memory scaling of $O(ov^2)$, but the limiting computation is the atomic orbital to molecular orbitals basis transformation, which has overall computational scaling of at $O(oN^4)$. However, by not requiring a full molecular orbital transformation of the electron repulsion integrals, the scaling is

decreased to $O(N^4)$. While having a computational scaling appropriate for larger systems, it has been shown to have accuracies similar to the other previously mentioned electron propagator methods.

4.2. Small Gas Phase Molecule Calibrations

Two of the methods mentioned above are benchmarked for their performance to gain a better insight into their applicability in molecular and materials systems. Testing TOEP2 and TOM across many different bonding environments is a rigorous way to determine their robustness. The core electron binding energies (cebe) were calculated using TOEP2 and TOM with Hartree-Fock and an uncontracted 6-31+G(d) basis set. The mean absolute deviation (MAD) of error or individual errors are reported for subset of the test set. Errors were calculated relative to shifts between experimental values reported by Eyermann and coworkers. Tables 4.1, 4.2, and 4.3 look at the performance of C(1s) in similar bonding environments. The MAD values were acceptable for both methods, with TOM outperforming the perturbation corrected TOEP2. Fluorinated systems gave the most performance issues, as fluorine is the most electronegative element and has the ability to change

the bonding environment of the carbon atom much more than other functional groups or substituents.

CO2 Ref	TOEP2	TOM
CS_2	0.27	0.11
HNCO	0.47	0.44
OCS	0.03	0.13
MAD	0.26	0.23

Table 4.1. Core electron binding energy shift errors (eV) relative to C(1s) carbon dioxide for TOEP2 and TOM.

CH_3OH Ref	TOEP2	TOM
CFH_3	0.06	0.07
CH_3Cl	0.04	0.01
CH_3NH_2	0.29	0.29
CH_3SiH_2Cl	0.12	0.10
CH_3SiH_2F	0.23	0.21
CH_3SiH_3	0.37	0.35
CH_4	0.27	0.27
MAD	0.20	0.19

Table 4.2. Core electron binding energy errors (eV) relative to C(1s) of methanol for TOEP2 and TOM. The mean absolute deviation (MAD) is reported for each method.

CCl_4 Ref	TOEP2	TOM
CCl_2F_2	0.91	0.56
CCl_2H_2	0.17	0.50
$CHCl_2SiH_3$	0.22	0.60
CCl_2O	0.41	0.00
CCl_3F	0.22	0.14
CCl_3SiH_3	0.11	0.49
CCl_3H	0.00	0.31
$CClF_3$	0.55	0.15
CF_2H_2	0.12	0.01
CF_2O	0.43	0.00
CF_3H	0.54	0.11
CF_3OCl	0.69	0.26
CF_4	0.93	0.49
MAD	0.41	0.28

Table 4.3. Core electron binding energy shift errors (eV) relative to C(1s) of carbon tetrachloride for TOEP2 and TOM. The mean absolute deviation (MAD) is reported for each method.

Further, to demonstrate the flexibility of the methods, asymmetric and symmetric organic molecules were used to test the flexibility of TOEP2 and TOM. For the asymmetric molecules, the results are presented in Table 4.4, showing computed differences between two different C(1s) cebe values in the same molecule. The results suggest that both methods perform with high accuracy except for the case of fluorinated systems. In the case of

symmetric systems, special treatment is needed to use TOEP2 and TOM effectively. The core orbitals, when equivalent, will produce an optimized wavefunction that are linear combinations of the two atomic orbitals when they are near degenerate. The choice of the orbital to half-occupy with TOM becomes a difficult problem, as the choice of molecular orbital will lead to different calculated cebe values. Using Boys localization[16] will create a wavefunction that does not have the linear combination of the two or more equivalent atomic orbitals, but rather as two non-combing atomic orbitals. This leads to far better performance, as shown in Table 4.5, with no ambiguity on the choice of orbital to use with TOM.

	Δ Exp	Δ TOEP2	Δ TOM
CF_3CO_2H	6.57	3.39	3.38
CH_2CF_2	4.77	4.76	4.73
CH_2CHCl	1.36	1.23	1.23
CH_3CF_3	1.57	7.20	7.18
CH_3CHCl_2	0.70	2.40	2.46
CH3CN	0.54	0.40	0.52
CH_3CO_2H	3.31	3.97	3.96
CH_3NC	0.70	0.92	0.86
H_2CCO	3.60	3.60	3.58
HCO_2CH_3	2.36	2.61	2.60

Table 4.4. Differences in core electron binding energy differences (eV) of non-equivalent C(1s) of reported small organic molecules using TOEP2 and TOM.

C_2H_2 Ref	TOEP2 Boys	TOM Boys	TOEP2 Standard	TOM Standard
C_2F_4	0.73	0.57	1.13	5.40
C_2F_6	1.67	1.51	1.80	5.52
C_2H_4	0.01	0.13	0.37	6.34
C_2H_6	0.35	0.21	0.54	6.78
$C_2O_2F_6$	1.86	1.69	1.65	4.93
C_2OF_6	1.86	1.69	1.64	5.23
C_2OH_6	0.58	0.44	0.59	6.23
C_2SH_6	0.43	0.32	0.61	5.87
C_6H_6	0.37	0.30	0.98	2.23
NCCN	1.25	1.15	1.56	6.70
MAD	0.91	0.80	1.09	5.52

Table 4.5. Core electron binding energy shifts (eV) relative to C(1s) of ethylene for TOEP2 and TOM. Two different wavefunctions (boys localized, and standard) are reported, demonstrating the usefulness of Boys localization for symmetric molecules. The mean absolute deviation (MAD) is reported for each method.

The same analysis as used for C(1s) cebe values in Tables 4.1, 4.2, and 4.3 has been performed on N(1s) and O(1s) systems. Ammonia and pyridine were used as references for N(1s) (Tables 4.6 and 4.7, respectively) while methanol and dichlorine monoxide were used as references for O(1s) (Tables 4.8 and 4.9, respectively). Fluorinated and nitrile functionalized species tend to be underperformers in Table 4.6 for the extreme differences in their bonding

environments. Table 4.7 has good performance since the test set contains singly substituted pyridine systems. The oxygen test systems had very good performance, which may be partially due to its strong electronegativity, allowing for a more consistent atomic charge with a wide variety of substituents.

NH_3 Ref	TOEP2	TOM
C_2H_5CN	0.16	0.09
$CClH_2CH_2NH_2$	0.48	0.46
$CF_3CH_2NH_2$	0.03	0.03
CF_3NO	0.96	0.92
CH_2CHCN	0.29	0.22
$N(CH_3)_2H$	0.25	0.23
$CH_3CH_2CH_2NH_2$	0.22	0.21
$CH_3CH_2NH_2$	0.21	0.20
CH_3CN	0.54	0.48
CH_3NH_2	0.10	0.10
CCl_3CN	0.90	0.92
$CClH_2CN$	0.84	0.86
ClCN	0.24	0.16
HCN	0.31	0.36
HNCO	0.01	0.03
$N(CH_3)_3$	0.38	0.36
NF_3	0.62	0.65
NH_2CHO	0.03	0.04
MAD	0.37	0.35

Table 4.6. Core electron binding energy shift errors (eV) relative to N(1s) of ammonia for TOEP2 and TOM. The mean absolute deviation (MAD) is reported for each method.

Pyridine Ref	TOEP2	TOM
2-Fluoropyridine	0.02	0.02
4-Fluoropyridine	0.04	0.04
2-Methoxypyridine	0.18	0.17
4-Methoxypyridine	0.14	0.15
2-Methylpyridine	0.15	0.14
3-Methylpyridine	0.09	0.09
4-Methylpyridine	0.14	0.14
MAD	0.11	0.11

Table 4.7. Core electron binding energy shift errors (eV) relative to N(1s) of pyridine for TOEP2 and the TOM. The mean absolute deviation (MAD) is reported for each method.

CH_3OH Ref	TOEP2	TOM
$(C_2H_5)_2O$	0.34	0.32
C_2H_5OH	0.01	0.01
C_6H_5OH	0.34	0.35
$(CF_3)_2CHOH$	0.13	0.13
CF_3OCF_3	0.61	0.60
CF_3OCl	0.08	0.11
CH_2CHOCH_3	0.39	0.37
$(CH_3)_2CHOH$	0.29	0.29
$(CH_3)_2O$	0.34	0.33
$(CH_3)_3CCOCl$	0.02	0.09
$CH_3CH_2CH_2OH$	0.20	0.20
CO	0.17	0.19
H_2O	0.18	0.16
MAD	0.24	0.24

Table 4.8. Core electron binding energy shift errors (eV) relative to O(1s) of methanol for TOEP2 and TOM. The mean absolute deviation (MAD) is reported for each method.

OCl_2 Ref	TOEP2	TOM
CF_2O	0.07	0.04
CH_2CCO	0.33	0.31
CH_2O	0.17	0.13
CH_3CH_2CHO	0.15	0.12
CH_3CHO	0.30	0.27
HNCO	0.01	0.04
MAD	0.17	0.15

Table 4.9. Core electron binding energy shift errors (eV) relative to O(1s) of dichlorine monoxide for TOEP2 and TOM. The mean absolute deviation (MAD) is reported for each method.

4.3. Surface Applications of TOEP2

4.3.1 Introduction

After having a better understanding of TOEP2's strengths and limitations, it is ready to be applied to problems in surface science. This is the first study describing the use of the TOEP2 method for describing core ionizations of organic functional groups attached to a silicon cluster representing the Si(111)(7x7) surface. The CEBE shifts of carbon and oxygen 1s orbitals of methanol and formaldehyde are reported for both adsorbed and thermally annealed methanol and formaldehyde on the Si(111)(7x7) surface. These values are compared to the previous experimental

work of Tanaka, Matsuzaki, and Toyoshima.[17] Agreement is found between our current work and experimental values. The accuracy of TOEP2 aids in elucidating the proper bonding environments of the single carbon and oxygen atoms adsorbed on the silicon surface.

4.3.2. Computational Details

Initial constrained bottom layer $Si_{27}H_{27}$ cluster geometries were optimized using the B3LYP functional in conjunction with the 6-311+G(d,p) basis set and MWB10 effective core potential added to the Si atoms. The 6 core uncontracted guassian basis functions were removed from the basis set for the Si atoms. TOEP2 calculations were performed with a truncated $Si_{15}H_{21}$ cluster, maintaining Si-H bonds to a distance of 1.48 Å. The initial wavefunction for the TOEP2 calculations was formed using the Hartree-Fock 6-31+G(d) orbitals with MWB10 effective core potential added to all Si atoms. All calculations were performed using a locally modified version of the development version of the Gaussian suite of programs.

4.3.3. Results and Discussion

There are two possibilities for the adsorption site of gas-phase methanol and formaldehyde on the Si(111)(7x7) surface, the adatom and restatom sites. Previous experimental and theoretical studies have shown a preference for methanol on the adatom site.[18] Using an appropriate cluster model that contains a Si(111)(7x7) adatom site is important to obtaining correct geometries and core binding energies. It is important for the cluster model to correctly describe the appropriate bonding interactions with the surface and rest atom layers with the adatom.

Using a smaller $Si_{15}H_{21}$ cluster, core electron binding energy (cebe) values of adsorption and thermal annealing processes for methanol and formaldehyde are calculated. The initial adsorption of methanol was shown experimentally to cause a substantial shift in the C(1s) and O(1s) core electron binding energies. The structure and cebe's for the initial dissociative adsorption of methanol that agree best with the experimental data are shown in Figure 4.1 and Table 4.10, respectively. The differences between the C(1s) and O(1s) core ionizations for the gas phase methanol and an adsorbed methoxy on a Si(111) cluster were calculated using TOEP2. These calculated shifts are in agreement with experiment but additional

error is present in the O(1s) shift, as that can be attributed to the larger change in the bonding environment, which makes the TOEP2 method start to perform less satisfactory for xps shifts. Similarly, Figure 4.2 and Table 4.11 contains the structures and cebe's for the relevant thermal decomposition process, which was heating the initial adsorption product from 123K to 773K. It was noted from Toyoshima and coworkers[17] that the cebe values of the sample were temperature dependent. The O(1s) binding energy changes by -0.8 eV but a larger change, signifying a dramatic change in bonding environment was for the C(1s) binding energy (-2.7 eV). The geometry that is in strongest agreement to the experimental cebe shifts is when the initial adsoption product decomposes to form a bridging Si—O—Si bond in the first atomic layer of the surface between the rest atom and adatom, which is a similar reaction for other small oxygen containing adsorbates.[19] It has also been known that methoxy on Si(111) is stable up to about 700K from previous work.[20] The difference between the experimental and computed cebe shifts is less than 0.1 eV, which are in very good agreement with what is experimentally observed.

Figure 4.1. Adsorption product of deprotonated methanol on Si(111)7x7 adatom site.

Atom	CH_3OH (eV)	Si-OCH_3 (eV)	ΔeV (eV)	Exp (eV)
O	538.727	537.083	-1.644	-1.2
C	293.189	293.091	-0.098	-0.2

Table 4.10. Computed xps shifts for methanol during adsorption on Si(111)7x7 adatom

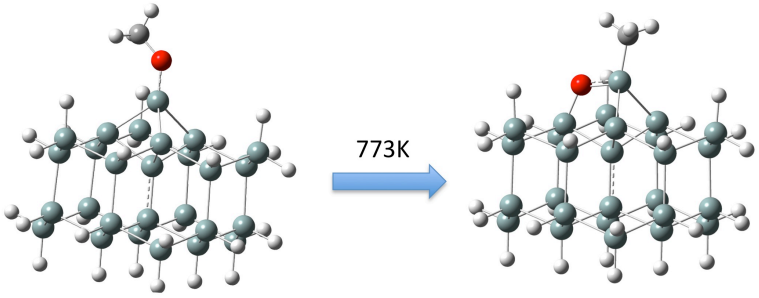

Figure 4.2. Geometries of adsorbed methanol on the Si(111)7x7 adatom site during annealing from 123K to 7733K.

Atom	Si-OCH_3 (eV)	Si-CH_3 (eV)	ΔeV (eV)	Exp (eV)
O	537.083	536.366	-0.717	-0.8
C	293.091	290.403	-2.688	-2.7

Table 4.11. Computed cebe values for adsorbed methanol during heating from 123K to 773K on Si(111)7x7 adatom.

A similar adsoption and annealing process occurs for formaldehyde adsorption and decomposition on Si(111)7x7. Initial adsorption at 298K leads to decomposition, as shown experimentally from their reported data. The adsorption product with the strongest agreement to the experimental observations has a bridging Si—O—Si oxygen atom in the first atomic layer of the

surface and methylene adsorbate on the silicon adatom, similar to the case of dissociative adsorption of methanol described above. After the sample is heated to 773K, a -1.0 eV C(1s) binding energy shift is observed, but the O(1s) does not undergo a notable change. A -1.0 eV shift is indicative of a methylene adsorbate being reduced to a methyl group, as shown by experimental work on the Cu(111) surface.[21] Furthermore, the cluster models that describe the reduction of methylene to a methyl adsorbate have associated core binding energies determined by the electron propagator that are in very good agreement with experiment. The geometries and cebe shifts are shown in Figure 4.3 and Table 4.12. The errors in our computed shifts are less than 0.1 eV, demonstrating the effectiveness of using TOEP2 for surface science applications.

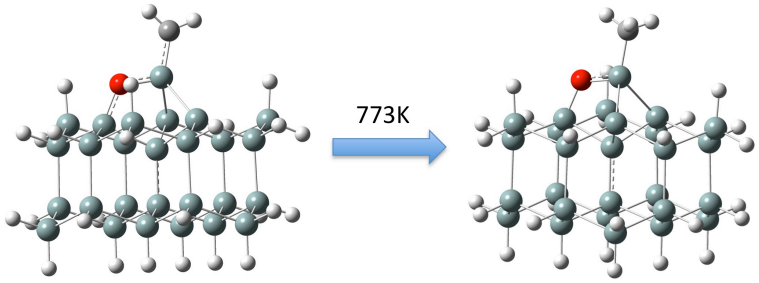

Figure 4.3. Geometries of adsorbed formaldehyde on the Si(111)7x7 adatom site during annealing from 123K to 773K.

Atom	Si-CH_2 (eV)	Si-CH_3(eV)	Δ eV (eV)	Exp (eV)
O	536.466	536.366	-0.080	≈0.0
C	291.427	290.403	-1.024	-1.0

Table 4.12. Computed cebe values for adsorbed formaldehyde during heating from 298K to 773K on Si(111)7x7 adatom.

After the initial reaction product is heated to 773K, the sample was cooled to 298K for 12 hours. During this procedure, the C(1s) cebe was observed to shift by 0.5 eV, which approximately at the midpoint between the C(1s) cebe of the initial adsorption and thermal annealing product. Toyoshima and coworkers[17] suggested the observation was from the following equilibrium:

$$CH_3 \leftrightharpoons CH_2 + H \leftrightharpoons CH + 2H \leftrightharpoons C + 3H$$

However, the model proposed below contradicts the previous authors' work, as they suggested that the equilibrium will shift to the right with heating. Agreeing with the previous Cu(111) study[21] , our cluster models and associated cebe shifts suggests that as the functionalized Si(111) surface is cooled, methylene adsorbates are reformed in a somewhat reversible manner. The computed shifts assume a 50% population of methylene and methyl adsorbates on the Si(111) adatoms. The structures and cebe shifts are shown in Figure 4.4 and Table 4.13. The results are in very strong agreement, with a 0.05 eV error.

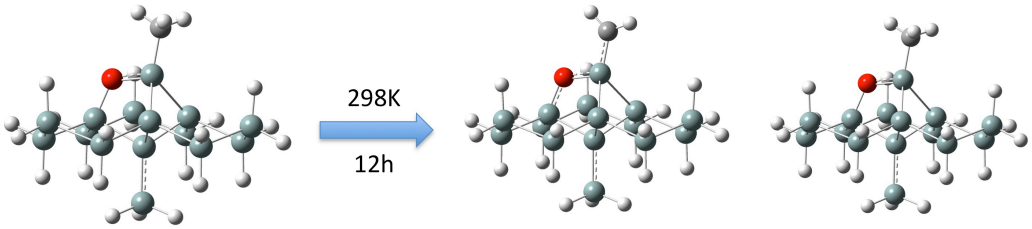

Figure 4.4. Adsorbed formaldehyde after cooling from 773K to 298K for 12 hours, assuming an equilibrium of methyl and methylene adsorbates.

Atom	Si-CH_3(eV)	Avg CH_2,CH_3	Δ eV (eV)	Exp (eV)
O	536.366	536.416	0.050	≈0.0
C	290.403	290.915	0.512	0.5

Table 4.13. Computed cebe values for adsorbed formaldehyde after cooling from 773K to 298K for 12 hours, assuming an equilibrium of methyl and methylene adsorbates

4.4. Shake-up Spectra

4.4.1. Introduction

The main peaks from x-ray photoelectron spectroscopy that are used to determine cebe values are not the only important features from the method's spectra. Furthermore, other signatures, referred to as satellites, are commonly observed in spectra obtained by XPS which have origins from several different processes caused from additional electronic excitations. Inelastic scattering processes, those from which the sample is induced to a bound excited state, can be observed as typically broad features found at lower kinetic energy values ranges of the system's spectra.[22] More complicated processes, such as shake-up, shake-down, and shake-out satellite peaks are also detected from this spectroscopic technique.[23] When an ejected core electron, induced by ionization, interacts with a higher lying electron, which in turn undergoes an electronic excitation, causes shake-up features of an x-ray photoionization spectra. Similarly, shake-down peaks are observed from electronic relaxation from the formation of the core hole. The third type of satellite feature, a shake-out peak, is similar to those of shake-down peaks but the electronic relaxation induces a second ionization of the system, but this second electron is

ejected from a higher lying orbital. These three different processes contribute different satellite features to spectra obtained by XPS and provide greater insight for electronic configurations and excited states.

Unfortunately, due to the complex processes that occur during XPS, assignment of satellite features can be formidable. Previously, different computational methods have been applied to aid in the determination and elucidation of observed satellite features with questionable results. This area of theoretical and computational chemistry has had a large focus towards the development of reliably accurate methods for main peaks, such as IP-CCSD, EOM-IP-CCSD,[11] MCSTEP,[24] FSMRCC,[25] TOEP2,[15] and TOM.[12d, 26] However, less development has been put forth towards the descriptions of satellite peaks formed. Slater's $\chi\alpha$ method,[27] equivalent core Kohn-Sham density function approach,[28] limited CI,[29] semi-empirical CI,[30] and semi-empirical CIS(D)[31] have been previously reported for use in shake-up peak assignments with qualitative accuracy.

Defining a tractable but accurate computational method to describe satellite peaks is important because of the prevalent use of XPS in the materials science community. The shake-up process

can be viewed as the adsorption of energy from two different steps at the adiabatic limit: core electron ionization and electronic excitation. It is important to capture both of these processes in order to obtain energies that describe shake-up peaks. Appropriate computational scaling of $O(N^5)$ or less is desired for modeling bulk systems, particularly those containing many heavy elements. Two computationally efficient methods, the Maximum Overlap Method[32] and TOEP2, have been previously reported to provide accurate core electron binding energies with a low computational cost. The Maximum Overlap Method (MOM) has been proposed by Gill and coworkers to describe core electron binding energies from XPS and electronic excitations induced form XAS, which undergoes electron excitations similar to those found in shake-up processes.[32a] It has been shown to be effective for describing these electronic states of small molecules by optimizing the single determinant wavefunction used to describe the system with a constraint that the occupied orbitals are not determined by the aufbau principle, but rather are chosen by which orbitals from the new set formed during the self-consistent field cycle most strongly overlap with the previous iteration's occupied orbitals. When an excited state can be described by a single determinant wavefunction, MOM provides accurate results for electronic excitations, core ionizations, and core excitations. Combining the two methods leads to a

computationally tractable model that can be used to accurately describe core electron binding energies of not only the ground state of a system, but also higher lying excited states.

4.4.2. Method

In an attempt to explore different models that have sufficient computational scaling for materials systems, shake-up satellite features are computed for a neon atom, water molecule, and pyridine with methods being based upon MOM, TOEP2, and CIS(D). Electronic excitations are typically correlated problems that can not simply be described by a single determinant wavefunction. All three of the models presented below propose to overcome this deficiency when calculating excited states.

One model presented below uses a ground state, neutral CIS(D) calculation to obtain an electronic excitation energy, which is then corrected by using TOEP2 on an equivalent single-reference wavefunction that is a Hartree-Fock solution using MOM. The difference between the ground state core electron binding energy and the excited state electron binding energy is added to the CIS(D) electronic excitation energy to describe the total energy involved in the shake-up process for each excited state. This should allow for

the determination of electronic excitations and core ionizations as two independent calculations to be summed together. When a single reference wavefunction cannot be defined for an excited state, multiple TOEP2 calculations are performed, and the contributions of these calculations to the shake-up peak is defined by the CIS coefficients. The second approach attempts to account for orbital relaxation and electronic excitation in the same calculation by using a ground state core ionized wavefunction obtained by the maximum overlap method as the reference wavefunction for CIS(D). Further, making assignments of an electronic excited state from a single one-electron excitation with CIS(D) can be challenging or impossible. When the alpha and beta spaces are not equal, spin, for a given excited state, can also be challenging to assign. In an attempt to avoid these pitfalls, the third approach is to apply the transition operator method to both the alpha and beta space[29] will allow for excited states that have indistinguishable spin cases and normal spin assignments since the coefficients of the CIS solutions are the same or of opposite sign. In order to improve the accuracy of the excited state energies for CIS(D), EOM-CCSD corrections are added to this method.

4.4.3. Results and Discussion

To demonstrate this new proposed model's effectiveness, it has been applied to three small gas phase systems with clear shake-up satellite features detected by XPS. Neon, water, and pyridine have been studied and modeled for features of their shake-up spectra. Providing comparisons to previous peak assignments and calculated peak energies will be useful in asserting the utility of this model.

Neon has important shake-up features for 3p←2p transitions. The low and high limits of the shake-ups are 37.35 eV and 40.76 eV, respectively. The results from the three methods are shown in Table 4.14.

CIS(D) + ΔTOEP2	CIS(D) Core Ion	(α,β)-TOM-CIS(D)
35.5	36.1	36.8
38.3	39.1	40.4

Table 4.14. Computed 3p ← 2p transitions of neon using the three different methods described above. Energies are reported in eV.

All three of the methods underestimate the 3p ← 2p transitions. However, the CIS(D) using a core ion reference wavefunction has the closest values to the experimental data. The spread between the highest and lowest excitation values is found experimentally to be 3.41 eV, which is also most closely matched with the (α,β)-TOM-CIS(D) calculation with the EOM-CCSD correction.

Water has a much more complicated spectra, having shake-up peaks at 20 eV, 22 eV, 24 eV, and 34 eV. The data for the three different methods are reported in Tables 4.15, 4.16, and 4.17. With CIS(D) + ΔTOEP2, it is possible to make assignments to these peaks from the data outside of the experimental peak value of 34 eV, which the method does not describe the higher energy excitations as well. Similar results are obtained using CIS(D) with the ionized core reference wavefunction as well, but the $3b_2 \leftarrow 1b_2$ transition can be used to assign the 34 eV experimental peak. CIS(D) with the half-ionized core orbitals in alpha and beta space leads to similar overall results that can be used to make peak assignments. The three methods agree for some of the peak transitions, as the 20, 22, and 24 eV feature is described as $2b_1 \leftarrow 1b_1$, $5a_1 \leftarrow 3a_1$, and $6a_1 \leftarrow 3a_1$ within 1 eV for all three methods. This shows that the methods are somewhat self-consistent with each other in their qualitative analysis of features of a shake-up spectra.

Transitions	CIS(D) + ΔTOEP2
$2b_1 \leftarrow 1b_1$	20.0
$5a_1 \leftarrow 3a_1$	21.9
$6a_1 \leftarrow 3a_1$	24.9
$2b_2 \leftarrow 1b_2$	22.5
$3b_2 \leftarrow 1b_2$	27.6
$4a_1 \leftarrow 2a_1$	37.1
$7a_1 \leftarrow 3a_1$	36.8

Table 4.15. Computed shake-up transitions of water with CIS(D) + ΔTOEP2, calculated by adding the shift computed in cebe from the difference between the core ionizations of the ground and excited states to CIS(D) electronic excitation energies. Values are reported in eV.

Transitions	CIS(D) Core Ion
$4a_1 \leftarrow 3a_1$	15.3
$4a_1 \leftarrow 3a_1$	16.8
$2b_2 \leftarrow 1b_2$	19.9
$2b_1 \leftarrow 1b_1$	19.7
$5a_1 \leftarrow 3a_1$	21.2
$2b_1 \leftarrow 1b_1$	21.5
$2b_2 \leftarrow 1b_2$	22.6
$6a_1 \leftarrow 3a_1$ $2b_2 \leftarrow 1b_2$	23.9
$2b_1 \leftarrow 1b_1$	24.9
$3b_1 \leftarrow 1b_1$	26.9
$1b_2 \leftarrow 3b_2$	28.3
$3b_2 \leftarrow 1b_2$	34.0
$5a_1 \leftarrow 1a_1$	36.4

Table 4.16. Computed shake-up transitions of water with CIS(D) using a core ionized reference wavefunction obtained by MOM. Values are reported in eV.

Transitions	(α,β)-TOM-CIS(D)
$4a_1 \leftarrow 3a_1$	15.6
$4a_1 \leftarrow 3a_1$	18.1
$2b_2 \leftarrow 1b_2$	21.1
$5a_1 \leftarrow 3a_1$	22.7
$6a_1 \leftarrow 3a_1$	23.6
$6a_1 \leftarrow 3a_1$	23.9
$2b_2 \leftarrow 1b_2$	25.4
$2b_2 \leftarrow 3b_2$	26.8

Table 4.17. Computed shake-up transitions of water with CIS(D) using a reference wavefunction that contains ½ α and ½ β ionized core orbitals. EOM-CCSD corrections are added to the excited state energies. Values are reported in eV.

Pyridine also has an experimentally known shake-up spectrum, with peaks at 5.7 eV, 7.2 eV, 8.6 eV, and 11.4 eV. The results from the three different computational methods are listed in Tables 4.18, 4.19, and 4.20. Assignments of the peaks can be made using CIS(D) with the electron propagator with some caution, as the peak energies can be different by about 0.5 eV. Table 4.18 shows that CIS(D) with the core ionized reference wavefunction also leads to similar results, but the peaks are difficult to assign. The peak assignment at 7.2 eV does match qualitatively, describing the transition as having $2a_2 \leftarrow 1a_2$ character, along with the other

two methods. CIS(D) using a half-ionized alpha and beta core orbital also gives results that can be used to qualitatively match the shake-up spectrum of pyridine. The results for this method are not reported with the EOM-CCSD correction, but also can successfully make a peak assignment for 11.4 eV peak, which is described as 3a2 ← 1a2, the same transition as the CIS(D) + ΔTOEP2 method.

Transitions	CIS(D) + ΔTOEP2
$2a_2 \leftarrow 1a_2$ $3b_2 \leftarrow 2b_2$	4.6
$3b_2 \leftarrow 2b_2$ $2a_2 \leftarrow 1a_2$	5.1
$2a_2 \leftarrow 1a_2$ $3b_2 \leftarrow 2b_2$	7.3
$3b_2 \leftarrow 2b_2$ $2a_2 \leftarrow 1a_2$	8.9
$3b_2 \leftarrow 1b_2$	7.0
$3a_2 \leftarrow 1a_2$	11.2

Table 4.18. Computed shake-up transitions of pyridine with CIS(D) + ΔTOEP2, calculated by adding the shift computed in cebe from the difference between the core ionizations of the ground and excited states to CIS(D) electronic excitation energies. Values are reported in eV.

Transitions	CIS(D) Ion
$2a_2 \leftarrow 1a_2$	5.1
$3b_1 \leftarrow 2b_1$	5.1
$3b_1 \leftarrow 2b_1$ $3a_2 \leftarrow 2a_2$	6.5
$2a_2 \leftarrow 1a_2$	7.9
$3b_1 \leftarrow 1b_1$	9.3

Table 4.19. Computed shake-up transitions of pyridine with CIS(D) using a core ionized reference wavefunction obtained by MOM. Values are reported in eV.

Transitions	(α,β)-TOM-CIS(D)
2a2 ← 1a2	5.0
3b2 ← 2b2	5.1
3b2 ← 2b2	6.5
3b2 ← 2b2 2a2 ← 1a2	7.9
3b2 ← 1b2	9.3
3a2 ← 1a2	11.5
3a2 ← 1a2	11.9

Table 4.20. Computed shake-up transitions of pyridine with CIS(D) using a reference wavefunction that contains ½ α and ½ β ionized core orbitals. Values are reported in eV.

4.5. Conclusions

Overall, the project is still in development, as there are many challenges in calculating core ioinized excitation energies. An analysis of core electron binding energies suggests that reasonable performance can be expected for computing shifts in spectra if the bonding environments are similar between the reference and sample molecules. Further, it was demonstrated that the electron propagator using the transition operator method can be successfully applied to Si(100) surface studies. Finally, three different models to compute shake-up features were explored. Current challenges and possible improvements to the calculation of shake-up peaks is described in the prospectus. However, these results presented can be used as tools to qualitatively describe the electronic processes that occur in x-ray photoelectron spectra.

4.6. References

1. (a) Hossain, M. Z.; Kato, H. S.; Kawai, M., Fabrication of Interconnected 1D Molecular Lines along and across the Dimer Rows on the Si(100)–(2 × 1)–H Surface through the Radical Chain Reaction. *The Journal of Physical Chemistry B* **2005,** *109* (49), 23129-23133; (b) Ferguson, G. A.; Than, C. T.-L.; Raghavachari, K., Line Growth on the H/Si(100)-2 × 1 Surface: Density Functional Study of Allylic Mercaptan Reaction Mechanisms. *The Journal of Physical Chemistry C* **2009,** *113* (43), 18817-18822; (c) Madachik, M. R.; Teplyakov, A. V., Coadsorption of Ethylene and Nitrobenzene on Si(100)-2 × 1: Toward Surface Patterning at the Molecular Level. *The Journal of Physical Chemistry C* **2009,** *113* (42), 18270-18275; (d) Barlas, T. R.; Dmitruk, N. L.; Kotova, N. V.; Mayeva, O. I.; Romanyuk, V. R., Self-assembling of metal nanoparticles on patterned semiconductor surfaces (Au/GaAs). *Superlattices and Microstructures* **2005,** *38* (2), 130-141; (e) Onclin, S.; Ravoo, B. J.; Reinhoudt, D. N., Engineering Silicon Oxide Surfaces Using Self-Assembled Monolayers. *Angewandte Chemie International Edition* **2005,** *44* (39), 6282-6304.

2. Konečný, R.; Doren, D. J., Adsorption of water on Si(100)-(2×1): A study with density functional theory. *The Journal of Chemical Physics* **1997,** *106* (6), 2426-2435.

3. Higashi, G. S.; Chabal, Y. J.; Trucks, G. W.; Raghavachari, K., Ideal Hydrogen Termination of the Si(111) Surface. *Applied Physics Letters* **1990,** *56*, 656-658.

4. Fidélis, A.; Ozanam, F.; Chazalviel, J. N., Fully methylated, atomically flat (111) silicon surface. *Surface Science* **2000,** *444* (1–3), L7-L10.

5. Gelius, U.; Basilier, E.; Svensson, S.; Bergmark, T.; Siegbahn, K., A high resolution ESCA instrument with X-ray monochromator for gases and solids. *Journal of Electron Spectroscopy and Related Phenomena* **1973,** *2* (5), 405-434.

6. Turner, D. W., Photoelectron Spectroscopy. *Annual Review of Physical Chemistry* **1970,** *21* (1), 107-128.

7. Moore, A. M.; Weiss, P. S., Functional and Spectroscopic Measurements with Scanning Tunneling Microscopy. *Annual Review of Analytical Chemistry* **2008,** *1* (1), 857-882.

8. Thiry, P. A., Vibrations measured at surfaces by HREELS : An updated review. *Journal of Electron Spectroscopy and Related Phenomena* **1983,** *30* (1), 261-273.

9. Chabal, Y. J., Surface infrared spectroscopy. *Surface Science Reports* **1988,** *8* (5–7), 211-357.

10. Holm, R.; Storp, S., ESCA: Eine Methode zur Bestimmung von Elementen und ihren Bindungszuständen in der Oberfläche von Festkörpern. *Z. Anal. Chem.* **1978,** *290* (4), 273-288.

11. Golubeva, A. A.; Pieniazek, P. A.; Krylov, A. I., A new electronic structure method for doublet states: Configuration interaction in the space of ionized 1h and 2h1p determinants. *The Journal of Chemical Physics* **2009,** *130* (12).

12. (a) Ortiz B., J. V.; Öhrn, Y., Electron propagator theory of molecular anions. *The Journal of Chemical Physics* **1980,** *72* (10), 5744-5751; (b) Ortiz, J. V., Calculation and interpretation of total energies in electron propagator theory. *The Journal of Chemical Physics* **1995,** *103* (13), 5630-5639; (c) Ortiz, J. V., Electron propagator theory: an approach to prediction and interpretation in quantum chemistry. *Wiley Interdisciplinary Reviews: Computational Molecular Science* **2013,** *3* (2), 123-142; (d) Ortiz, J. V.; Basu, R.;

Öhrn, Y., Electron-propagator calculations with a transition-operator reference. *Chemical Physics Letters* **1983,** *103* (1), 29-34; (e) Purvis, G. D.; Öhrn, Y., The transition state, the electron propagator, and the equation of of motion method. *The Journal of Chemical Physics* **1976,** *65* (3), 917-922.

13. Beste, A.; Vázquez-Mayagoitia, Á.; Ortiz, J. V., Direct Δ MBPT(2) method for ionization potentials, electron affinities, and excitation energies using fractional occupation numbers. *The Journal of Chemical Physics* **2013,** *138* (7).

14. (a) Goscinski, O.; Pickup, B. T.; Purvis, G., Direct calculation of ionization energies. Transition operator for the ΔESCF method. *Chemical Physics Letters* **1973,** *22* (1), 167-171; (b) Williams, A. R.; deGroot, R. A.; Sommers, C. B., Generalization of Slater ' s transition state concept. *The Journal of Chemical Physics* **1975,** *63* (2), 628-631.

15. Flores-Moreno, R.; Zakrzewski, V. G.; Ortiz, J. V., Assessment of transition operator reference states in electron propagator calculations. *The Journal of Chemical Physics* **2007,** *127* (13).

16. Boys, S. F., Construction of Some Molecular Orbitals to Be Approximately Invariant for Changes from One Molecule to Another. *Reviews of Modern Physics* **1960,** *32* (2), 296-299.

17. Tanaka, K.; Matsuzaki, S.; Toyoshima, I., Photodecomposition of adsorbed methoxy species by UV light and formaldehyde adsorption on silicon(111) studied by XPS and UPS. *The Journal of Physical Chemistry* **1993,** *97* (21), 5673-5677.

18. (a) Xie, Z.-X.; Uematsu, Y.; Lu, X.; Tanaka, K.-i., Dissociation mechanism of methanol on a Si(111)-(7x7) surface studied by scanning tunneling microscopy. *Physical Review B* **2002,** *66* (12), 125306; (b) Xu, X.; Wang, C.; Xie, Z.; Lu, X.; Chen, M.; Tanaka, K., Adsorbate lone-pair-electron stimulated charge transfer between surface dangling bonds: methanol chemisorption on Si(111)-7x7. *Chemical Physics Letters* **2004,** *388* (1–3), 190-194.

19. (a) Wang, S.; He, J.; Zhang, Y.; Xu, G. Q., Adsorption of O2 and CO2 on the Si(111)-7x7 surfaces. *Surface Science* **2012,** *606* (17–18), 1387-1392; (b) Nishijima, M.; Edamoto, K.; Kubota, Y.; Tanaka, S.; Onchi, M., Vibrational electron energy loss spectroscopy of the Si(111)(7×7)–H2O(D2O) system. *The Journal of Chemical Physics* **1986,** *84* (11), 6458-6465.

20. Edamoto, K.; Kubota, Y.; Onchi, M.; Nishijima, M., Observation of methoxy species on the Si(111)(7×7) surface — A vibrational study. *Surface Science Letters* **1984,** *146* (1), L533-L539.

21. Chuang, T. J.; Chan, Y. L.; Chuang, P.; Klauser, R., The surface chemistry of methyl and methylene radicals adsorbed on Cu(111). *Journal of Electron Spectroscopy and Related Phenomena* **1999,** *98–99* (0), 149-173.

22. Trajmar, S.; Williams, W.; Kuppermann, A., Electron impact excitation of H2O. *The Journal of Chemical Physics* **1973,** *58* (6), 2521-2531.

23. Bagus, P. S.; Ilton, E. S.; Nelin, C. J., The interpretation of XPS spectra: Insights into materials properties. *Surface Science Reports* **2013,** *68* (2), 273-304.

24. Heryadi, D.; Jones, C. T.; Yeager, D. L., A small optimal complete active space (CAS) for multiconfigurational spin tensor electron propagator method (MCSTEP) ionization potentials: Application to methane, acetylene, ethylene, and ethane. *The Journal of Chemical Physics* **1997,** *107* (13), 5088-5093.

25. Dutta, A. K.; Gupta, J.; Vaval, N.; Pal, S., Intermediate Hamiltonian Fock Space Multireference Coupled Cluster Approach to Core Excitation Spectra. *Journal of Chemical Theory and Computation* **2014,** *10* (9), 3656-3668.

26. Campoy, G.; Poulain, E.; Morales, J.; Palma, A., Binding energies and peak intensities of light hydrocarbon molecules through TOM I. Methane and acetylene. *International Journal of Quantum Chemistry* **1986,** *30* (S20), 555-561.

27. (a) Bristow, D. J.; Tse, J. S.; Bancroft, G. M., Experimental and theoretical shake-up studies. The rare gases. *Physical Review A* **1982,** *25* (1), 1-6; (b) Slater, J. C., The self-consistent field for crystals. *International Journal of Quantum Chemistry* **1969,** *4* (S3B), 727-746.

28. Deng, Y.; Gao, B.; Deng, M.; Luo, Y., A comparative theoretical study on core-hole excitation spectra of azafullerene and its derivatives. *The Journal of Chemical Physics* **2014,** *140* (12).

29. Svensson, S.; Ågren, H.; Wahlgren, U. I., SCF and limited CI calculations on the ls shake-up spectrum of H2O. *Chemical Physics Letters* **1976,** *38* (1), 1-8.

30. Distefano, G.; Guerra, M.; Jones, D.; Modelli, A.; Colonna, F. P., Experimental and theoretical study of intense shake-up structures in the XPS spectra of nitrobenzenes and nitrosobenzenes. *Chemical Physics* **1980,** *52* (3), 389-398.

31. Keane, M. P.; de Brito, A. N.; Correia, N.; Svensson, S.; Lunell, S., Experimental and theoretical study of the N1s and C1s shake-up satellites in pyridine and aniline. *Chemical Physics* **1991,** *155* (3), 379-387.

32. (a) Besley, N. A.; Gilbert, A. T. B.; Gill, P. M. W., Self-consistent-field calculations of core excited states. *The Journal of Chemical Physics* **2009,** *130* (12); (b) Gilbert, A. T. B.; Besley, N. A.; Gill, P. M. W., Self-Consistent Field Calculations of Excited States Using the Maximum Overlap Method (MOM)†. *The Journal of Physical Chemistry A* **2008,** *112* (50), 13164-13171.

Chapter Five

Prospectus

5.1. Introduction

In the research presented from the previous chapters, further developments towards computational models that can be applicable to the nanotechnology, surface science, and semiconductor communities have been discussed. Further improvements can be made in these areas to expand their robustness, scope, and general applicability to molecular and materials systems. Using composite methodologies to describe systems without specific interactions, either spurious through approximations made when describing the system to make it appropriate for computation or physically motivated interactions such as hydrogen bonding have been demonstrated to be useful in decomposing energetic and geometric contributions of a system. Pseudoatoms that have been used to describe the fully covalent bonding environment in bulk silicon materials can be further extended for applications in other environments, ones that contain mixtures of ionic and covalent bonds. Furthermore, Electron propagator techniques can be improved for applications in x-ray photoelectron spectroscopy to help identify and predict peaks that

are derived from complex electronic processes. New developments, applications, and challenges are described in this chapter related to these areas.

5.2. Further generalization of a composite scheme to selectively remove interactions of a molecule and applications to strained systems

The use of a composite energy scheme was shown to be an effective method to quantitate the geometric and energetic contributions of intra-system hydrogen bonding. Examples in Chapter 4 refer to intramolecular hydrogen bonds in small organic diols and a large example with dissociated ammonia on a Si(100) surface cluster. Hydrogen bonding is an important attractive interaction that can occur with various conformations of a system, which typically creates an energetic stability. However, the same composite methods should be extended to quantitate and observe repulsive interactions have great chemical consequence.

Steric interactions are important weak interactions that can dictate conformations, which in turn determine the reactivity and selectivity of a reactant. Creating models to determine conformational preferences and their associated reaction pathways

can allow for a better prediction of products, particularly ones that contain stereoselective centers, to choose appropriate target molecules for use in a synthetic pathway.

An important type of steric interaction is known as allylic strain.[1] Two types of this class of strain are 1,3-strain and 1,2-strain. Each of the nomenclatures describes the substituent-substituent repulsions based upon the positioning in the molecule with respect to the olefin. These interactions occur because sp^2 hybridized carbons, which have a significantly large barrier of rotation, contain groups that cause repulsive forces that cannot be remedied without rotation of the allyl group's double bond. These important interactions have been useful in the formation of large molecules containing many stereocenters. Similar allylic strains exist for cyclic molecules that contain sp^2 hybridized carbons.

As a Connectivity-Based Hierarchy scheme (CBH), similar to other fragmentation-based methods[2] has been previously applied and proven successful for hydrogen bonding systems, the same approach can be further generalized and applied to systems containing steric repulsions. It is defined in a general way that is flexible to treat fragments of any given size and remove selected fragment-fragment interactions. The hierarchy is defined to create

cancellation of overlapping fragments in order to avoid double counting of energies in a general manner. Combining these many excised fragments together has led to effective results in a simple fashion, appropriate for energies and geometry optimizations.

The concept of rungs can be evoked, similar to that defined in CBH. The lowest rung of CBH is known as CBH-0, which is a bond-centric rung, where the each atom's bonding is preserved. Similarly, the lowest run of the CBH-scheme proposed preserves the user defined fragment atoms, which can be of any general size, up to the size of the total molecular system. The next rung, which is known to be a "bond-centric" rung, can be an analogous "fragment-bond-centric" rung, where the bonds between any two fragment regions are preserved. Progressing further up the ladder captures more information about the total system, oscillating between odd "fragment-centric", and even "fragment-bond-centric" rungs, up to N-1 rungs, where N is the total number of user defined fragments for the molecular system.

Each rung above rung zero is defined with the same rules as defined by CBH, but with the exception that each atom has been replaced by a fragment, i.e. each fragment is treated in the same manner as an atom from the CBH scheme. However, at the lowest

rung, the stoichiometry does not match that of the full molecular system after forming each of the composite fragments. To avoid these complications, H_2 systems are added at each region between two fragments to account for the hydrogen link atoms employed during the formation of the subcalculations. To negate the forces from contributing at this rung, optimized H_2 molecules are used in this model.

Considering this general method, the first choice to use for testing sterically strained systems is the first "fragment-bond-centric rung", where nearest neighbor fragments are considered. This leads to the same composite scheme defined in Chapter 3 for use in intramolecular hydrogen bonding systems. The test molecules and fragments defined for each are shown in Figure 5.1. For all calculations described with these molecules, the MP2/6-31+G(d,p) model chemistry was chosen for energies and geometry optimizations.

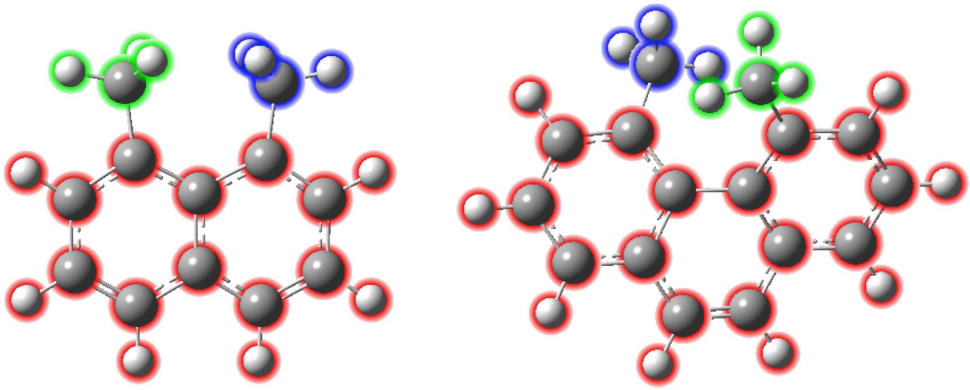

Figure 5.1. MP2 geometry optimized molecules tested with the composite energy method to determine the amount of strain caused from steric repulsions. Carbon atoms are grey and hydrogen atoms are white. Each outer color (red, green, and blue) represents a chosen fragment defined for the method. The molecules depicted are 1,8-dimethylnapthalene (left), and 4,5-dimethylphenanthrene (right).

The two systems depicted in Figure 5.1 are analyzed in a manner similar to the reported energetic and geometric relaxations discussed in Chapter 3. The difference calculated between the standard MP2 optimized structure's energy and newly discussed composite energy defines the energetic contribution from steric repulsion. The energy from geometric distortions due to the steric repulsions can also be determined as the difference between the composite energy at the MP2 optimized structure and the

associated method's optimized structure. Similarly, the difference between the energies of the MP2 optimized structures at the standard optimized and composite optimized geometries are used to report the total energy change related to having no strain contained in the molecular systems. Results are reported in Table 6.1.

System	Total Relaxation	Geometry Relaxation	Steric Repulsion
1,8-dimethylnapthalene	-5.9	-2.5	-3.4
4,5-dimethylphenanthrene	-3.3	-3.1	-0.2

Table 6.1. Summary of results for the set of eight strained molecules depicted in Figure 5.1. Energies are reported in kcal/mol.

When 1,8-dimethylnapthalene relaxes without the presence of steric repulsions, as evident from the geometries reported in Figure 5.2, the carbon-carbon distance decreases from 2.966 Å to 2.607 Å, indicative to how the major contributor to the geometric relaxation comes from the distortion from the methyl-methyl repulsion, which is calculated to be 2.5 kcal/mol. The steric repulsions do not minimize with respect to rotation of the methyl group, as the dihedral angles change by less than 1º between the

MP2 optimized geometries through standard and composite energy methods.

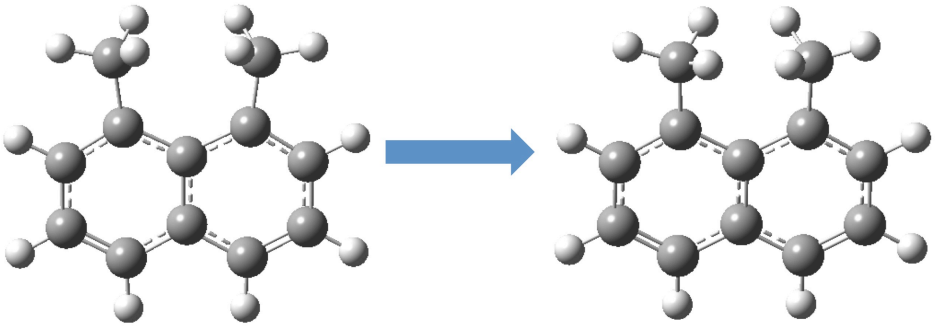

Figure 5.2. 1,8-dimethylnapthalene optimized geometries with standard MP2/6-31+G(d,p) (left) and composite method (right).

In a more extreme example of steric repulsion, 4,5-dimethylphenanthrene was investigated with the composite model. The geometries are depicted in Figure 5.3. The molecule does not become fully planar without the presence of the steric methyl-methyl repulsions. The dihedral angle defined connecting carbon atoms 4 and 5 decreases from 32º to 29º when employing the composite method, indicative of a decrease in geometric distortion of the molecule. Phenanthrene has a planar geometric minimum, so some other repulsive forces still exist when using this composite method, possibly from two of the fragment subcalculations that are formed, 4-phenanthrene and 5-phenanthrene. However, with carbon-carbon methyl distance of 2.968 Å, the composite energy at

the MP2 optimized geometry may still be appropriate for evaluating the steric energy contribution.

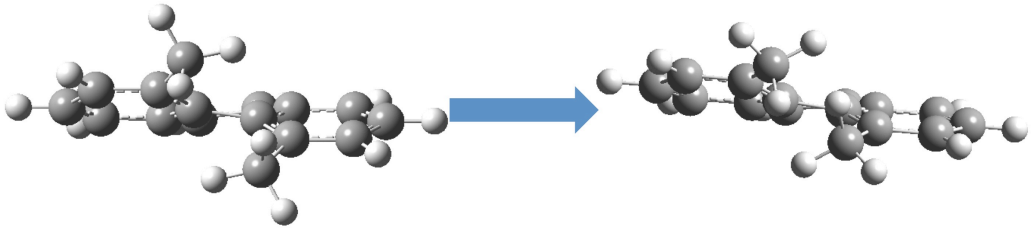

Figure 5.3. 4,5-dimethylphenanthrene optimized geometries with standard MP2/6-31+G(d,p) (left) and composite method (right).

From these results, we find that the overall energies seem in consistent with one another, particularly in molecules with similar sterically hindered groups, with relaxation energies that are in the weak interaction regime. Approximations from the scheme do lead to artifacts that can be corrected either by development of further composite methods that are also general but utilize multiple types of model chemistries, attempting to use a higher rung with more user defined fragments, or by a carefully chosen scale factor to account for spurious forces when fragments of interest are at sufficiently close distances to cause repulsions with link atoms caused by truncation.

5.3. Improvements to electron propagator techniques for satellite peaks

Using a single reference determinant leads to two major challenges for an electron propagator technique based upon perturbation theory. Excited states are correlated problems, so as an example, any singlet excited state has at least coupling between alpha and beta electrons, if not more excited configurations being used to describe an excited state, as reflected in solutions found by configuration interaction using an unrestricted Hartree-Fock wave function. This leads to difficulties in using methods to use ground state methods for excited state electronic configurations.[3] Along with these difficulties to using a single reference wavefunction, perturbation theory leads to numerical instability for degeneracies in orbital eigenvalues,[4] particularly relevant for calculating low-lying excited states of the same symmetry as the ground state, such as those that contribute to shake-up peaks in x-ray photoelectron spectroscopy. Two strategies are described below to overcome this challenges.

One possible way to use a single determinant wave function that provides correlation is to use solutions to use solutions that contain a number of electrons that have partial occupancy across

many orbitals.[5] As an example, an excited state which has two main excitations contributing to an excited state, as determined by configuration interaction, could be described by one electron that have non-integer occupancy that is divided into two orbitals, with the percent contributions of each excitation determining the fraction of the electron that is placed in the higher lying orbitals. Similar work has previously been done using fractional occupation numbers to describe excited states, and this may be an approximate way of describing this correlated problem, so the method defined by TOEP2 can be applied to excited state systems with higher accuracy.

The failures of using perturbation theory for reference wave functions that contain degeneracies can be avoided by rewriting the electron propagator in terms of an equation of motion - coupled cluster singles and doubles.[6] The one-particle, two-hole; two-particle, one-hole, and correction terms would need to be calculated in this formalism. The computational cost of EOM-CC2 is $O(N^5)$, and since only a partial transformation of the atomic orbitals to molecular orbitals is required, it can equally be applied to materials systems. Martinez et. al have reduced the scaling of EOM-CC2 to $O(N^4)$ through a resolution of identity formalism, so it may be possible to reduce the overall scaling of the electron

propagator to $O(N^3)$. These methods do have promise, when using the transition orbital method, to increase accuracy of core electron binding energies at a low computational cost.

5.4. Development of pseudoatoms for III-V semiconductors

More sophisticated pseudoatoms can be defined and implemented for improving truncation error for systems unique to the problem solved by the divalent pseudoatom, where two covalent bonds are cut to the same atom that is being removed from the complete system. In indium phosphide and other group III-V semiconductors, ionic and covalent interactions contribute to the overall bonding because indium and phosphorus have different numbers of valence electrons as well as different electronegativities. Using hydrogen link atoms to truncate this system would lead to a very poor description of indium phosphide's electronic structure, geometry, and properties.[7] A rigorous analysis of how the pseudoatom is defined is necessary in order for it to perform in a manner that has the correct description of ionic and covalent interactions.

An initial starting point for designing pseudoatoms for III-V semiconductors would be to design a monovalent pseudoatom that

can be applied to InP clusters at regions of truncation. Typically, phosphine groups have appropriate dative bonding that helps maintain the correct electronic structure for InP clusters, and using a single atom to replace a phosphine decreases the degrees of freedom, allowing more efficient geometry optimizations of these systems. The appropriate atom as a starting point for replacing the phosphine groups would be the isoelectronic argon atom with the phosphorus basis set and associated pseudopotential. Adding additional fitted effective core potential terms to this pseudopotential may be an effective strategy to obtaining an atom with similar dative bonding to that of a phosphine group. These terms can either be fitted by properties listed in Chapter 1, where a function defined in terms of errors for various geometric parameters and populations were minimized with respect to each parameter, or by fitting to different orbital energies in a way that attempts to make the atomic orbital basis of argon similar to the lower lying molecular orbitals of phosphine.

In order to obtain a proper optimization of the added effective core potential parameters, an appropriate initial guess must be used. Starting values of zero for coefficients and one for exponents has proven to be ineffective in previous explorations of pseudoatom development. Part of the success in the development

of silicon divalent pseudoatoms was from using an initial set of hand fit parameters provided by Dr. Ujjal Das. Defining a systematic method of creating a quality initial guess that can be easily implemented will be beneficial to the efficiency of developing new pseudoatoms.

A previous fitting method that is worth improving upon is to modify the currently defined terms in the pseudopotential, as used in SDD, but vary the coefficients contained in each angular momentum term while keeping the exponents fixed. The highest angular momentum coefficient is minimized with respect the bond angle errors in the fitting molecules. Next, the next lowest angular momentum coefficient is varied to optimize the pseudoatom bond lengths. Finally, with those two parameters hand fit, the lowest angular momentum coefficient is optimized to decrease the error in the population analysis. As each of these variables are changed, it will affect the results of the bond angles, bond lengths, and Mulliken charges, so this should be done in an iterative manner until results are satisfactory.

The procedure mentioned does have deficiencies, as it would be more desirable to define a pseudoatom by adding additional corrections to the overall effective core potential instead of using a

completely new set of coefficients and exponents. Previous hand fitting attempts with silicon have proven a failure in the potential energy surface formed from opening a bond angle, which is drastically underestimated by this procedure. Understanding the dependence of the energy cost to create a linear bond angle with respect to the set of coefficients and exponents may lead to more robust parameter optimization procedures. Special care must be taken during hand fitting parameters or using optimization techniques that use numerical derivatives, as regions in the parameter space lead to non-smooth changes to the properties of interest, so the optimizer must use penalty functions or carefully avoid these regions.

Using the methodology from the development of a monovalent pseudoatom that can be used in dative bonding environments, divalent pseudoatoms that replace the phosphorus groups truncating an InGaP(001) surface can be obtained. As seen in a typical 2-dimer InGaP(001) cluster model shown in Figure 5.4, two different types of phosphorus atoms truncate the cluster, one that is trivalent, the other is tetravalent. The divalent PH group needs its own definition of a pseudopotential using an isoelectronic sulfur atom, compared to the divalent PH_2 truncating group which

should use a chlorine atom, as they have their own unique bonding environments.

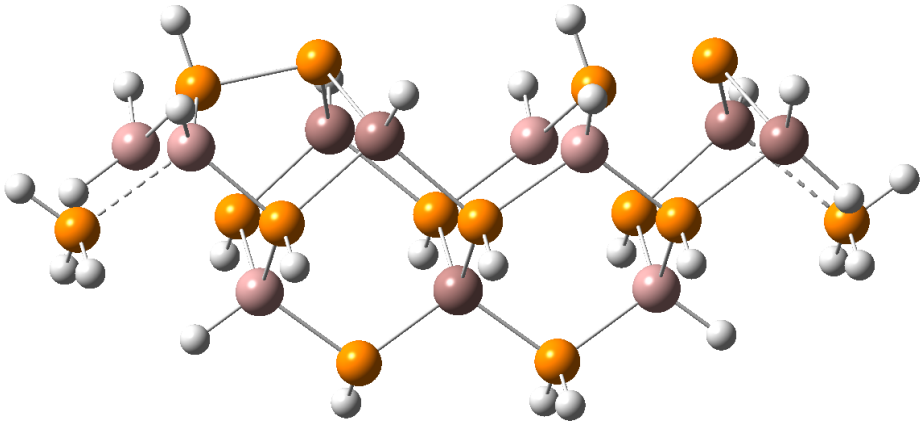

Figure 5.4. A phosphorus-rich 2-dimer InGaP(001) model, optimized with B3LYP and a double-zeta basis set with SDD pseudopotentials on indium and gallium atoms.

5.5. References

1. (a) Hoffmann, R. W., Allylic 1,3-strain as a controlling factor in stereoselective transformations. *Chemical Reviews* **1989,** *89* (8), 1841-1860; (b) Johnson, F., Allylic strain in six-membered rings. *Chemical Reviews* **1968,** *68* (4), 375-413; (c) Tietze, L. F.; Schulz, G., Investigations into the biosynthesis of porphyrins and corrins—calculations on 1,3-allylic strain and [1,5]-sigmatropic rearrangements in pyrroles, furans, and thiophenes. *Chemistry – A European Journal* **1997,** *3* (4), 523-529.

2. (a) Ramabhadran, R. O.; Raghavachari, K., Theoretical Thermochemistry for Organic Molecules: Development of the Generalized Connectivity-Based Hierarchy. *Journal of Chemical Theory and Computation* **2011,** *7* (7), 2094-2103; (b) Ramabhadran, R. O.; Raghavachari, K., Connectivity-Based Hierarchy for Theoretical Thermochemistry: Assessment Using Wave Function-Based Methods. *The Journal of Physical Chemistry A* **2012,** *116* (28), 7531-7537; (c) Gordon, M. S.; Fedorov, D. G.; Pruitt, S. R.; Slipchenko, L. V., Fragmentation Methods: A Route to Accurate Calculations on Large Systems. *Chemical Reviews* **2011,** *112* (1), 632-672.

3. Dreuw, A.; Head-Gordon, M., Single-Reference ab Initio Methods for the Calculation of Excited States of Large Molecules. *Chemical Reviews* **2005,** *105* (11), 4009-4037.

4. Mori-Sánchez, P.; Wu, Q.; Yang, W., Orbital-dependent correlation energy in density-functional theory based on a second-order perturbation approach: Success and failure. *The Journal of Chemical Physics* **2005,** *123* (6).

5. (a) Beste, A.; Vázquez-Mayagoitia, Á.; Ortiz, J. V., Direct Δ MBPT(2) method for ionization potentials, electron affinities, and excitation energies using fractional occupation numbers. *The Journal of Chemical Physics* **2013,** *138* (7); (b) Slavíček, P.; Martínez, T. J., Ab initio floating occupation molecular orbital-complete active space configuration interaction: An efficient approximation to CASSCF. *The Journal of Chemical Physics* **2010,** *132* (23); (c) Steinmann, S. N.; Yang, W., Wave function methods for fractional electrons. *The Journal of Chemical Physics* **2013,** *139* (7).

6. Hohenstein, E. G.; Kokkila, S. I. L.; Parrish, R. M.; Martínez, T. J., Tensor Hypercontraction Equation-of-Motion Second-Order Approximate Coupled Cluster: Electronic Excitation Energies in

O(N4) Time. *The Journal of Physical Chemistry B* **2013,** *117* (42), 12972-12978.

7. Raghavachari, K.; Fu, Q.; Chen, G.; Li, L.; Li, C. H.; Law, D. C.; Hicks, R. F., Hydrogen Adsorption on the Indium-Rich Indium Phosphide (001) Surface: A Novel Way to Produce Bridging In–H–In Bonds. *Journal of the American Chemical Society* **2002,** *124* (50), 15119-15124.

Benjamin C. Gamoke

Education

- Ph.D. in Physical Chemistry, Indiana University 2009-2015
  - Research Advisor: Krishnan Raghavachari
- B.S. in Chemistry, University of Wisconsin – Stevens Point 2005-2009
  - Research Advisor: Jason S. D'Acchioli

Research

- A novel composite energy method termed PBC-LC (Periodic Boundary Conditions – Low Coverage), has been developed to perform adsorbate studies at low coverages on periodic surfaces with the use of computationally efficient unit cells.
- Pseudoatoms are custom-designed to remove truncation effects from calculations by defining a modified effective core potential along with an appropriate basis set. We developed divalent pseudoatoms that solve the problems encountered with truncated Si(100) cluster/slab models.
- Interaction deletion is a new composite energy scheme that effectively cancels unphysical link atom interactions in cluster models for surfaces. The resulting hybrid potential energy can be minimized with respect to the geometrical parameters, yielding structures that are not adversely impacted by the unphysical interactions. A generalized method is being developed to aid in the understanding of hydrogen bonding interactions in molecules and materials.
- A variety of applications to problems in surface chemistry are being carried out with the recently developed methods as well as traditional methods. A study on the group III sublattice growth in the alloy semiconductor $InGaP_2$ semiconductor has been recently published.

Awards

- Felix Haurowitz Award for exceptional research performance — 2012-2013
  - Department of Chemistry, Indiana University, Bloomington, IN
- Felix Haurowitz Award for exceptional research performance — 2011-2012
  - Department of Chemistry, Indiana University, Bloomington, IN
- Departmental Fellowship for academic proficiency — 2009-2010
  - Department of Chemistry, Indiana University, Bloomington, IN
- Kallader Award for academic performance in inorganic chemistry — 2008
  - Department of Chemistry, University of Wisconsin – Stevens Point, Stevens Point, WI

Publications

8. **Benjamin C. Gamoke**, Nicholas J. Mayhall, Krishnan Raghavachari, "Interaction Deletion: A Method for Selectively Removing Atom-Atom Interactions", (In preparation).
7. **Benjamin C. Gamoke**, Ujjal Das, Hrant P. Hratchian, and Krishnan Raghavachari, "Divalent Pseudoatoms in Cluster Modeling of Si(100) Surfaces", **2013,** 164708.
6. **Benjamin C. Gamoke** and Krishnan Raghavachari, "Cluster Model Studies of Atomic Ordering in Group III Sublatice Growth over P-rich $InGaP_2$ Surfaces", *Journal of Physical Chemistry C,* **2013,** 117, 2078-2083.
5. **Benjamin C. Gamoke**, Nicholas J. Mayhall, Krishnan Raghavachari, "A Composite Energy Treatment for Sterically Hindered Cluster Models for the Si(100) Surface", *Journal of Chemical Theory and Computation,* **2012,** 8, 5132-5136.
4. **Benjamin C. Gamoke**, Nicholas J. Mayhall, and Krishnan Raghavachari, "Modeling Non-Periodic Adsorption on Periodic Surfaces: A

Composite Energy Approach for Low-Coverage Limits", *Journal of Physical Chemistry C,* **2012,** 116, 12048-12054.

3. Jordan P. Merz, **Benjamin C. Gamoke**, Matthew P. Foley, Krishnan Raghavachari, Dennis G. Peters, "Electrochemical Reduction of (1R,2r,3S,4R,5r,6S)-hexachlorocyclohexane (Lindane) at Carbon Cathodes in Dimethylformamide", *Journal of Electroanalytical Chemistry.* **2011,** 660, 121-126.
2. **Benjamin Gamoke**, Diane Neff and Jack Simons, "Nature of PO Bonds in Phosphates", *Journal of Physical Chemistry A,* **2009,** 113, 5677-5684.
1. Robert C. Badger, Jason S. D'Acchioli, **Benjamin C. Gamoke**, Sang Bok Kim, Tracey A. Oudenhoven, Dwight A. Sweigart and Robin S. Tanke, "Chemical, Electrochemical, and Theoretical Investigations of [(Cp)Ru(CO)3]+ and [(Ind)Ru(CO)3]+", Organometallics, **2009,** 28, 418-424.

Presentations

- Divalent Pseudoatoms in Cluster Modeling of Si(100) Surfaces, 246th ACS National Meeting, Indianapolis, IN (Poster Presentation) — September 2013
- Modeling Non-periodic Adsorbates on Periodic Surfaces, 44th Midwest Theoretical Chemistry Conference, University of Wisconsin, Madison, WI. (Oral Presentation) — June 2012
- Modeling Non-periodic Adsorbates on Periodic Surfaces, 43rd Midwest Theoretical Chemistry Conference, University of Notre Dame, South Bend, IN. (Poster Presentation) — June 2011
- Theoretical Studies of Metastable Anions in Phosphate Groups, Departmental Seminar, Department of Chemistry, University of Wisconsin – Stevens Point, Stevens Point, WI (Oral Presentation). — December, 2008